Degradation of Mechanical Properties of Bovine Cortical Bone During Long-Term Whole Bone Storage.

Lia Carstens

Master of Science in Biomechanical Engineering
in the Department of Mechanical Engineering
Faculty of Engineering and the Built Environment
University of Cape Town

2024

Declaration

I, Lia Carstens, hereby:

(a) grant the University of Cape Town free license to reproduce the above thesis in whole or in part, for the purpose of research;

(b) declare that:

(i) the above thesis is my own unaided work, both in concept and execution, and that apart from the normal guidance from my supervisor, I have received no assistance apart from that explicitly stated in the Acknowledgements.

(ii) neither the substance nor any part of the above thesis has been submitted in the past, or is being, or is to be submitted for a degree at this University or at any other university.

I am now presenting this thesis for the degree of Master of Science in Biomechanical Engineering.

L. Carstens

2024

Abstract

Understanding the mechanical properties and behaviour of bone is critical for predicting fractures and failures in the human skeletal system. Mechanical testing has been the conventional method for characterizing bone materials. However, due to the limited wall thickness of whole bones, only small cortical bone specimens can be obtained which creates challenges when accurate modulus measurements are required. Large-scale universal testing machines often introduce global compliance errors that obscure precise displacement data, in addition to localized compliance at the specimen-platen interface. These compliance effects are especially acute when conducting tests on quasi-brittle materials like cortical bone, that exhibit low failure strains.

A thorough review of existing literature shows that there is a gap regarding the storage protocols for bone specimens prior to mechanical testing. While storage methods are generally well described, important parameters such as the interval between donor death and bone retrieval, or the time between specimen preparation and testing, are seldom reported. As bone degrades after removal from the donor, understanding this degradation is crucial to determining the duration that stored specimens remain representative of in-vivo conditions.

This dissertation investigates the effects of long-term storage on the mechanical properties of bovine cortical bone, comparing two protocols: "machined-frozen" (MF) and "frozen-machined" (FM). While degradation was observed in both cases, FM samples retained their mechanical integrity slightly better than machined specimens. The elastic moduli for both groups were at the lower end of expected values after one month of storage, with a significant decline by the third month.

The work described above required the development of specialized testing techniques. In particular, this work addresses compliance errors by utilizing a micron-accurate sub-press equipped with novel frustum platens designed to centralize and uniformly distribute loads. These platens, enabled precise theoretical and

experimental evaluations of localized compliance, ensuring accurate modulus measurements for small specimens. Validation was achieved by comparing results from compressive tests on cylindrical polymethyl methacrylate (PMMA) and aluminium (Al) specimens of varying heights against three alternative methods i.e. stress wave propagation, tensile extension, and three-point bending, each of which typically require larger specimens. A high degree of correlation between the methods demonstrates the accuracy and utility of this approach in small-specimen testing.

Acknowledgements

I would like to express my gratitude to my supervisor Dr. Trevor Cloete for their invaluable guidance, support, and encouragement throughout this project. Trevor, thank you for providing me with valuable knowledge and insights and for pushing me to exceed even my own expectations. Your experience and mentorship has been invaluable, and I could not have asked for a better supervisor during this journey.

To Nicholas Daras, whose foundational research provided the groundwork for this project, thank you. Taking over from your work has been both a challenge and a privilege, and I am grateful for the solid base you laid. Thank you for not only the academic support, but also your friendship. You never hesitated to lend me your hand; ear; shoulder; or anything else I may need. Your encouragement and constant cheering from the sidelines is what kept me positive and kept me going. To Sherlyn Gabriel, thank you for the off-campus lunches, the cake and coffee sessions, and for always being willing to drop everything to help the people you care about. Your generosity and friendship got me through some of the toughest parts of this degree.

To my BISRU family, thank you all for showing an interest not only in my work, but also in my personal well-being. Dr. Reuben Govender, thank you for your mentorship outside of my project and for immensely building my confidence, it has been a pleasure being your teaching assistant and colleague for the past two years. To Shivasi Mashau, thank you for always being a good sport in whatever ridiculous activities I planned for our socials. Sa-aadat Parker, thank you for always being up for a chat in the staff room. To, Joshua Malan, who has been through the trenches with me, both at Tuks and here at UCT, I thank you for your friendship. Finally, to Prof. Steeve Chung Kim Yuen, thank you for always putting a smile on my face, even on the dreariest of days.

A massive thanks to all the staff in the UCT workshop who helped machine all the apparatuses and specimens used in this research. Pierre, Thulani, Wayne

and especially Grant for machining all of my bone specimens, regardless of how unpleasant that got sometimes. A big thanks to Penny Louw in CME for her assistance when configuring and operating the UTM and for making my testing a fun and enjoyable experience. Thank you to Heinrich Rautenbach at Bill Riley Meat for supplying the cow femurs used for the bone tests.

To my friends and loved ones who were always there for me, you are all immensely appreciated and I could not have got through any of this without each and every one of you.

Finally, to my mother, Lizette and my father, Riaan thank you guys for always supporting me in everything I do, no matter how outrageous. Thank you for giving me this opportunity and thank you for your continued love and encouragement and support. To my partner, Lohan, thank you for your unwavering support and patience throughout this journey. To my brother, Heinrich, thank you for the all of the coding assistance, banter and loving mutual bullying.

Contents

List of Figures

List of Tables

Chapter 1

Introduction

The mechanical properties of bone have been a subject of interest in engineering research for more than 50 years [1]. However, despite this, there appears to be a large disparity in the literature about the mechanical properties of bone. The literature hypothesizes that these inconsistent results are due to the highly complex nature and structure of bone, as well as a lack of standard testing and storage techniques among studies. Specimen storage protocols used in bone investigations, in particular, are not thoroughly reported in the literature. Storage protocols reported, range from dry freezing [2] to storage mediums such as saline [3], formalin [4] or phosphate buffered saline [5]. Furthermore, there is no agreement on whether storage duration influences the reported mechanical properties of bone specimens, or what an acceptable duration is for bone to be stored before the properties no longer represent in-vivo conditions, with a number of studies reporting conflicting findings.

Most importantly, there does not appear to be any specific investigation wherein fresh bones (within 24 hours of death of the donor for the purpose of this dissertation) are tested or even an agreed-upon definition of what the term 'fresh' means when it comes to bone. This raises the question of whether prolonged storage can skew test results. The characterisation of bone is further confounded by the need for a highly accurate testing apparatus to precisely evaluate features such as the failure strain of such small specimens, and achieving this degree of accuracy appears to have received insufficient attention in the literature.

Even though testing machines are calibrated for a specific accuracy, the inherent compliance of large testing machines can notably influence the measured properties when testing small specimens [6]. Consequently, machines generally employed for assessing the mechanical properties of bone specimens need supplemental systems or specialized techniques to achieve precise displacement measurements [7].

This research broadly aims to enable the future development of patient-specific numerical models capable of predicting and depicting skeletal responses under various strain rates. However, before such a sophisticated model can be created, it is essential to accurately characterize the material properties of bone through experimental testing on small specimens.

1.1 Aim and Scope

The primary aim of this research is to characterize the degradation behaviour of bovine cortical bone in an effort to develop improved bone specimen curation protocols. To conduct this degradation study, quasi-static compression tests were performed using a custom sub-press. The sub-press accuracy was validated and the compliance was estimated to determine its effect on measured mechanical properties and to determine its suitability in small specimen/low modulus compression tests.

1.2 Objectives

The objectives of this dissertation are:

- To investigate the effects of two storage protocols, namely "machine-freeze" (MF) and "freeze-machine" (FM), on the mechanical properties of bovine cortical bone over time.
- To validate the sub-press accuracy.
- To investigate local platen compliance with three distinct platen variations.
- To evaluate the performance of the sub-press by comparing it to the results from three distinct testing machines and methods.

1.3 Document Outline

This dissertation is divided into the following chapters:

- Chapter 2: Literature Review

  The aim was pursued firstly, through a thorough literature review. Several topics were researched such as the hierarchical structure of bone, intrinsic factors that affect the response of bone to stress, species-specific responses, the strain rate dependence of the mechanical properties of bone, specimen storage methods and duration, as well as the specialised equipment needed to test bone.

- Chapter 3: Methodology

  This chapter describes the design and modifications of the sub-press, the sub-press accuracy validation, the estimation of the sub-press compliance, the bone specimen machining and storage, the experimental set-up and testing methods, as well as the data processing steps followed.

- Chapter 4: Experimental Results

  This chapter contains the results after all data processing for all QS tests from the degradation study, with special interest in the apparent modulus and maximum compressive strength.

- Chapter 5: Discussion

  This chapter offers an analysis of the results, beginning with a short summary of literature findings, followed by the validation of sub-press accuracy, the estimation of the sub-press compliance and assessment of the sub-press platen variations, and concluding with the findings from the degradation study.

- Chapter 6: Conclusion and Recommendations

  The study concluded with a summary of key findings and recommendations for future research.

Chapter 2

Literature Review

Reviewed here is the literature relevant to the research to be presented. There are sections on the hierarchy of bone, intrinsic factors that affect stress response, impact of storage and testing conditions, bone structure and strain rate on bone response, among other topics. This section concludes with a review of the specialised equipment required to analyse cortical bone.

2.1 Hierarchical Structure of Bone

Bone is a complex biological substance with several organizational levels ranging from macro-scale to nano-scale. An overview of the hierarchical structure of bone is provided here, including details on how the structure of bone may vary between species.

2.1.1 Bone Physiology

On a macro-scale bone can be split into two categories namely cortical and trabecular bone. On a micro-scale bone consists of osteons (primary and secondary), Haversian canals and collagen fibrils. On a nano-scale, bone contain collagen molecules and hydroxyapatite nano-crystals.

There are several different types of bones in the human skeleton, including short (e.g. carpal bones in the hands), long (e.g. humeri in the upper arms), irregular

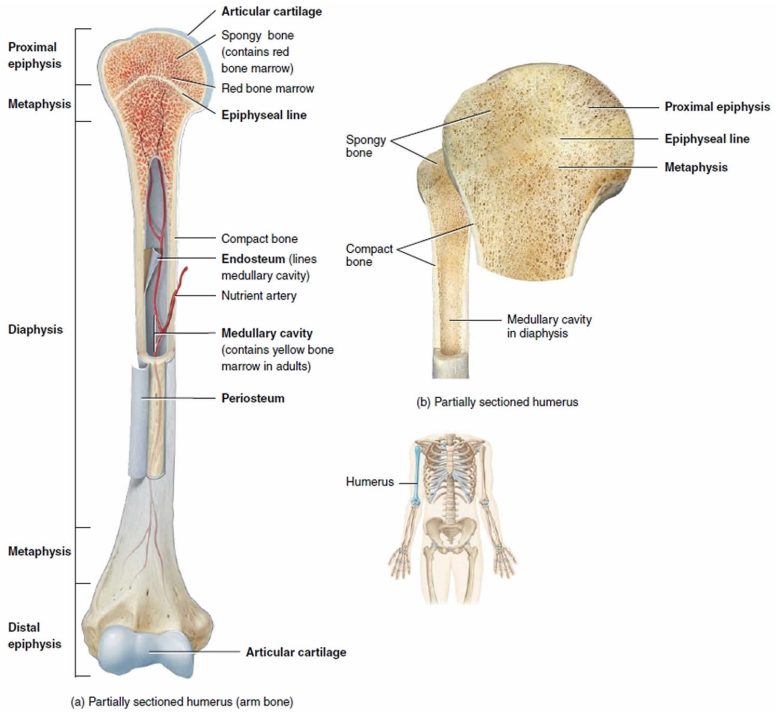

Figure 2.1 Long bone anatomy [9]

(e.g. vertebrae in the spine) and flat bones (e.g. ribs) [8]. The research presented here will focus solely on long bones. Long bones, such as femurs or humeri, are identified by their appearance as having a long, hollow centre (the diaphysis) and rounded ends (the epiphyses) on either side [8]. Figure 2.1, which depicts a typical human humerus, demonstrates the fundamental architecture of a long bone.

At the macro-scale, two distinct bone morphologies are evident when a long bone is sectioned. These are trabecular bone, also referred to as spongy bone, and cortical bone, also referred to as compact bone. It is also crucial to keep in mind that the term 'bone' can be a somewhat ambiguous because it can refer to both the material i.e. trabecular or cortical, and the overall structure i.e. whole bones.

Cortical bone is a densely packed tissue (containing less than 10% soft tissue) that forms the external layer of all bones and is found particularly in diaphysis of long bones [10]. Cortical bone represents 80% of the skeletal mass and therefore supports most of the mechanical function [11]. Trabecular bone is made up of trabecules shaped as plates or rods interspersed between bone marrow that repre-

sents more than 75% of the trabecular bone volume and is found mainly between the cortices of smaller flat and short bones such as scapulae, vertebrae, and pelvis [10]. Trabecular bone is only 20% of the skeletal mass but is metabolically four times more active per unit volume than cortical bone [11]. Thus, the metabolic function is equally distributed between cortical and trabecular bone [11].

At the nano-scale, the two primary constituents of cortical bone tissue are collagen molecules and hydroxyapatite crystals [12]. These components are organized in several ways at the micro-structural scale. Four basic descriptions are used to group these micro-structural variations namely woven bone, lamellar bone, fibrolamellar bone (also called plexiform) and osteons (also known as Haversian canals).

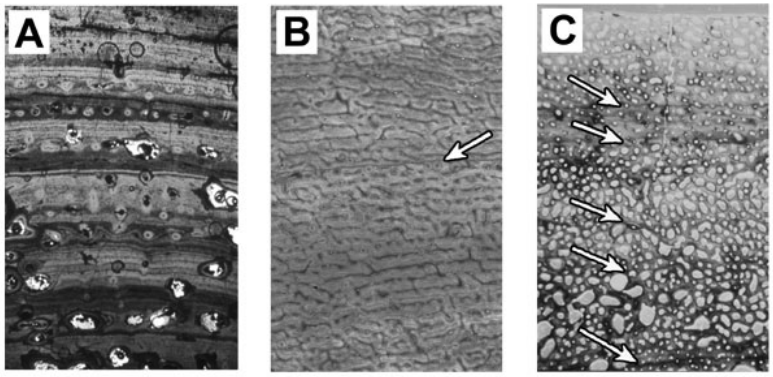

Figure 2.2 A. Lamellar bone. B. Woven bone. C. Fibrolamellar bone. Arrows indicate Lines of Arrested Growth (LAGs) [13].

Additionally, the micro-structure of bone will modify and adapt as it grows. Stress causes micro-damage in the bone, which prompts remodelling - the process of removing and replacing bone tissue [14]. In fully developed skeletal structures, changes in bone mass are mostly caused by bone remodelling [15]. This has an impact on the micro-structure of the bone and material composition, both of which have a significant impact on the bone strength [15]. It has been hypothesized that excessive or insufficient bone remodelling can make bones more brittle [16]. The porosity of cortical bone rises with high levels of remodelling, such as those that take place during menopause [15]. In contrast, if the quantity of remodelling is too low, the amount of micro-cracks in the bone would significantly rise [15]. Healthy bones need to go through a complex natural cycle of injury and remodelling in

order to be fracture-resistant [16]. The differences are evident in newly created bone located at the outer surface of the whole-bone compared to established bone found farther inside the whole-bone [17].

Woven bone as shown in Figure 2.2 B, forms very rapidly (such as is found in juveniles with corresponding high rates of growth) [18], with collagen fibres showing a variety of orientations and having an undefined and random structure with a disorganized appearance, which causes an isotropic bone response [19, 18]. The bone has a flexible structure because it is not densely compacted [19]. Due to the unpredictability of its orientation, woven bone grows more quickly but is weaker than lamellar bone [19]. However, the speed at which woven bone can be formed means that it is often found in bones that require rapid growth, such as during growth spurts in young individuals.

Lamellar bone as shown in Figure 2.2 A, is composed of layers of aligned collagen fibrils laid down on top of one another at a slower rate than woven bone [19]. Despite the fact that these layers may be oriented differently from one another, each layer has its fibres aligned in a specific, recognizable direction [17]. The hydroxyapatite crystals will also be lined up with one another in each of these sub-layers. However, from layer to layer, the crystal inclination will vary [17]. As a result of this lamellar bone appears 'plywood-like' [17].

Fibrolamellar, or plexiform bone (also known as laminar bone, not to be confused with lamellar bone) seen in Figure 2.2 C, is a combination of woven and lamellar bone. An initial framework of woven bone is rapidly laid down, then replaced with lamellar bone at a more reasonable pace during remodelling [19]. Remodelling entails the resorption of old or damaged bone, followed by the deposition of new bone material [20]. Primary osteons may also arise within the woven bone framework in a range of orientations in this sort of micro-structure [18].

Osteons can be primary or secondary and are made up of layers of bone around the perimeter. Primary osteons are highly elongated and fill voids left by fast bone development [17]. Secondary osteons, which frequently have a cylindrical shape and are formed during the remodelling of pre-existing bone, are also known as Haversian systems [17]. These Haversian systems have a distinct outer boundary known as the cement line and form through previously produced bone tissue [18]. It has been observed that an increase in the number of secondary osteons

present results in a reduction in the ultimate compressive strength of the bone [21], ultimate tensile strength [22], and apparent modulus [21, 22]. Haversian bone displays somewhat transversely isotropic behaviour, due to the symmetry found in the structure of the Haversian systems [23].

2.1.2 Bone Structure in Different Species

Different species have cortical bone with distinctly different micro-structures [24, 25, 26]. To qualitatively distinguish bone samples from various species, Brits *et al*. [24] examined the configuration of principal vascular canals as well as primary and secondary osteons. Vascular canals are small open channels in bone through which blood vessels run, and are found both as stand-alone features, and in the centre of primary and secondary osteons. Brits *et al*. [24] examined a number of different species, but the results they found about sheep, non-human primates, and human bone were of particular interest. The sheep bone was predominantly made up of vascular longitudinal bone, but it also had bands of primary osteons that were closer to the centre of the bone. The non-human primate bone showed a mixture of avascular bone and irregular Haversian bone. Bone that has either very few or no circulatory canals is said to be avascular.

Brits *et al*. [24] found juvenile and adult human bone to have distinct properties and placed them in separate categories. The adult human bone displayed a mixture of primary vascular longitudinal bone along with dense and uneven Haversian bone. The osteons were either dispersed or closely packed, depending on their density. By contrast, the adolescent human bone primarily displayed uneven Haversian bone, along with sporadic secondary osteons and sizeable Haversian canals.

In keeping with the findings of Brits *et al*. [24], Spatz *et al*. [27] found that cortical bone from the femur, tibia, and metatarsus of an adult sheep is primarily fibrolamellar, with only a very little proportion of Haversian bone present.

Similar to the findings of Brits *et al*. [24], Martiniakova *et al*. [25] investigated the micro-structure of sheep bone and found primarily primary vascular fibrolamellar bone with a few dispersed secondary osteons. Since baboons have been shown to undergo bone remodelling, some Haversian systems can be expected in mature baboon bone [28], which is also consistent with the results of Brits *et al*. [24]. [24].

Crocodylian micro-structure can be divided into two main categories namely lamellar bone interspersed with longitudinal vascularisation, organized into zones within the bone (also known as lamellar zonal bone) [29] and fibrolamellar bone [29] as shown in Figure 2.3. Fibrolamellar bone is commonly found in captive crocodylians, and is the most likely configuration to be seen in the specimens collected for the research to be presented.

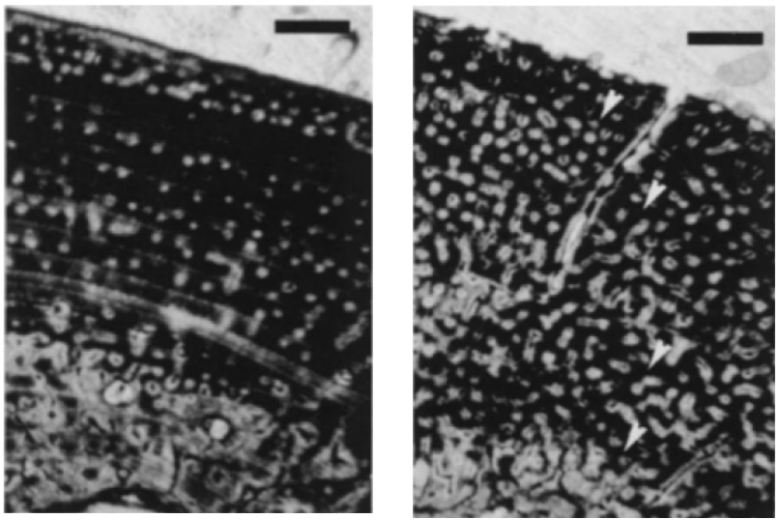

Figure 2.3 Left: An example of lamellar zonal bone tissue seen in crocodylians, with 919 micrometer scale bar. Right: An example of fibrolamellar bone seen in crocodylians, with white arrows marking boundaries between areas of fibrolamellar bone (Scale bar 919 micrometer). [29]

There are conflicting reports on the micro-structural organisation of ostrich bone. Spatz *et al* . [27] found ostrich cortical bone to be primarily fibrolamellar with minimal Haversian bone present by, which is consistent with the description provided by Castanet *et al* . [30]. By contrast, Currey [19] reports that ostriches frequently have substantial Haversian bone present. Furthermore, within a single species, the way in which the femur bears load will affect the specific micro-structures present [31].

2.2 Intrinsic Factors that Affect the Response of Bone to Stress.

The factors that affect the mechanical properties of bone are challenging to evaluate separately due to their mutually interactive nature [15]. Intrinsic factors that influence bone response include the age and sex of the specimen donor, the age and curation of the specimen post-mortem, the porosity of the specimen and mineral content, and the anisotropy of bone itself.

2.2.1 The Effect of Age

Several studies have shown that the mechanical properties of a bone specimen are influenced by the age of the donor at death [32, 33, 34, 35]. The post-mortem age, or the interval between bone harvest and bone testing, has also been shown to have an impact [5, 36].

2.2.1.1 Age of Donor

The effects of age are intertwined with the effects of bone remodelling and micro-structure on bone response [26]. Enlow [26] found that as an individual ages, more bone remodelling will take place, and the underlying micro-structure may change. Ebbesen *et al*. [33] found that the compressive strength of an individual's bone declines with age, however, Martin & Atkinson [34] found that the material strength of bone actually increases initially up to the age of about 30, after which the strength starts to decline. Martin & Atkinson [34] attributed this to the fact that bone does not initially form as secondary osteons, but as primary bone, which becomes secondary bone through remodelling as an individual ages.

According to Augat & Schorlemmer [32] the overall porosity of cortical bone increases with every remodelling of the tissue, due to the fact that not all of the previously removed material is fully replaced. Moreover, as an individual ages, there is more time for micro-damage to occur and accumulate, due to repeated loading of the bone [32, 37]. This is supported by a study reported by Hui *et al*. [38], which revealed an increase in fracture occurrence in bones from older individuals. It should be emphasized that this specific study [38] combines infor-

mation on fractures in the shafts of long bones with fractures in areas such as the head of the femur.

Ebbesen *et al*. [33], who particularly examined the mineral composition of trabecular bone, observed that trabecular bone has a lower bone mineral density as it ages. As opposed to this, Currey *et al*. [35] found that mineral content increases with age. However, they [35] did find that toughness decreases with age, which concurs with the other studies mentioned. Similar to Currey *et al*. [35] a study performed on porcine bone by Feng & Jasiuk [39] showed age-related changes in the structure and chemical composition of cortical bone and that mineral content and mineral-to-organic-ratio increased with age. In this study [39] sections from femoral cortical bone from 6, 12, and 42 months old swine were studied to quantify the age-related changes in bone structure. Lamellar bone was a prevalent structure in 6 months and 12 months old animals, resorption sites were most pronounced in 6 months old animals, while secondary osteons were the dominant features in 42 months old animals. The structural and chemical changes with age corresponded to an increase in local elastic modulus (the elastic modulus measured at specific regions within the bone, accounting for microstructural differences and measured using techniques such as nano-indentation), and global elastic modulus (which represents the overall averaged stiffness of the bone obtained from macroscopic mechanical tests such as tensile or compression testing) and ultimate tensile strength as bone matured [39].

In conclusion, the manner in which each study evaluated mineral content is one potential explanation for this discrepancy. By measuring the initial volume of each specimen from unprocessed cancellous bone, Ebbesen *et al*. [33] studied the ash weight and ash density from the specimens. This implies that where the marrow had been in the samples, there would still be very sizeable voids. This provides an apparent ash density estimate since it is challenging to determine the volume of bone tissue alone in cancellous bone samples. Ash content was defined by Currey *et al*. [35] as the proportion of a dried, de-fatted sample that remained as ash following the ashing method. All samples were solely cortical. As with the testing of cancellous materials, the porous volume is not included in this. It was also found that there is no statistically significant difference between the static elastic modulus (the modulus of elasticity measured under slowly applied loads, assuming no significant time-dependent effects such as visco-elasticity or creep) of

cortical bone in children and the static elastic modulus in the elderly [40]. This is consistent with the hypothesis that as people age, their cortical bone develops to an optimum level and then declines [40].

2.2.1.2 Postmortem age of Specimen

Three studies, Lee & Jasiuk [5], Welgemoed [36] and Daras *et al*. [41] investigated the effect of post-mortem age on the mechanical response of bone. The storage protocols used in these studies are discussed in more detail in Section 2.7.

Lee & Jasiuk [5] studied the impact of freeze-thaw cycles on trabecular porcine bone. Three groups of femurs were examined: fresh bone, bone stored in the freezer at -20°C for one year, and bone stored for five years. The bones were wrapped in gauze soaked with Phosphate Buffered Saline (PBS) and stored in sealed zip lock bags before freezing. After thawing, the machined specimens were tested within 48 hours. The bone frozen for five years exhibited lower Young's modulus and ultimate strength compared to fresh bone. Moreover, the correlation between mechanical properties and parameters such as porosity and apparent density weakened in the long-term frozen bone, especially for Young's modulus.

Welgemoed [36] tested femurs from four different species were to examine the impact of long-term storage on bone properties. The bones were cut and machined into two series. The first series underwent gradual defrosting, storage in saline solution, and freezing at -31°C until needed. The second series was machined later to assess the effects of longer storage times. Both series were tested, and the results showed ageing effects, with a decrease in the apparent modulus between the first and second series. However, the compressive strength showed less variation between the series.

Daras *et al*. [41] investigated the effects of long duration storage on the measured mechanical properties of bovine cortical bone. Three different storage protocols were compared; namely machined-refrigerated, machined-frozen and frozen-machined-frozen. Degradation effects were evident for both refrigerated and frozen specimens and the results demonstrated that testing bone specimens after more than one week in storage may not provide representative in-vivo properties. In addition, specimens exhibited severe degradation after six months in storage regardless of the storage protocol.

Overall, all three studies suggest that post-mortem age and long-term freezing significantly affects the mechanical properties of bone. There is evidence of decreased apparent modulus and weakened mechanical behaviour in bones that underwent longer storage periods. Lee & Jasiuk [5] concluded that this may be attributed to the formation and enlargement of ice crystals causing structural damage, as well as the continued activity of cellular enzymes at freezing temperatures. The findings also indicate that the predictability of the mechanical properties of bone may be compromised with prolonged storage, making it challenging to establish correlations between porosity and mechanical behaviour in aged bones [5].

2.2.2 The Effect of Donor Sex

Females have been reported to have lower bone mineral content (in g) and lower mean bone mineral density (in g/cm^2) than males of the same age [33]. However, it was observed by Ebbesen *et al*. [33] using a number of testing techniques that women often had slightly greater bone densities in their younger years, with a faster loss in density than men and ultimately end up having lower bone densities than men in later years, yet, the variation in density between the sexes is so negligible that it is largely ignored [33]. A study by Martin & Atkinson [34] that likewise revealed no discernible difference in the density of bone specimens obtained from human males and females lends support to this. It was found that specimens from females showed a significantly lower maximum compressive load, due to the difference in overall size of the bone tested, but no significant difference in maximum compressive stress [33]. Also, Wu *et al*. [42] found that there were no significant differences in the apparent modulus of bone due to the sex of the specimen donor.

The second moment of area (moment of inertia) in females grows until the age of 35, at which point it begins to rapidly decline [34], according to observations of the cross-section of the shaft of a human femur. It rises in males throughout their lives, however it does so at a slower pace [34]. This may explain why specimens from older females show weaker material strengths, as this decreasing second moment of area couples with any other factors that would reduce the maximum load the bone is able to carry. The ever-increasing second moment of area in males works to counterbalance the other material weakening mechanisms [34]. Moreover,

the cortical layer of bone in females thins while remaining relatively constant in thickness in males [34].

Crenshaw *et al*. [43] conducted a study on the effects of sex in swine bone, and found similar differences. They found that there was no difference in withstandable force between the sexes. Similar to the research of Martin & Atkinson [34], a variation in the second moment of area between males and females was found which is only of concern when testing whole bones and not small bone specimens. This was offset by a slight difference in the mineralisation of the bones, with males having less mineralised bone than females.

2.2.3 The Effect of Mineral Content

Bone mineral content, which is typically quantified in grams or milligrams, is the amount of mineral (primarily calcium and phosphorus) at a particular skeletal site, such as the femoral neck, lumbar spine, or total body [44]. It is frequently displayed as ash weight (g) or as a percentage of the material that remains after ashing[1] (mg/g). Bone ash is defined as the residue obtained when bones are burned in air.

According to Currey *et al*. [35], the mineral concentration of cortical bone rises with advancing age. Up until the age of 25, there is a consistent and obvious increase in mineral content. Ageing from 25 years onwards exhibits a less pronounced increase, but it is evident that the increase in mineral content with age continues in these later years when viewing the logarithmic relation between ash content and age. Baboons exhibit the same rise in mineral content with ageing [28].

Research by Currey [45, 46] also demonstrated a positive association between tensile yield stress and mineral content, albeit a looser one than that between Young's modulus and mineral content, as well as an increase in Young's modulus with a rise in mineral content across several species.

Bovine bone was tested in untreated, de-mineralised, and de-proteinised stages. Novitskaya *et al*. [47] observed that untreated bone had the maximum compressive strength, indicating that total bone is more robust than the sum of its individ-

[1] the act of roasting de-gelatinised bone

ual components. Lower porosity and a larger (but not excessively high) mineral content in cortical bone increase strength [15]. This further shows that bone is a intricate substance that ought to be evaluated as closely as possible to in-vivo conditions.

2.2.4 The Effect of Location and Anisotropy

The spatial arrangement of bone material, both at the macro-structural and micro-structural levels, as well as the mechanical characteristics of a particular bone, will have a significant impact on how it responds to stress [16]. This leads to a complex material that, to be fully understood, needs to have many different properties and failure processes explored.

Bone is highly anisotropic [47, 48, 49, 50, 51] and thus the direction in which specimens are cut has a significant impact on their mechanical responses. While cutting a bone specimen, the longitudinal, transverse, and radial axes - depicted in Figure 2.4 - should be taken into account.

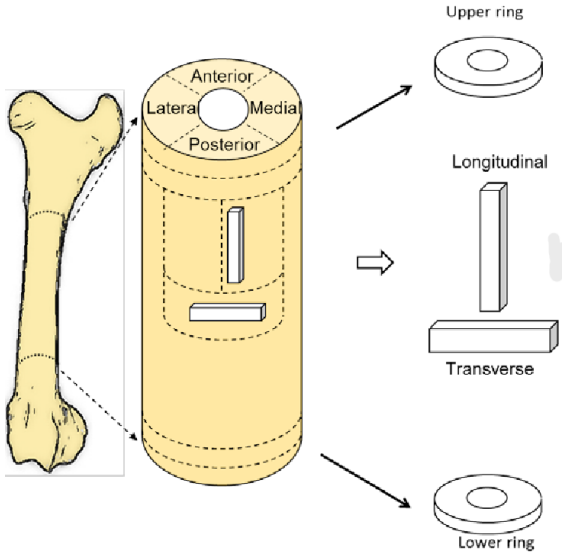

Figure 2.4 A depiction of how transverse and longitudinal specimens relate to a portion of a long bone shaft [52]

The medial, lateral, anterior, and posterior regions of each of the four sides of a bone are keywords when referring to location [31]. The region closest to the centre

of the skeleton will be the medial area. Given its distance from the centreline of the skeleton, the lateral area will be the outer-most side of the bone. The front-most part of the bone is called the anterior, while the rearmost is called the posterior. Two other keywords are proximal and distal, which refer to locations that are near or far from the head, respectively.

When comparing tests conducted in the longitudinal and transverse directions, there are obvious differences in the ultimate tensile and compressive stress, as well as the ultimate tensile and compressive strain, with longitudinal specimens consistently displaying higher failure stress and lower failure strain values than transverse specimens. [47, 53, 49, 50].

Oddly, Novitskaya *et al*. [47] found that the compressive radial strength of bovine bone is greater than the compressive longitudinal strength. The reason given for this was that the radial specimens tested primarily had a lamellar structure, and the longitudinal had osteons present, thus attributing it to differences in microstructure. The specimens tested were taken from adjacent portions of bone, although where on the bone was not stated.

Further anisotropic behaviour is observed when analysing the stiffness of bone. In bovine cortical bone, Novitskaya *et al*. [47] found that the longitudinal specimens had the highest stiffness, followed by the transverse specimens. The lowest stiffness was measured in the radial specimens.

The location from where the specimen is cut on the diaphysis of the femur (proximally, distally, laterally, anteriorly, etc.) might significantly affect the mechanical properties [54]. A longitudinal specimen taken from the anterior side of a bone may exhibit properties different from those found on the posterior side of the same bone, demonstrating that cortical bone is not only anisotropic but also extends to having different properties around the circumference of the same bone [31].

According to a study by Evans and Lebow [55] on the human femur, in particular the cortical bone, specimens taken from the lateral portion of the diaphysis of bone had the highest ultimate tensile strength, while specimens taken from the anterior portion had the lowest, with no discernible differences in elastic modulus throughout the circumference of the bone. The mid-diaphysis of human bone exhibits higher ultimate tensile strength and elastic modulus than either the distal or proximal sections of the diaphysis and bone extracted from either end of the

diaphysis exhibits distinct attributes to specimens collected from the mid-diaphysis [55]. The proximal diaphysis displayed the lowest elastic modulus and the worst ultimate tensile strength in wet specimens [55].

The type of loading (compressive or tensile) has an effect on the properties measured. The response of bone has been found to exhibit higher values of ultimate strength in compression than in tension, both in the longitudinal and transverse directions [50]. It has been found that the apparent modulus of specimens loaded in tension is 6% higher than the apparent modulus of specimens loaded in compression [56].

Wu *et al* . [42] evaluated osteonal human cortical bone and the bone tissue between osteons (also referred to as interstitial bone). They found that the interstitial bone had a higher indentation modulus than the osteonal bone. However, this testing was done using nano-indentation, meaning these results are from testing at a micro-structural level. It is not certain that this will be an accurate representation of the macroscopic properties as well.

The macroscopic stress response of bone may be influenced by additional elements, such as the cement lines between osteons, which may not be adequately captured by nano-indentation testing [57]. This is not to argue that it is unimportant to understand how distinct micro-structural components react; rather, it is to emphasize that it is crucial to understand how these components react when they interact as they would in entire bone.

2.2.5 The Effect of Porosity and Density

The mechanical properties of bone can be significantly influenced by its porosity and density. Elastic modulus and ultimate strength similarly drop with increasing porosity, which is accompanied by a corresponding decline in apparent density [21, 58]. The impact of inhomogeneities inside each specimen itself should also be considered. It has been found that inhomogeneities can have a significant impact on the measured mechanical properties and can lead to significant variations between measured properties even in small specimens [56]. Different micro-structure can explain some of these inhomogeneities, but there are other explanations, including variations in porosity and mineralization [56].

When investigating density effects and comparing literature, however, it is important to note which density is being presented, as there are multiple different densities which may be presented: Areal bone mineral density (aBMD, measured in g/cm^2) is presented when a bone surface is scanned to determine the bone mineral content, and is presented as the surface mineral content in grams divided by the area scanned. Volumetric bone mineral density (vBMD, measured in g/cm^3) is a measure of the bone mineral content throughout a sample, and is equal to the bone mineral content of the entire specimen in grams divided by the sample volume. In practice however, an apparent density (measured in g/cm^3) is often presented, as it is much easier to measure. The apparent density includes both the mineral and organic components of the bone sample, and is the weight of the entire specimen divided by the volume of the entire specimen. Dry apparent density (measured in g/cm^3) may be presented, which is similar to apparent density, but the sample is first dried in an oven to remove as much of the water content as possible. The dry apparent density is the weight of the dried sample divided by the volume of the dried sample. Lastly, apparent ash density (measured in g/cm^3), which is the density of only the mineral component of the bone, may be presented. The apparent ash density is the ash weight divided by the volume of the sample before ashing. The ash weight of the bone sample is the weight of the ash left over after burning the sample in an oven until only the mineral ash remains.

The amount of porosity for a particular volume of bone will fluctuate significantly depending on the micro-structure of the bone, such as lamellar versus secondary osteonal bone, as was previously shown. This could explain the variations in material response that we observe in bones with various micro-structures. This is supported by the differences reported in studies looking at bone from a single species, such as, Wright & Hayes [21], who observed that secondary Haversian bone displayed noticeably lower values for both ultimate strength and apparent modulus. Seemingly contrary to this, Grimal *et al*. [54] found a weak correlation between apparent density and strength, as well as between apparent density and stiffness. However, this was attributed to the small range of densities present in the specimens used, and was not found to be contradictory with previous studies showing a relationship between density and strength or stiffness - it simply requires a larger range of densities to show the true relationship. It was also suggested by the authors [54] that due to the small range of densities displayed in the specimens,

that the differences in response were more likely to be due to the organisational differences possibly present in the bone.

2.3 Effect of Micro-structural Variations on Bone Response

A study by Weiner *et al* . [17] sought to assess the function of lamellar bone specifically, and focused only on bone specimens taken from mammals. The authors concluded that lamellar bone was likely capable of performing a variety of mechanical tasks, depending on the environment to which the individual bone was exposed [17]. It should be emphasized that they define lamellar bone to include both osteonal bone and circumferential lamellar bone. Combining these two categories, which are typically referred to as independent in other studies, may have obscured relations between structure and function. Furthermore, after comparing data from other studies using micro-hardness measurements [59, 60, 61, 62], sonic velocity measurements [63, 64, 65] and testing on tibia bones taken from young baboons treated with large doses of the anti-osteoporotic drug alendronate[2] [66], Weiner *et al* . [17] found no definitive answer as to the link between structure and function, although they did note that osteonal bone was better able to absorb aspects of damage (such as micro-damage or fatigue damage) than lamellar bone. Moreover, they observed that osteonal specimens held together better after failure than lamellar bone [17].

According to Novitskaya *et al* . [47], specimens with lamellar bone and no osteons exhibited greater compressive strength than specimens with osteons. It has been suggested that the interactions at the cement lines between secondary osteons affects the stress response by allowing the initial formation of cracks, but preventing crack growth [57]. As osteonal bone is frequently present in bones and sections of bones sustaining a heavy load, offering good fatigue and impact resistance [57]. Study by Abdel-Wahab *et al* . [67] concurs and contends that cement lines influence the distribution of maximum stresses within a bone and prevent micro-scale fracture. Haversian systems have been found to be extremely vulnerable to micro-

[2]It is very difficult, if not impossible, to obtain natural specimens of lamellar bone in different orientations. There is however a way around this, like using bone from an animal that has been treated with a drug that reduces or eliminates remodelling, so that macroscopic volumes of parallel arrays of lamellae are available.

damage in compression, where cracks can both start and spread inside the system [68]. Moreover, variations in the different Haversian systems themselves, such as the degree of mineralization and size, affect how sensitive to breaking Haversian bone is [68]. Haversian bone has been observed to be less rigid and weaker than fibrolamellar bone [27, 23, 46].

In their study of the failure of human cortical bone under compression, Ebacher *et al*. [69] observed that longitudinal specimens showed the development of cracks that were oblique to the osteonal direction and occasionally even had a step-like appearance. Many uncracked fibril bundles remained connected across the crack as it mostly followed the circumference of the circular lamellae surrounding the osteons. The crack was found to consist of many small micro-cracks, as well as displaying evidence of some small crack interaction with present canaliculi - which are defined as tiny canals between natural bone cavities, although cracks were much more sensitive to the Haversian canals themselves and to osteocyte lacunae - which are defined as small cavities in the bone [69].

The consensus in literature seems to be that lamellar bone with primary osteons show larger elastic moduli and higher final strengths than Haversian bone [31].

2.4 Species specific responses

Human and bovine bones have been the subjects of the majority of studies on the mechanical properties of cortical bone [1], with little information on other species. Studies involving multiple species are uncommon [45, 46] and often include information gathered from numerous independent test series. Rarely do multiple species appear in a single test series, making it challenging to distinguish between changes in a species' natural traits and those brought on by various storage or testing techniques.

A study reported by Rampersadh *et al*. [70] investigated cortical bone samples from the femurs of four different animal species: baboons, crocodiles, sheep, and ostriches. In this study, a single researcher followed consistent testing techniques to test specimens in the quasi-static and upper intermediate strain rate regimes. The findings demonstrated that all species had a similar strain rate dependency, i.e., the modulus exhibits insignificant rate effects in the quasi-static zone but significantly increases at intermediate strain rates. This implies that the stiffness of the bone

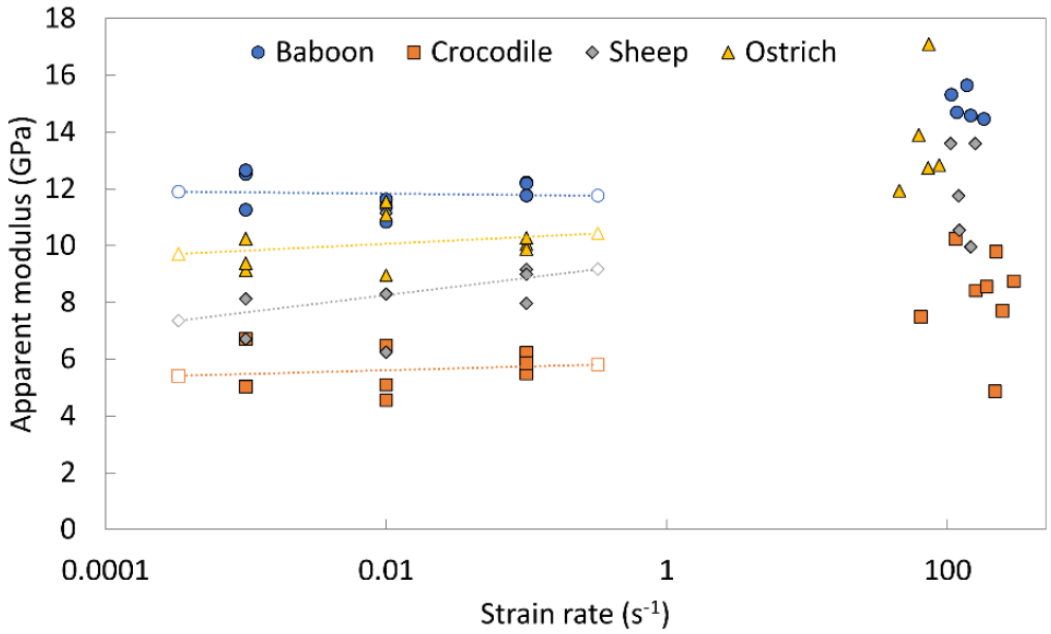

Figure 2.5 Comparison of apparent moduli for all species across all strain rates tested from Rampersadh *et al*. [70].

is species-dependent although strain rate may have a species-independent impact on bone stiffness [70].

Figure 2.5 displays the apparent modulus findings from quasi-static and intermediate strain rate compression testing for all species [70]. According to the results, baboon bone exhibits the stiffest behaviour among the examined species with the highest apparent modulus, followed by ostrich bone, sheep bone, and finally crocodile bone which displays the lowest apparent modulus. The range of values recorded for a single species over the quasi-static strain rate regime did not change significantly. However, while transitioning from the quasi-static to the intermediate strain rate regime, a clear and noticeable rise in moduli was seen across all species, displaying absolute changes in the range of 2.6-4.0 GPa. The bones from crocodiles, sheep, and ostriches had the most scatter in the results of the intermediate strain rate. This may be explained by the fact that, because to the more aggressive character of the test, higher strain rate testing is likely to bring to light any faults in the material or imperfections in specimen fabrication [70].

The following section presents a comparison of the results from more literature that was found for different species that might also be of interest namely cow, crocodile, sheep, baboon, pig and ostrich.

2.4.1 Bovine (Cow)

Adharapurapu *et al*. [49] investigated the bending strength of bovine cortical bone using a split Hopkinson pressure bar in a three-point bending configuration at various strain rates (low, intermediate, and high). The bending strength of wet and dry bone were measured and compared in both the longitudinal and transverse directions. Overall, the fracture strength of cortical bone was found to be lower in the transverse direction than in the longitudinal direction. Dry bone fractured at higher stresses but lower strain rates than wet bone. The phenomenon of very low fracture toughness of bone at high loading rates was also observed.

Cloete *et al*. [71] reported strain-rate sensitive behaviour of bovine cortical bone comparable to Adharapurapu *et al*. [49], demonstrating consistency of results regarding the dynamic and fracture strength of bovine cortical bone. In this study [71], the importance of testing bone at near constant strain rates to avoid discrepancies in experimental results, was emphasized.

To achieve constant strain rates, Adharapurapu *et al*. [49] and Cloete *et al*. [71] used different pulse-shaping techniques which will be discussed in Section2.9. Cloete *et al*. [71] reported that the expected apparent moduli of bovine cortical bone when tested at ISRs should be in the order of 10 GPa.

2.4.2 Crocodili (Crocodile)

Currey researched the bones of alligators and crocodiles [46, 45]. They reported apparent moduli in the vicinity of 6-8.5 GPa in the crocodile investigation [46] but provided no information on the testing procedure or the location of the sample collection. For specimens obtained from the femur, an apparent modulus of 13.0 GPa at a strain rate of 0.2 $s^{-1}$was found in the alligator investigation [45]. The quasi-static values from Rampersadh *et al*. [70] (4.56–6.71 GPa) fall below and on the lower end of the Currey crocodile range [46], but the intermediate re-

sults from Rampersadh *et al*. [70] (4.87–10.2 GPa) fall, for the most part, on the top end [46].

Zapata *et al*. [72] subjected alligator crania to an ultrasonic test in a 2010 study, and found that the apparent modulus varied from 8.8 GPa in the least stiff direction to 10.7 GPa in the most stiff direction to 0.5 GPa in all three directions.

2.4.3 Ovine (Sheep)

The typical ultimate tensile strength of healthy, normal cortical bone is 250 MPa, according to constant strain rate studies on sheep femora by Moreno & Forriol [73]. They conducted three-point loading test to determine the ultimate tensile strength of bone strips.

Spatz *et al*. [27] reported apparent moduli for sheep bone as 26-31.5 GPa. Long bone specimens were used in the Spatz [27] investigation, which examined them under quasi-static strain conditions (and an unknown strain rate). The apparent moduli observed in the investigation by Rampersadh *et al*. [70] were all much lower than values published by Spatz *et al*. [27] for both quasi-static (4.74-11.2 GPa) and intermediate strain rates (9.95-13.6 GPa). The Spatz values appear to be rather high, nevertheless, given that apparent moduli for human and bovine bone typically vary from 5 to 25 GPa [1].

2.4.4 Papio (Baboon)

Wang *et al*. [74] investigated baboon bone using ultrasonic testing at 5 locations in the skull. They studied the modulus in three different orientations and found that the stiffest orientation had a modulus of 17.2 GPa, while the modulus of the least stiff orientation ranged from 9.2 GPa to 12.2 GPa. In comparison, the quasi-static data captured by Rampersadh *et al*. [70] (10.8-12.7 GPa) falls mostly within the lower range reported by Wang *et al*., whereas the intermediate strain data (14.5-15.7 GPa) falls within the mid-range reported by Wang *et al*. [74].

Similar research was conducted on macaque mandibles by Dechow & Hylander [75], who measured apparent moduli ranging from 9 GPa in the direction with the least stiffness to 23.9 GPa in the direction with the highest stiffness. This

suggests that the baboon bone and bones from other members of the same family may share at least some similarities.

2.4.5 Porcine (Pig)

Parish *et al*. [76] used a split Hopkinson tension bar to investigate the high strain-rate behaviour of pig bone under tensile loading at nominal strain rates ranging from 300 $s^{-1}$to 1000 s^{-1}. The axial ultimate tensile strength (UTS) of pig bone increased from 50 MPa to 220 MPa with increasing strain rates within the dynamic testing range, according to the experimental results. It was also observed that when the gage section is dehydrated, the ultimate strength in the pig bones decreases significantly [76].

Fresh porcine ribs were subjected to dynamic 3-point bending tests in a study conducted by Ayagara *et al*. [77]. In this study, both fractured and non-fractured bone was tested, and the static fracture strain value for cortical bone was 2 x 10^{-2} m/m. The force response of bone in the absence of fracture showed three distinct phases. Phase A: During this brief period (up to 300 x 10^{-6} s), the input force increases dramatically while the output force remains constant. The sample is not in a state of equilibrium. Phase B: The rib is subjected to forces applied by the two output bars (between 300 x 10^{-6} s and 700 x 10^{-6} s). The input force and the resultant output force are nearly equal, indicating small oscillations. Phase C: After 700 x 10^{-6} s, a dynamic equilibrium is established between the input force and the resultant output force, and the oscillations disappear. Because no fracture occurred, there was no sudden decrease (similar to a discontinuity) in the contact force signals. The force response of bone with fracture revealed that, similar to tests without fracture, a sudden increase in input force is observed during the dynamic equilibrium phase, followed by a plateau phase. In this case, a dynamic equilibrium is reached at 600 x 10^{-6} s. The authors [77] concluded that the key feature of this type of response is that crack propagation and fracture occur during the equilibrium phase. The rib fracture corresponds to the rapid drop in force signals. During the non-equilibrium phase, the results revealed fracture characteristics. There is no time for the sample to find an equilibrium between the input force and the resultant output force. Rib fracture occurs around 500 x 10^{-6} s before equilibrium is established.

It is important to note that the findings of these studies are influenced by a variety of factors, including the age, sex, and anatomical location of the bone specimens, as well as the testing methods and conditions.

2.4.6 Struthio (Ostrich)

Reed & Brown [78] performed four-point bending tests on emu bone, at three strain rates, namely 1.67 x 10^{-4} s^{-1}, 3.3 x 10^{-4} $s^{-1}$and 5 x 10^{-4} s^{-1}. They measured the apparent modulus at each of these rates and found them to be 13.05 GPa, 14.14 GPa and 15.86 GPa respectively. They also measured the yield and ultimate strengths at 5 x 10^{-4} $s^{-1}$and found them to be 126.54 MPa and 154.6 MPa respectively. This apparent modulus data is comparable to apparent modulus data on ostrich bone in tension, reported by Yamada [79]. Yamada reported values for cortical ostrich bone in both compression and tension. In compression, the ultimate strength was reported as 117.72 MPa, and the apparent modulus as 5.297 GPa. In tension, the ultimate strength was reported as 69.65 MPa, and the apparent modulus as 13.64 GPa.

Cuff *et al*. [80] generated other values for the elastic modulus of cortical ostrich bone, using nano-indentation (5.03 GPa) and by generating post-hoc values within their model (10 GPa and 7 GPa). This is a wide range of possible moduli. Cuff *et al*. [80] also noted that their tests were performed on specimens from the inner region of the bone, which may have differing properties than tough outer surfaces.

Spatz *et al*. [27] found that cortical ostrich bone (mostly radial specimens tested at a quasi-static strain rate) showed a range of Young's moduli from 17 GPa to 22.3 GPa, the highest out of all literature. The study reported by Rampersadh *et al*. [70], however, found that cortical ostrich bone showed a range of Young's moduli from 8.96 GPa to 11.6 GPa for quasi-static tests and 11.9 GPa to 17.1 GPa for intermediate strain rate tests.

Casinos and Cubo [81] performed tests on whole avian bones, and while these results are not specifically relevant to the properties of ostrich cortical bone, they did find that ultimate compressive strength and apparent modulus tended to decrease with decreased body mass.

Table 2.1 *Mechanical Properties of Cortical Bone in Different Species*

Source	Species	Apparent Modulus (GPa)	Ultimate Strength (MPa)	Bone Source	Type of Testing & Strain Rates Tested At
Rampersadh *et al*. [70]	Baboon	10.8 - 12.7 14.5 - 15.7	N/A	Femora	Quasi-Static Intermediate
Rampersadh *et al*.[70]	Ostrich	8.96 - 11.6 11.9 - 17.1	N/A	Femora	Quasi-Static Intermediate
Rampersadh *et al*. [70]	Sheep	4.74 - 11.2 9.95 - 13.6	N/A	Femora	Quasi-Static Intermediate
Rampersadh *et al*. [70]	Crocodile	4.56 - 6.71 4.87 – 10.2	N/A	Femora	Quasi-Static Intermediate
Adharapurapu *et al*. [49]	Bovine	N/A	N/A	Femora	Bending Strength Test at Various SR
Cloete *et al*. [71]	Bovine	approximately 10	N/A	Femora	N/A
Currey [45, 46]	Crocodile	6.0 - 8.5	N/A	Femora	N/A
Zapata *et al*. [72]	Crocodile	0.5 - 10.7	N/A	Crania	Ultrasonic Test
Moreno & Forriol [73]	Sheep	N/A	250	Femora	Three-Point Loading Test
Spatz *et al*. [27]	Sheep	26 - 31.5	N/A	Long Bones	Quasi-Static
Wang *et al*. [74]	Baboon	9.2 - 17.2	N/A	Skull	Ultrasonic Testing
Dechow & Hylander [75]	Baboon	9.0 - 23.9	N/A	Mandibles	N/A
Parish *et al*. [76]	Pig	N/A	50 - 220	Femora	Tensile Testing at High Strain Rates 300 s^{-1} to 1000 s^{-1}
Ayagara *et al*. [77]	Pig	N/A	N/A	Ribs	Dynamic 3-Point Bending Test
Reed & Brown [78]	Ostrich	13.05 - 15.86	126.54 - 154.6	N/A	Four-Point Bending Test 1.67 x 10^{-4} s^{-1}, 3.3 x 10^{-4} s^{-1}, 5 x 10^{-4} s^{-1}
Yamada [79]	Ostrich	5.297	69.65	N/A	N/A
Cuff *et al*. [80]	Ostrich	5.03 - 10	N/A	N/A	Nanoindentation
Casinos & Cubo [81]	Ostrich	N/A	N/A	Whole Avian Bones	N/A

2.5 Strain rate dependence

The effect of strain rate on material properties is an important aspect of bone response under impact conditions. Bone is a complex material that has been found to be highly strain rate dependent [67, 22, 48, 49, 21, 82].

As strain rate increases, the behaviour of the bone changes from ductile to brittle [21]. It is important to note that bone can never be ductile despite how frequently the term is used in literature. The term "ductile" merely refers to a period of incipient failure, followed by a decreasing load-bearing capacity, as opposed to short, sharp failure (i.e., "brittle" failure).

According to Sanborn *et al*. [53], longitudinal and transverse specimens both exhibit significant strain rate dependence under compression, with larger values for both compressive failure strength and Young's modulus appearing at higher strain

rates. The approximate strain rates used in their testing were 10^{-3} s^{-1}; 1 $s^{-1}$and 10^{3} s^{-1}.

A study by Abdel-Wahab *et al* . [67] demonstrated that when strain rate increased from 10^{-5} $s^{-1}$to 10^{-3} s^{-1}(also known as the creep range), both fracture stress and elastic modulus increased in bovine cortical bone. Also, they observed that the fracture stress rises significantly more (by 60%) when the strain rate is changed from 10^{-5} $s^{-1}$to 10^{-3} s^{-1}than when it is changed from 10^{-3} $s^{-1}$to 1 s^{-1}(only rising by 11%) [67]. Contrary to the findings of the other reviewed studies, they came to the conclusion that the elastic modulus did not change considerably when measured at strain rates of more than 1 s^{-1}. Nevertheless, they didn't do any actual research at strain rates greater than 1 s^{-1}, they only used extrapolation from the data they produced to draw their conclusions.

Evans *et al* . [83] found, in contrast to prior investigations, that the ultimate tensile strength of equine bone increased and subsequently dropped with increasing strain rate (across a range of 10^{-4} $s^{-1}$to 1 s^{-1}). Unfortunately, there was a large amount of scatter and a tiny sample size. Their conclusions on the relationship between strain rate and Young's modulus are in line with those of earlier studies, specifically that Young's modulus rises as strain rate does. They also found evidence demonstrating that stress transitions from pseudo ductile (exhibiting shearing type failure with a wider "ductile" response zone) to brittle (shorter, sharper failure) at some terminal strain rate, typically in the range of 10^{-1} $s^{-1}$to 10 s^{-1}. This is consistent with the findings of McElhaney & Byars [84], who found that bone showed shearing-type failure up to strain rates of 1 s^{-1}. Bone specimens showed splintering failure, when numerous tiny bone fragments developed, over 1 s^{-1}. According to research by Currey [45] and Paul [85], bone yields at a given strain rather than a certain stress, with a lower yield strain in bone that has a greater Young's modulus.

For both fresh bovine and embalmed human bone, research by McElhaney & Byars [84] demonstrated a clear strain rate dependence of apparent modulus and compressive strength.

Human cancellous bone exhibits a rise in ultimate strength with increasing strain rate, according to a study reported by Carter & Hayes [82], which examined the bone under compression in the strain rate range of 10^{-4} $s^{-1}$to 10 s^{-1}. Strain

rate and yield strength as well as strain rate and ultimate strength showed a strong positive association in tensile experiments on bovine cortical bone [22, 48, 21]. Similar to Crowninshield & Pope [48], who tested at strain rates between 10^{-3} $s^{-1}$and 200 s^{-1}, Wright & Hayes [21] explored in the range of 5.3 x 10^{-4} $s^{-1}$to 237 s^{-1}. Furthermore, prior studies indicated a strong positive association between apparent modulus and strain rate [22, 21]. The correlations shown in Currey's [22] work are also valid, but it is important to note that the strain rates used in his experiments were not constant, so any values for mechanical properties may not be completely accurate as bone is highly strain rate dependent in certain regions. The higher strain rate tests conducted by Crowninshield & Pope [48] were not done at a constant strain rate, which had the same problem. In lower strain rates, testing is often done using a displacement controlled servo-hydraulic machine, which provides a constant strain rate, despite this not being focused on before testing.

No prior studies could be found that concentrated on delivering a near constant strain rate, particularly in higher strain rate experiments, until a study done by Adharapurapu *et al*. [49]. Using cortical bovine bone, they used servo-hydraulic testers to conduct quasi-static compression experiments covering strain rate ranges of 10^{-3} $s^{-1}$to 1 s^{-1}. They also used a modified Split Hopkinson bar (SHB) to conduct high strain rate experiments at 10^{-3} s^{-1}. This appears to be the first attempt at such strain rate control, and the experiments were conducted on both longitudinal and transverse specimens, at a near constant strain rate. These tests on bovine bone further show that cortical bone is indeed strain rate sensitive, with an increase in strain rate leading to a proportional increase in stiffness and strength. The observed decrease in failure strain serves as an illustration of how brittle behaviour worsens as strain rate rises.

Equine cortical bone was the subject of a study by Kulin *et al*. [86] that covered a range of strain rates. They used a pulse shaper, which consisted of a small piece of malleable material between the striker and incidence bar, in an effort to account for strain rate, but it was insufficient. An apparent modulus change could be seen in the specimens' stress vs strain graph. However, they believed that their strain rate was stable enough to make inferences about the yield strength as measured in compression. They observed that compressive yield strength improves with an increase in strain rate, which is consistent with prior studies.

A model of the behaviour of bone was developed by Johnson *et al*. [1], who focused on cortical bone. They performed a highly valuable comparison of available data across a range of strain rates, as seen in Figure 2.6. As a result, it is clear that there is a large amount of scatter in bone characteristics, 5 to 20 GPa in the quasi-static domain to be precise. However, even after accounting for that scatter, a rate effect is still evident.

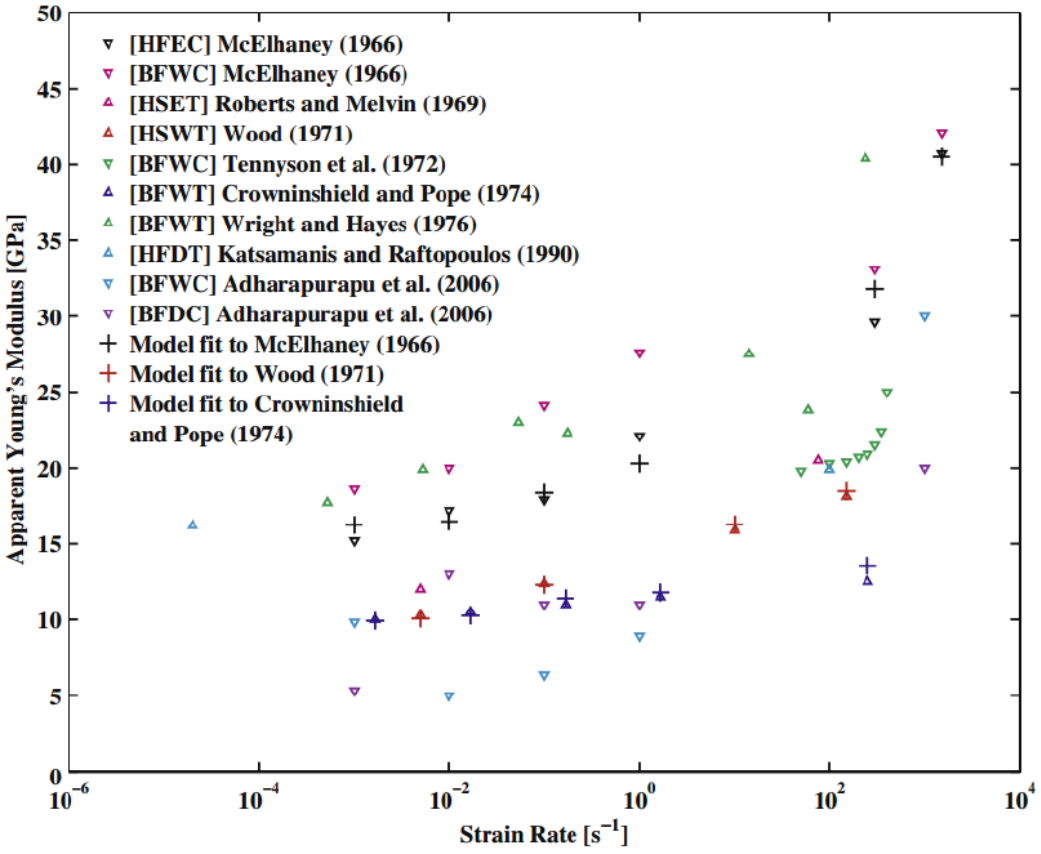

Figure 2.6 A comparison of cortical bone data from various investigations over a variety of strain rates from Johnson *et al*. [1]. The letters that come before each source denote the following testing conditions: H – human bone, B - bovine bone, F - femur, S - skull, E - embalmed, W - hydrated, D - dehydrated, C - compression, T - tension.

Cloete and co-workers [87, 85, 71] demonstrated that a conical striker may deliver a near-constant strain rate in bovine bone specimens evaluated at dynamic rates. It was reported that bovine bone has higher stiffness in the dynamic strain rate regime than in the quasi-static, and that fracture stress increases with strain rate [87]. They further expanded on this by developing the Cone-in-Tube (CiT) striker and conducted more testing of bovine bone, including data in the intermediate strain rate range [85, 71]. The data showed that the compressive strength of longitudinal bone is strain rate dependent and revealed a distinct transition zone between quasi-static and dynamic zones, where the majority of the rise took place. This shift happened in the intermediate range, between 1 $s^{-1}$and 10 s^{-1}.

Welgemoed [36] conducted a multi-species study of the properties of cortical bone over a range of strain rates. To carry out the testing, two changes to a standard SHB set-up were investigated: using a tandem momentum trap and a CiT striker. The design of the CiT striker was inspired by the work of Cloete *et al*. [71] and Paul [85]. The strain rate dependence in the link between material properties and strain rate in this study was readily apparent [36]. There were only slight variations in the apparent modulus within the quasi-static range (10^{-1} s^{-1}, 10^{-2} $s^{-1}$and 10^{-3} s^{-1}) but when switching from the quasi-static to high intermediate strain rate regimes (between 40 $s^{-1}$and 200 s^{-1}), there was a clear, noticeable rise. All of the tested species showed this. When compressive strengths were taken into account, it was possible to observe a slight, steady rise in strength with a rise in strain rate in the quasi-static regime. At the high intermediate range, no increase was observed, in fact, a slight decrease was observed in some cases. At these higher strain rates, larger apparent moduli were observed, suggesting that the strain at failure reduced as strain rate increased. Thus, the aggressive testing techniques used for the greater strain rate testing may be to blame for these very low strength findings [36]. Both the maximum compressive strength and the 0.2% offset yield strength showed this association across all examined species.

2.6 Specimen Geometry

Biomechanical numerical models require precise modulus values of bone. To obtain these values in sufficient quantities for statistical significance, it is essential to extract as many specimens as possible from a single donor bone to reduce the chance of different donor bones having different material properties [45], even

when bones are retrieved from the same donor animal, necessitating the use of small specimens. Additionally, machining numerous large specimens for bending tests is challenging, and testing bone in tension is particularly difficult due to its quasi-brittle nature. Consequently, compression testing with small specimens is preferred.

Furthermore, due to the material properties of bone not being consistent in all regions of a particular donor bone [88, 89], the testing of large or whole bone samples cannot offer definitive material characteristics reiterating the need to test small specimens, where the macroscopic material properties can be considered near constant throughout the test specimen. Therefore, a priority must be placed on being able to conduct a large number of tests on small specimens within in a short time period. The short time period is necessitated by bone being a biological material that is susceptible to drying out when removed from the donor, such that the mechanical properties would not be representative of in-vivo bone [90].

There are no standards for compression testing of bone specimens. The most applicable standard to use in this case, based on tests for materials with similar material properties, would be the standards used for rigid plastics. For example, the ASTM D695 [91] or ISO D604 [92] standards. However, these standards require that specimens intended to determine elastic modulus have a height of 50.8 mm and a diameter of 12.7 mm; a height-to-diameter ratio of 4:1 [91]. Obtaining specimens that adhere to this ratio with a reasonable diameter from a donor bone, is exceedingly difficult as a result of the typically narrow thickness and inconsistent cross-sectional shape of cortical bone regions. Additionally, if one donor bone is to be used to produce all specimens, obtaining a large, statistically significant number of specimens, as outlined in the standards mentioned above, becomes impractical. As a result of these factors, it is not uncommon to find small specimens with geometries closer to a 1:1 ratio in the literature. Van Haaren *et al*. [2], McElhaney [93] and Rampersadh *et al*. [70] tested cortical bone specimens with a maximum aspect ratio of 2:1 and with dimensions in the order of a few millimetres. Daras *et al*. [94] conducted both QS and dynamic tests to demonstrate the strain rate sensitivity of cortical bone. A requirement for these dynamics tests to be valid is that the specimens are in a stress equilibrium i.e. a 1:1 height-to-diameter ratio, and using such tall specimens would make achieving this stress state very difficult.

2.7 Specimen Storage

The storage solution in which specimens are maintained after machining has an effect on the measured mechanical properties [95, 96]. Stefan *et al*. [95] observed that cortical specimens preserved in alcohol-glycerine solution had a significantly enhanced Young's modulus and lower plastic energy absorption. This is assumed to be related to water loss within the bone when soaking in alcohol, which can be corrected by rehydrating with normal saline [95, 96]. This demonstrates the need of keeping the bone specimens adequately hydrated before testing. Properly hydrated specimens, which mirror the normal state of bone, exhibit visco-plastic behaviour, whereas alcohol-stored specimens exhibit more brittle behaviour [96]. This appears to be consistent across the evaluated literature.

Van Haaren *et al*. [2] observed that when bone is preserved in formalin (a buffered formaldehyde solution) the mechanical characteristics of bone remained unaffected, even after a year. In contrast, Stefan *et al*. [95] observed that after 6 months of formalin storage, there was a considerable decrease in energy absorption and ultimate strain in human cortical bone. This is consistent with the findings of Goh *et al*. [97], who found that complete bones preserved in formalin for only three weeks exhibited a considerable difference in energy absorption capabilities, causing the bone to behave in a more brittle fashion than fresh bone. They also observed that there was no substantial change in stiffness or maximum loading capacity [97]. Finally, Ohman *et al*. [4] found that specimens held in formalin solution for eight weeks showed a considerable change in Young's modulus, yield strain, and ultimate strain.

Kaye *et al*. [98] found that freezing a "dead bone" specimen, i.e. bone that is no longer within a living body, with diminished enzyme and cellular activity, has no effect on mechanical qualities as long as the freezing temperature is above -70°C [98] and this remains true for up to a year, according to findings by Van Haaren *et al*. [2].

Moreno & Forriol [73], observed that frozen specimens had higher bending strength than fresh bone. It should be emphasized, however, that it is unclear whether or not the frozen specimens were thawed before testing. They also found that frozen specimens had more phosphorus than fresh ones, which they attributed to the continuous enzyme activity that can occur at a freezing temperature of -20°C.

Welgemoed [36] observed ageing effects due to long-term storage in a study that involved the testing of femurs from four different species. Two series of specimens were machined from these bones. In the first series, the mid-diaphysis of each bone was cut and machined after gradual defrosting. These specimens were stored in saline solution and frozen at -31°C until needed. A second series of specimens was machined later to assess degradation due to longer storage times. Both series underwent the same testing methods. Results showed ageing effects with a decrease in the apparent modulus between the first and second series. Compressive strength, however, showed less variation between series [36].

Daras *et al*. [41] investigated the effects of three storage protocols on the degradation of the mechanical properties of bovine cortical bone during long-term storage. Four whole humeri were extracted from two mature bovine cattle, and the bone was machined into specimens. Following preparation, all specimens were stored in saline solution, with a small number kept refrigerated at 4°C, while the majority (including some whole-bones) were stored in a biological freezer at -32°C. The study considered three storage protocols: machined-refrigerated (MR), machined-frozen (MF), and frozen-machined-frozen (FMF). In the MR protocol, specimens were machined from fresh bone and stored refrigerated, never being frozen. The MF protocol involved machining fresh bone specimens and storing them at -32°C. In the FMF protocol, whole-bones were frozen immediately in saline, and after a set period, thawed, machined into specimens, and then refrozen. One FMF donor bone was frozen for two months, while the other was frozen for 11 months before machining. The study found that refrigerated specimens that were never frozen exhibited inconsistent results after just one day, recommending that such specimens should be tested within 24 hours of harvest. Specimens machined from fresh or previously frozen bone must be tested within a week post-machining for results to reliably reflect in-vivo mechanical properties. Freezing whole bones prior to machining extends the viable testing period by several months, but cortical bone specimens stored for more than six months exhibit significant degradation, regardless of the protocol used. The authors [41] also noted that, due to the non-linear degradation process, a simple rate of daily loss is not adequate for correction, and a 'half-life' model better characterises this behaviour.

Lee & Jasiuk [5] investigated the impact of freeze-thaw cycles on the structure and mechanical properties of trabecular porcine bone. To conduct their experi-

ment, femurs were harvested and divided into three groups: fresh bone (group A), bone stored in the freezer at -20°C for one year (group B), and five years (group C). Prior to freezing, the bones were wrapped in gauze soaked with Phosphate Buffered Saline (PBS)[3] and sealed in zip lock bags to prevent drying. The bones were allowed to fully thaw before machining. The machined specimens were stored in PBS at 4°C, and all tests were completed within 48 hours of thawing. The bone frozen for five years exhibited lower Young's modulus and ultimate strength compared to fresh bone. Another notable difference between the groups was the extent to which mechanical properties correlate with parameters such as porosity and apparent density [5]. The fresh bone aligned closely with the previously reported trend that porosity strongly influences Young's modulus and ultimate stress. In contrast, the long-term frozen bone exhibited a weaker correlation, particularly for Young's modulus. The findings suggest that long-term freezing not only weakens bone but also hampers the predictability of the mechanical properties of bone. Possible reasons for this effect include the formation and enlargement of ice crystals, which cause structural damage, as well as the continued activity of cellular enzymes at -20°C [5]. It should be noted, however that it is not recommended to freeze PBS. During freezing, phosphoric acid is formed and could negatively affect the protein stability in biological specimens [99, 100, 101]. Thus, when the intention is to freeze specimens for long-term storage, it is advised against using a phosphate buffer but to rather use a saline (0.9% NaCl) instead.

2.8 Testing Conditions

The conditions under which bone specimens are tested have an impact on the material qualities measured.

The temperature of the specimen being tested has been found to affect the material properties of bone [102]. The final compressive strength of cortical bone is relatively stable at temperatures above 27°C and increases as temperature falls below 27°C [102]. Sedlin & Hirsch [3] evaluated mechanical characteristics of human femoral cortical bone at 21°C and 37°C temperatures. In keeping with prior studies, they observed that the maximum stress and apparent modulus remain

[3]PBS (phosphate buffered saline) is a pH-adjusted blend of ultra-pure grade phosphate buffers and saline solutions which, when diluted to a 1X working concentration, contains 137 mM NaCl, 2.7 mM KCl, 8 mM Na2HPO4, and 2 mM KH2PO4.

rather constant in this temperature range. However, they observed a considerable increase in deflection to failure at higher temperatures. Smith & Walmsley [103] found that in a temperature range of 5°C to 43°C, the deflection under a specific load increases as temperature increases. However, they found that as temperature rises in this region, Young's modulus drops.

Dry bone has been found to be more brittle than wet bone, with higher failure stresses and lower total strains [49], as well as a higher elastic modulus and hardness [55]. Nyman *et al*. [90] argued that this makes sense, as the collagen component of bone, which affects toughness and elasticity, would be more affected by changes in the water content of bone than the mineral component. The collagen component will be most compliant and tough when properly hydrated. When dry, the bone material becomes substantially less flexible, resulting in higher failure stresses and lower strains [90].

There is evidence that the size of the specimen being examined may affect the measured attributes [51]. Allena *et al*. [51] observed that cylindrical specimens of bovine cortical bone with a small diameter (4 mm) had higher failure stresses than those with larger diameters (6, 8, and 10 mm). They hypothesized that this could be because of a lack of uniformity in the stress induced in their specimens, or because the smaller a specimen is, the more it corresponds with the micro-structure present. The smaller the specimen, the closer it is to the dimensions of any cement lines, or portions thereof, that may be present. However, Ebacher *et al*. [68] found that when bending complete tibia and cortical specimens (35 mm x 4 mm x 3 mm), they failed similarly in terms of both the macro-visible fracture pattern and how the micro-damage proceeded.

2.9 Equipment and Testing Methods

There is a large variety of testing equipment that can be used to test across different strain rate regimes. In this section the relevant equipment is discussed. The strain rate regimes of interest are the low or quasi-static strain rate regime (less than 1 s^{-1}); the intermediate strain rate regime (1 $s^{-1}$to 100 s^{-1})[4] and the high or dynamic strain rate regime (100 $s^{-1}$to 10 000 s^{-1}). To test across all these regimes,

[4]There is no agreement on what the intermediate strain rate regime is, but for the purposes of this review, it is between 1 $s^{-1}$and 100 s^{-1}.

three different devices are required: a conventional quasi-static testing machine, a wedge-bar (WB) apparatus and a conventional split Hopkinson pressure bar (SHPB) implemented with a cone-in-tube (CiT) striker and a tandem momentum trap.

These 3 regimes are of interest because, according to the literature [71], it is the crucial zones where the shift in response is thought to occur. As seen in Section 2.5, the intermediate and high strain rate regions typically have the fewest data points accessible, due to the difficulty of testing in these areas, and specialized equipment was thus needed. The research also required a near-constant strain rate, which also necessitated the use of specialized equipment (again, see Section 2.5 for more information). A description of this specialized equipment can be found in this section.

2.9.1 Universal Testing Machine

Quasi-static compression tests are used to determine a material's behaviour under applied crushing loads. Compressive testing is performed similar to tensile testing using a universal testing machine (UTM). The gripping jaws are replaced by anvils or platens (which are usually flat) and the cross-head moves toward the stationary grip as compared to pulling away, applying compressive pressure to a test specimen usually of either a cuboid or cylindrical geometry [104]. These compression tests are usually performed on large specimens and are not typically used to determine modulus per se but rather to assess the plastic behaviour of materials [105]. The most common measurement obtained from a compression test is the compressive strength.

During compression testing, there are various techniques for measuring strain, including machine cross-head displacement, strain extensometer, and strain gauges. Strain can be measured using the conventional platens testing method through the motion of the test machine cross-head. This technique operates on the assumption that the deformation of the specimen is equal to the displacement of the platens. This assumption introduces error when measuring the relatively small deformations of bone specimens, due to deflection of the entire load frame of the machine when under stress. This effect is related to the stiffness of the test machine apparatus and is known as "machine compliance" [6]. Therefore, studies utilizing this

method of strain measurement should correct for machine compliance to ensure that the strain measured represents the specimen alone.

A review paper by Zhao *et al*. [7] titled "Standardizing compression testing for measuring the stiffness of human bone" examined 4 712 abstracts, with 177 papers included in the final analysis. Among these, 20 studies directly analysed compression testing techniques to improve accuracy. The most common method for strain measurement was found to be through machine cross-head displacement. However, only 12 of these studies applied a machine compliance correction when using this method, none of which applied localized platen compliance correction and just one study [106] provided specific details on the compliance correction algorithm. Other studies utilized extensometers and electric resistance wire strain gauges for strain measurement.

Machine compliance may be determined directly by loading the system without a specimen or with a standard uniform material specimen such as steel with known properties. Anderson *et al*. [106] determined machine compliance using the no-specimen testing method. However, the challenge with this approach is that the UTM does not load and unload in exactly the same manner each time, leading to variations in the measured compliance with each test. Augat *et al*. [32] reported systematic measurement errors in their investigation because strain was measured across machine platens rather than the specimen itself, emphasising the influence of specimen interaction and the importance of including the specimen in compliance correction. According to Odgaard & Linde [107], strain is frequently greater around the specimen face edge than in the centre of cut specimens. This can result in an overestimation of the average strain across the specimen and a subsequent underestimation of modulus [108, 107, 109].

An important application of compression testing on small specimens, where machine compliance should be of critical importance, is the measuring of the modulus and stiffness of bone. Biomechanical numerical models require precise modulus values of bone. To obtain these values in sufficient quantities for statistical significance, it is essential to extract as many specimens as possible from a single donor bone to reduce the chance of different donor bones having different material properties [45], even when bones are retrieved from the same donor animal, necessitating the use of small specimens. Additionally, machining numerous large specimens for bending tests is challenging, and testing bone in tension is partic-

ularly difficult due to its quasi-brittle nature. Consequently, compression testing with small specimens is preferred.

Furthermore, due to the material properties of bone not being consistent in all regions of a particular donor bone [88, 89], the testing of large or whole bone samples cannot offer definitive material characteristics reiterating the need to test small specimens, where the macroscopic material properties can be considered near constant throughout the test specimen. Therefore, a priority must be placed on being able to conduct a large number of tests on small specimens within in a short time period. The short time period is necessitated by bone being a biological material that is susceptible to drying out when removed from the donor, such that the mechanical properties would not be representative of in-vivo bone [90] .

To test cortical bone in compression using standard testing apparatuses without the influence of machine compliance on the small specimen geometries, a custom sub-press as shown in Figure 2.7, was designed to operate within a universal testing machine (UTM) [94]. A Zwick 1484 UTM was used in conjunction with this custom sub-press for all quasi-static compression tests performed in this study. The sub-press was designed to eliminate the compliance of large testing machines that can introduce significant errors when assessing strain and strain rate in small, quasi-brittle materials. Daras *et al* . [94] demonstrated that the sub-press offers a simple, cost-effective, repeatable and routine means of measuring displacements in the order of a micron through the novel use of AMS AS5311 Hall Effect Sensors and Bogen MS10-300 Magnetic Multi-pole Strips, and outperforms the Zwick and Visual Extensometre (VE) testing methods in terms of accuracy and consistency, respectively. Its ability to conduct numerous tests rapidly reduces degradation effects on biological specimens, which is its primary advantage.

The sub-press consists of a base, a sleeve, a plunger and a pre-load nut, all of which, when assembled, fit into a UTM. A specimen is compressed between two platen surfaces formed by the bottom of the plunger (upper platen), which is completely flat and the top of the base (lower platen), which has a slight conical raise, creating a 10 mm diameter stage for specimen placement. All the components were manufactured from a mild steel. The pre-load nut interacts with the 10 kN load cell via a proprietary load transfer pin and threaded component supplied with the UTM. The plunger features four recessed slots along its length. The multi-pole magnetic strips, used to measure the displacement of the plunger, are secured into

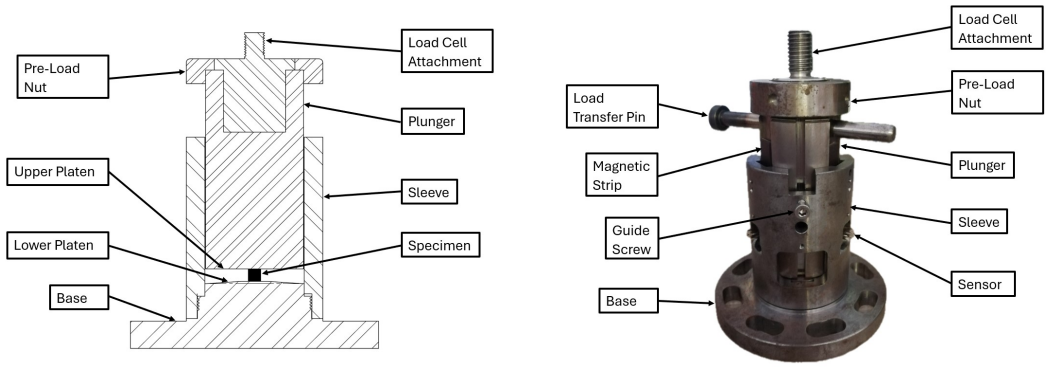

(a) **(b)**

Figure 2.7 The sub-press as designed by [94] with (a) A schematic and cross-section of the sub-press with a specimen in the testing location and (b) A side-on view of the assembled sub-press.

three of these slots, while the fourth engages with a guide screw, which prevents any rotational motion between the plunger and the sleeve.

2.9.2 Wedge-bar Apparatus

A wedge bar (WB) apparatus [71], shown in Figure 2.8, was designed to make testing in the intermediate strain rate regime possible.

The wedge-bar layout consists of a load frame assembly and three 20 mm diameter steel bars. The striker, wedge bar, and stopper bars are all essentially identical except for a shallow wedge that has been machined into the wedge bar. The load frame assembly, which comprises of a load frame, backing plate, load cell, and sliding anvil with a lower surface machined to match the wedge, can accommodate the movement of the wedge bar. Although the wedge bars' lengths and ratios range from 1500 mm and 500 mm for 1 $s^{-1}$to 500 mm and 200 mm for 10 s^{-1}, the greatest anvil displacement in each case is just 1 mm, which is enough to fracture the specimen. Further details of the wedge-bar technique are given by Cloete *et al*. [71].

During testing, a gas gun is used to discharge the striker, which impacts the wedge-bar and quickly reaches the desired test velocity before coming to rest. A small cylindrical specimen is compressed against the load cell by the sliding anvil

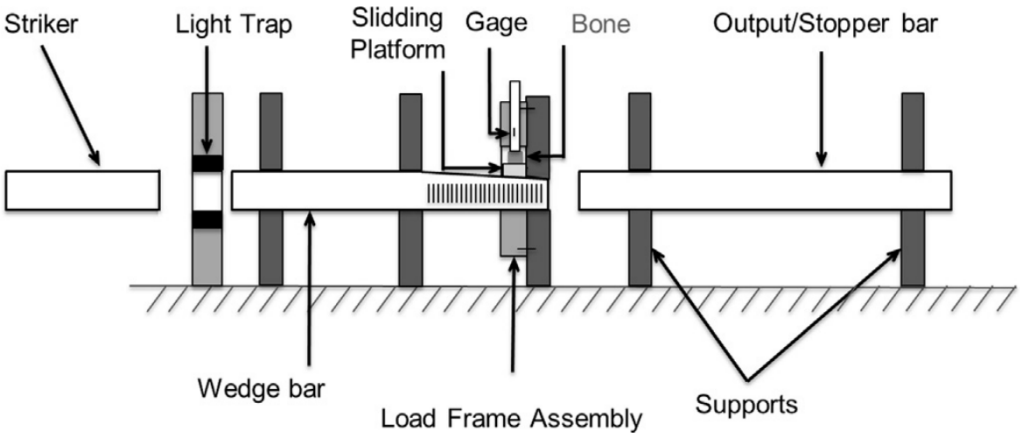

Figure 2.8 Wedge-bar apparatus system [71].

due to the wedge-bar action, which is recorded by a reflective object sensor and records the load history. The wedge bar motion, which is stopped by impact with the precisely placed stopper bar to allow specimen recovery at a well-defined final strain (between 5% and 10%, i.e., after the elastic range but before densification of the fractured trabeculae), indicates the specimen deformation. The ISR regime is appropriate for the wedge-bar. Without any fluid components or polymers and a short load path, the compact load frame assembly quickly reaches equilibrium.

Because the wedge-bar kinetic energy is much more than what is necessary to deform the specimen, the shallow wedge angle creates strong forces with a significant speed reduction. This ensures a near-constant deformation rate.

2.9.3 Cone-in-Tube Striker

A traditional SHB set-up is insufficient for high intermediate strain rate testing at a near-constant strain rate because of the complicated way that bone reacts to stress [36]. In a typical SHB, the specimen is positioned between two bars (the incident and transmitter bars). An incident wave would be created by firing a standard uniform striker (often by means of a gas gun) at the incident bar, travelling down the bar and into the specimen. A portion of this wave would be reflected back into the incident bar and a portion would be transmitted into the transmitter bar. Strain gauges mounted on each bar would be used to record these

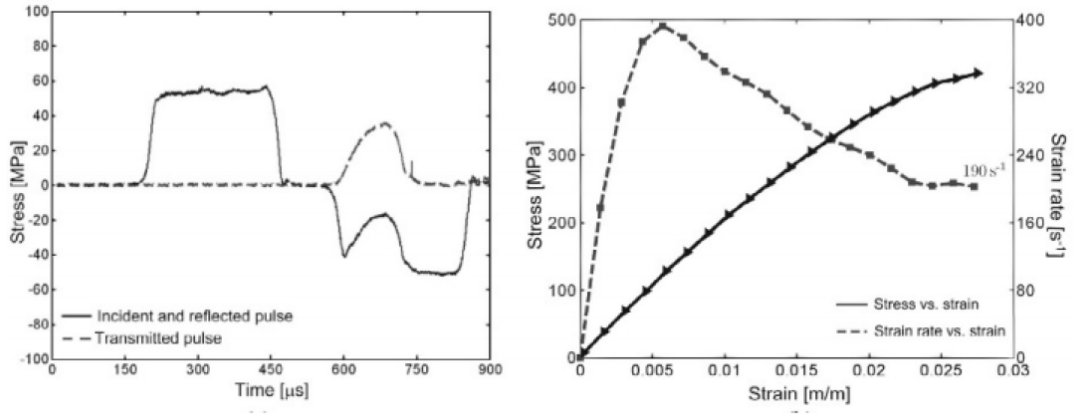

Figure 2.9 The square-shaped pulse from a standard uniform striker (shown on the left), and the decreasing strain rate seen over a test (shown on the right) from Cloete *et al*. [110].

waves. The results might then be translated into stress, strain, and strain rate in the specimen using stress wave theory [36].

A typical square-shaped wave would result from this as shown in Figure 2.9. This would result in a decreased strain rate throughout the test when applied to a material that hardens under strain. The pulse would need to be shaped in order to combat this [86]. As was done by Kulin *et al*. [86], a deformable material sandwiched between the striker and the incidence bar would be the most published way of pulse shaping. The rise time of the incident pulse was decreased, and any higher frequencies that were present were damped. As was found in the research by Kulin *et al*. [86], this method did not provide a sufficiently stable strain rate to assess apparent modulus at dynamic rates.

The pulse has to rise at roughly the same slope as the apparent modulus of the strain-hardening material being tested in order to determine the apparent modulus accurately. According to research by Cloete *et al*. [110, 71], a conical striker has been shown to be capable of producing this shape. Contrary to the uniform strikers that are typically used in SHB testing, the use of a conical striker enables control of the shape of the produced pulse, leading to a more stable strain rate [71]. Instead of the longer, more square wave seen in traditional testing, it produced a wave

with an increasing slope throughout the course of the test as shown in Figure 2.10.

Unfortunately, the conical shape also produces a 'tail' on the induced stress wave, which has a detrimental effect on the maximum achievable test duration. Additionally, it limits the strain rates that may be achieved by preventing the lower range of 40 s^{-1}that is desired [71]. The CiT striker was developed as a result of this. The CiT striker combines the shaped pulse attainable with a conical striker with a rapidly removed load. The tube, in which the cone is nested, would strike up against a large reaction mass simultaneously with the cone impacting the incident bar as shown in Figure 2.11. This would cause a stress wave to be generated in both the tube and cone, which travel at the same time back towards the large end of the cone. At best, this would reverse the direction of the CiT, and at worst, simply cause an immediate stoppage of load, which removes the stress 'tail' and enables a minimized strain rate and maximized test duration [71].

For impedance to be attached properly, the cone and tube should ideally be made of the same material and have the same cross-sectional area as the cone's large end [71]. A gas cannon barrel could be mounted the striker more easily with the tube present than with a striker that is only conical.

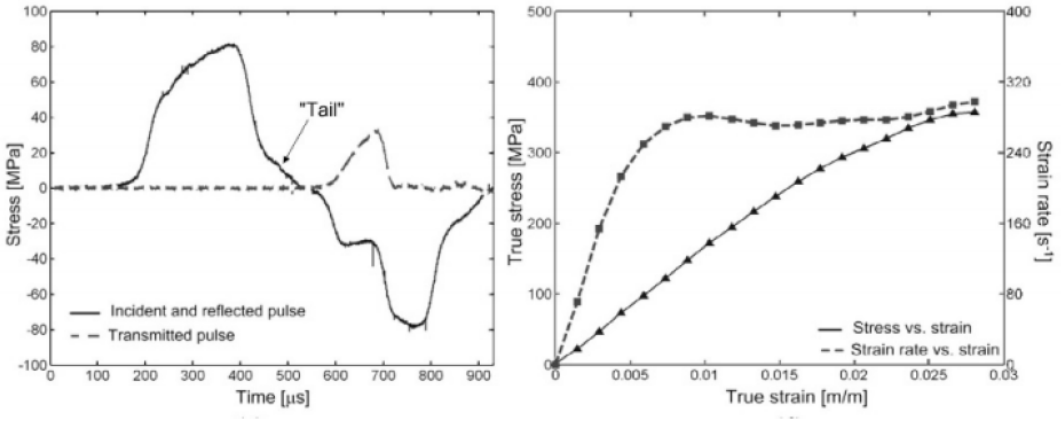

Figure 2.10 The increasing pulse from a conical striker, with the tail highlighted (shown on the left), with the more constant strain rate seen over the test (shown on the right) from Cloete *et al* . [110].

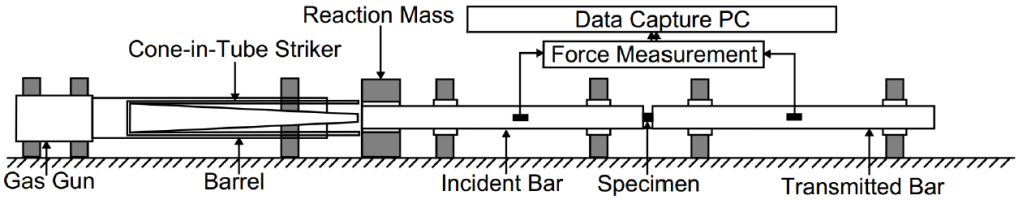

Figure 2.11 A schematic of a CiT striker in a practical set-up as designed by Paul (2014) [85].

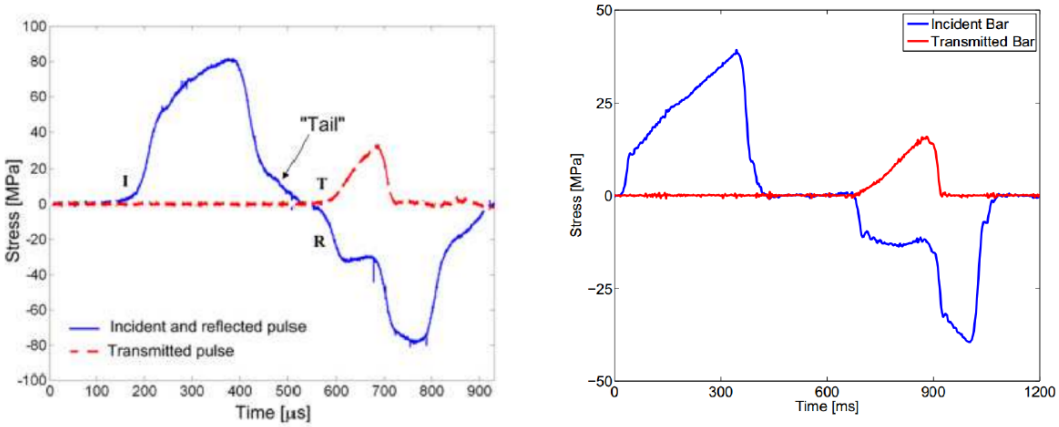

Figure 2.12 A pulse with a "tail" generated by a conical striker (shown on left) and a pulse generated by a CiT striker with no "tail" (shown on right), from Paul (2014) [85].

2.9.4 Momentum Trapping

The second piece of apparatus was built using Prot & Cloete's tandem momentum traps from 2016 [111]. Even when working with relatively delicate specimens, such as small specimens of cortical bone, the momentum traps' main function is to restrict the loading of the specimen to a single event, prevent reloading, and enable the specimen to be retrieved intact after testing for further inspection. The Prot & Cloete's [111] design is implemented as two nested tubes, each of which is impedance matched to a central bar. In the SHB configuration, this middle bar serves as the incident bar (see Figure 2.13).

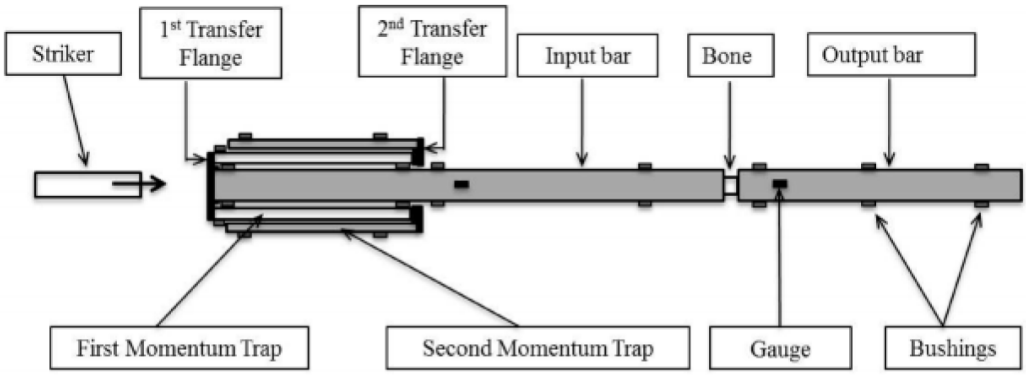

Figure 2.13 The original design for nested momentum traps by Prot & Cloete (2016) [111].

The tandem momentum traps function by preventing additional loading on the specimen by controlling the reflection of stress waves inside the bar and traps. Figure 2.14 depicts the progression of the wave through the system. This diagram illustrates the wave propagation via a collection of tandem momentum traps that are not nested, although the principle still holds true for the nested configuration.

The first momentum trap, which was attached to the incident bar by a flange, and the incident bar both experienced the initial compressive loading wave at the same time. The wave entered the second momentum trap after exiting the first momentum trap when it reached its terminus. It then reflected as a tensile wave after exiting the second trap. As a tensile wave could not be transferred over the first and second momentum trap boundaries by design, this led to the second trap separating from the first trap. This prevented the first trap from separating from the incident bar before it served its full purpose. At the same time as this was occurring, the wave that passed down the incident bar to the specimen was partially reflected back up the incident bar as a tensile wave. This tensile wave passed down the incident bar, along the flange and into the first trap, leaving the incident bar stationary. This tensile wave caused the inner trap to separate from the incident bar. On the other side of the specimen, the transmitter bar conveyed the compressive pulse that passed through the specimen. This reflected as a tensile pulse when it reached the end of the transmitter bar. The tensile wave then pulled

the transmitter bar away from the specimen, preventing reloading and any further damage to the specimen.

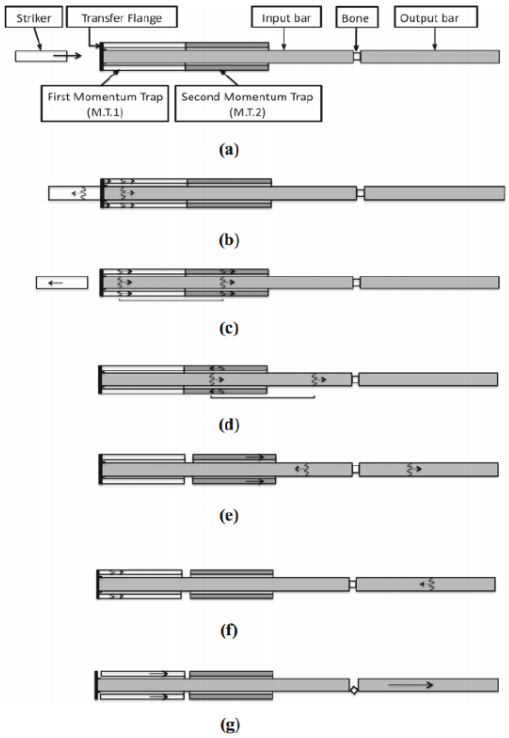

Figure 2.14 A schematic of how a wave propagates through a tandem momentum trap as depicted by Prot & Cloete (2016) [111]. (a) The striker just before impacting the system. (b) The initial compressive wave propagated down the incident bar and into the first trap. (c) The compressive wave propagated from the first to the second trap, and simultaneously down the incident bar. (d) The compressive wave continued down the incident bar, and was simultaneously reflected back as a tensile wave at the free end of the second trap. (e) The second trap separated from the first as the tensile wave reached the trap boundary. The compressive wave was reflected as a tensile pulse from the specimen back into the incident bar. A compressive wave was transferred to the transmitter bar. (f) The tensile wave in the incident bar transferred through the range into the first trap. There were no waves left in the incident bar. The compressive wave was reflected as tensile at the end of the transmitter bar. (g) The tensile wave pulled the first trap away from the incident bar. The tensile wave pulled the transmitter bar away from the specimen.

Chapter 3

Methodology

This chapter describes the methods used to prepare, store and test bovine cortical bone specimens. It details the processes for specimen machining and storage as well as the experimental set-up. The testing methodologies and the design, commissioning and validation of the sub-press, with novel platens, are explained in detail. In particular, the issue of testing machine compliance is addressed, both in terms of global and local compliance. The global compliance is eliminated using the sub-press. The local compliance, i.e. platen deformation in the vicinity of the specimen, is accounted for systematically and includes an extensive series of tests on PMMA and Al specimens.

The first four sections of this chapter covers the design of the test set-up and the modifications made to the sub-press and platens, followed by the validation of the measurement system, which includes a detailed discussion of the tests on PMMA and Al specimens. The last three sections detail the bone specimen curation protocols, i.e. the cortical bone specimen preparation process, the experimental set-up and procedure, and the data processing steps followed in this research.

3.1 Sub-Press Design and Modifications

To test small cortical bone specimens in compression using standard testing apparatuses without the influence of global machine compliance, a custom sub-press was designed to operate within a universal testing machine (UTM) [94], as mentioned

previously in Section 2.9.1. This section describes the commissioning, modification and application of this custom sub-press which offers a simple, cost-effective, repeatable and routine means of measuring displacements in the order of a micron through the novel use of Hall effect sensors and multi-pole magnetic strips.

3.1.1 Base Sub-press Design

The base sub-press designed by Daras *et al*. [94] is described in detail in Section 2.9.1 and consists of a base, a sleeve and a plunger. A specimen is compressed between two platen surfaces formed by the bottom of the plunger (upper platen), which is completely flat and the top of the base (lower platen), which has the form of an extremely shallow truncated cone, creating a slightly raised 10 mm diameter stage for specimen placement. All the components were manufactured from a mild steel.

The sub-press, shown in Figure 2.7, was designed with the intention of accurately characterizing small specimens with relatively low elastic moduli, by eliminating the testing machine compliance. For softer materials, such as PMMA, the sub-press performs as intended [94], however, even with the testing machine compliance accounted for, there is still compliance due to the local deformations of the platens in the region of the specimen. This local elastic deformation due to contact stresses alone can affect the modulus measurement [108, 107, 109]. The effect is not great for a relatively compliant material such as PMMA, but for stiffer materials it can be significant. In particular, the deformation is non-uniform due to localised compliance effects, which are discussed in detail in Section 3.3.

3.1.2 Sub-press Platen Modifications

While the base sub-press proved sufficient to accurately assess the stiffness of cortical bone, it produced large errors when testing stiffer materials. To resolve this and confirm that the base sub-press is accurate for soft materials, sub-press platen modifications were designed to address the localised compliance effects by removing material from the platens. This gives the platens a distinct truncated conical shape, thus promoting more uniform platen deformation. The reasons for this are discussed in detail in Section 3.3.

The first set of modified platens, shown in Figure 3.1, incorporate a redesigned base with a slightly curved conical frustum shape and a matching cap insert. This design provides more uniform deformation of the specimen. In addition it features a reduced specimen stage diameter of 6 mm, which enhances precision in centring the specimen on the platen.

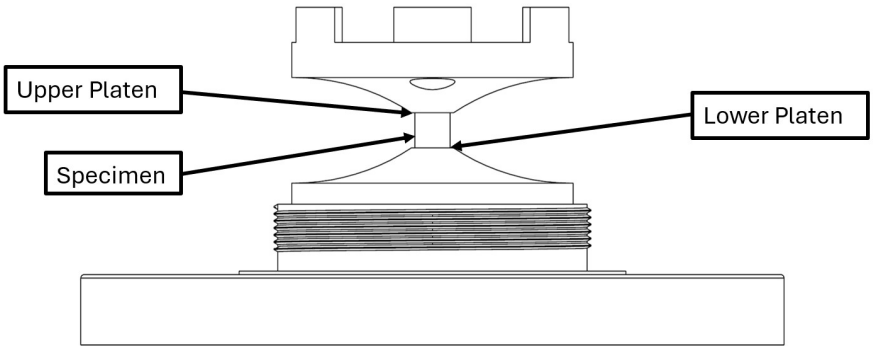

Figure 3.1 A Schematic of conical frustum platens for the modified sub-press.

The second set of modified platens, shown in Figure 3.2, further refines this concept by incorporating a strongly curved conical base, approximating a hyperbolic frustum, with a matching cap insert. This design removes additional material with the intention to provide completely uniform deformation of the specimen with a 5 mm diameter specimen stage, the same as the diameter of the specimen itself, ensuring optimal placement and support. Both sets of new platens were manufactured from stainless steel while all the other components of the sub-press remain unchanged.

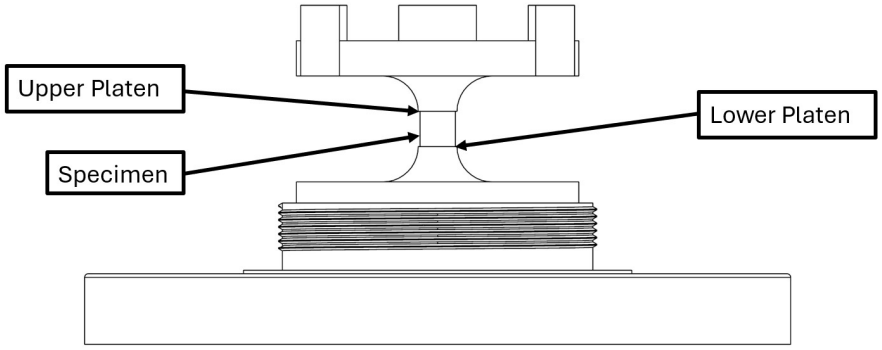

Figure 3.2 A Schematic of hyperbolic frustum platens for the modified sub-press.

3.1.3 Hall Effect Sensors and Magnetic Strips

As mentioned in Section 2.9.1 ,the sub-press utilises Bogen MS10-300 Magnetic Multi-pole Strips paired with AMS AS5311 Hall Effect Sensors to measure displacement. The use of three strip-sensor pairs, ensures that any non-axial motion of the plunger is accounted for, which can occur due to slight eccentricities in the load path or off-centred specimen placement. The arrangement of three hall effect sensors is sensitive enough to detect and correct for these otherwise imperceptible deviations, which is demonstrated in Section 3.2, whereas more remote conventional single measurement systems with linear variable differential transformers (LVDT) cannot capture this [7]. Stereoscopic digital image correlation (DIC) may be able to address this, in principle, although, the author's knowledge, this is yet to be demonstrated.

The resolution achieved with the hall effect sensor is dependent on the specification of the magnetic strip secured to the plunger, which has repeating segments with a 2 mm pole-to-pole distance. The hall effect sensor provides 12-bit digitization which, when paired with the magnetic strip, results in a displacement resolution of 0.488 μm. The signal from the hall effect sensor is captured using an Arduino UNO R3 micro-controller. The three data streams from each sensor are captured

separately and combined during signal processing to detect and account for any slight differences in the readings as a result of non-axial motion.

3.2 Sub-press Accuracy Validation

An assessment of the accuracy of the sub-press was considered essential for the bone tests pursued in this work. Calibration certificates for the magnetic strips and the hall effect sensors are included with their purchase and specify their resolution and accuracy, and, therefore, given this documentation, further validation of the individual strip-sensor pairs was deemed unnecessary. This following section outlines the process used to assess the overall accuracy of the combined measuring system i.e. three hall effect sensors each paired with a magnetic strip and mounted on the sub-press.

Daras *et al*. [94] reported that the sub-press was designed in such a way that the critical features could be machined, primarily, using a lathe, for its inherent accuracy. In particular, individual parts were designed such that the platen and mating surfaces could be machined in a single operation, i.e. without needing to reposition and re-secure a part. This ensured that the plunger and sleeve would have near-perfect concentricity, which, in turn, ensured that the upper and lower platens remained parallel within a close tolerance. Consequently, there is a high degree of confidence that a specimen will experience pure axial compression between two flat and parallel platen faces. Additionally, the bottom face of the sleeve is perpendicular to the axis of the plunger and sleeve, making it an ideal datum for validation testing. A similar approach was taken with the modifications.

The first step of the commissioning process, was to assess the accuracy of the sub-press in measuring displacement. This was done using a Mitutoyo depth micrometer, marked with 10 μm increments and a SMZ745T Nikon microscope. The base of the sub-press was removed, and the sleeve was secured to a specially designed mounting fixture shown in Figure 3.3 such that all unwanted motion was restricted. The plunger was inserted to the sleeve such that upper platen face was flush with the bottom face of the sleeve.

The mounting fixture with the sub-press secured inside, was placed under the microscope for image capturing and processing. The depth micrometer was secured against the bottom face of the sleeve such that the dial could clearly be seen

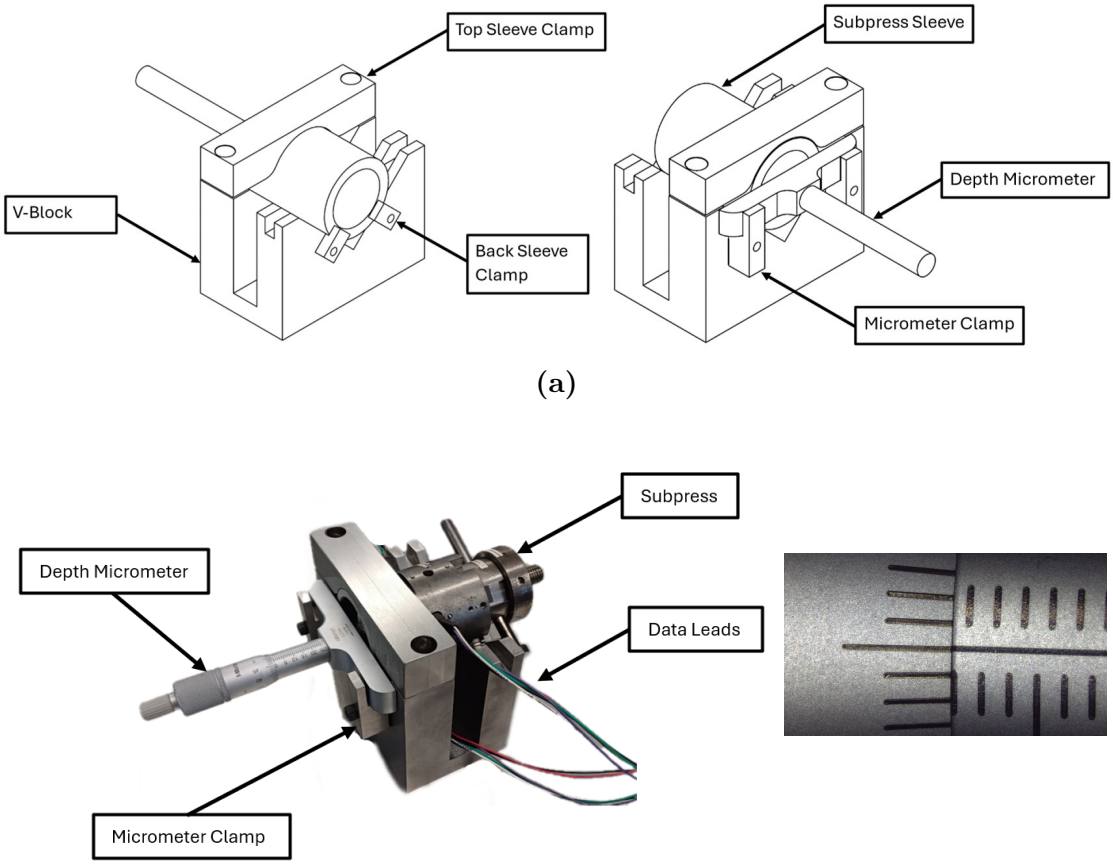

Figure 3.3 The commissioning test set-up with (a) A schematic of the mounting fixture design, (b) A view of the calibration set-up as would go under the microscope, and (c) A typical image captured of the depth micrometer dial by the microscope.

through the microscope as shown in Figure 3.3c. The micrometer was manually incremented in nominal 10 μm steps across a total displacement of 100 μm and between each step a period of time was allowed to pass in order to obtain distinct steps in the final displacement-time plots. Great care was taken never to wind the micrometer dial back, but always forward, even if the increment was slightly overshot. The raw data from the sub-press (i.e. hall effect sensors) and the images captured by the microscope were analysed and compared.

Figure 3.4 The sub-press and mounting fixture placed under the microscope.

During manual adjustment of the micrometer dial, the intended displacement of 10 μm per increment was not always achieved due to occasional overshooting or undershooting. To determine the actual displacement, image processing software was employed. By analysing the captured images of the micrometer dial, the deviations from the intended 10 μm increments were quantified. These deviations were then used to correct the intended displacements, providing an accurate measurement, as close as 0.1 μm (based on the pixel resolution of the microscope), of the actual displacement for each increment.

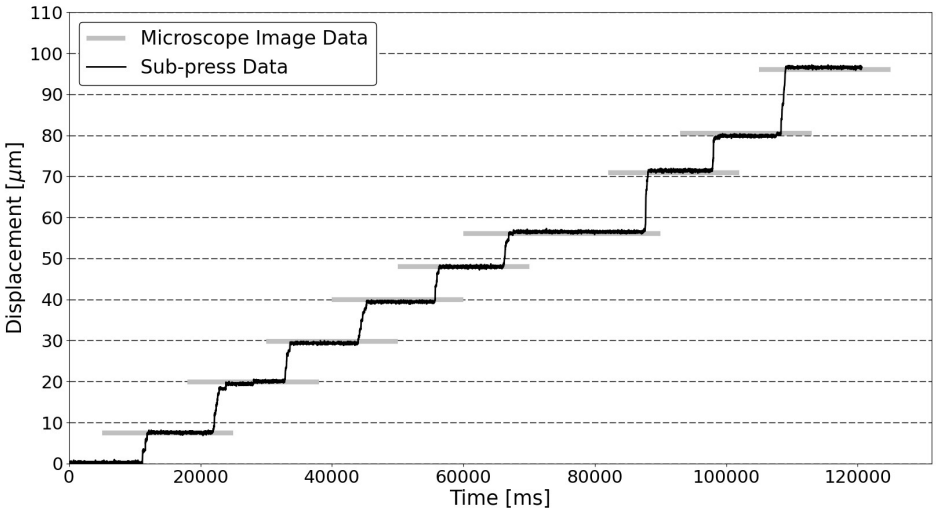

Figure 3.5 A displacement vs time plot of the sub-press data (in black) during an incremented displacement test using a manually adjusted micrometer where the grid lines represent the intended displacement increments and the short, grey horizontal lines represent the actual displacements as obtained from the microscope images.

A typical displacement-time plot is presented in Figure 3.5. The commissioning test described above was conducted ten times in order to ensure consistency and repeatability, and similar results were obtained. The sub-press is sensitive enough to measure each step with clarity. The average difference between the sub-press readings and the micrometer displacements (as obtained from the image processing) is 0.051 μm with a standard deviation of 0.466 μm.

A Bland-Altman plot [112], shown in Figure 3.6 was used to assess the agreement between displacement measurements obtained from the Hall Effect sensor and the microscope across various time intervals. The plot visualizes the differences between the two measurement methods, with the red dashed line representing the mean difference and the blue dashed lines indicating the upper and lower limits of agreement (LoA), calculated as the mean difference $\pm$ 1.96 times the standard deviation of the differences [112]. The closer the data points are to the

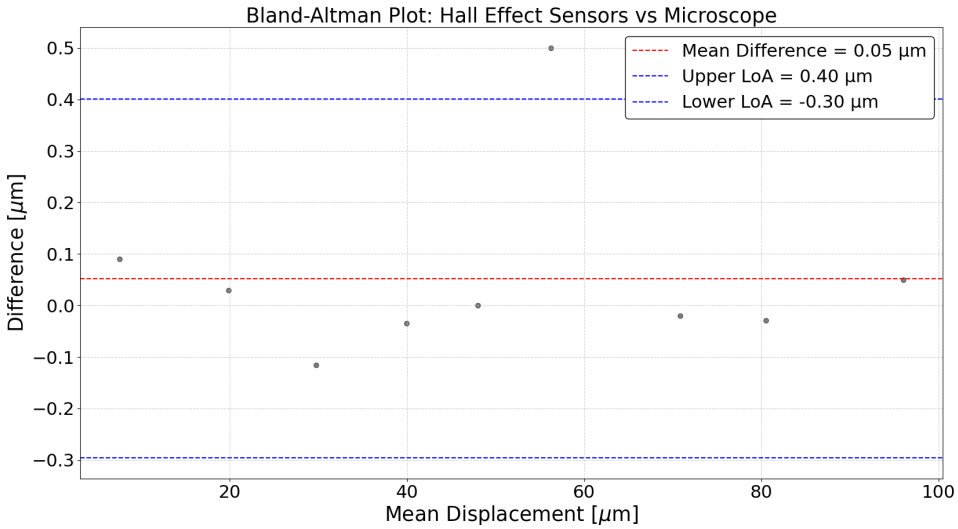

Figure 3.6 A Bland-Altman plot of the agreement between displacement measurements obtained from the Hall Effect sensor and the microscope across various time intervals.

mean difference line and the smaller the scatter within the LoA, the better the agreement between the two methods. A narrow distribution of points within the LoA, thus suggests that both methods provide consistent measurements.

The average difference of 0.051 μm is remarkable in that it is a order of magnitude smaller than the resolution of the sensors. This is possible due to a process similar to 'dithering' in image processing, where noise enhances sub-pixel accuracy [113, 114, 115]. Some noise can be observed in the output signal in Figure 3.5, which is attributed to random environmental noise rather than sensor error. Due to the digital output of the sensors the data points are spread over a few discrete intervals, with most clustered near the true position. With a sufficiently high sampling rate, applying a moving average to the signal can achieve greater accuracy than the resolution of the sensors. This is explained in greater detail in the paper by Daras *et al*. [94].

While the results are at or beyond the conventional accuracy of both the sensors and micrometer, it is considered unlikely that the measurements would be both incorrect and show such consistent agreement. Thus, it is evident that the addi-

tional analysis steps taken, i.e. dithering and image processing, have resulted in the required resolution.

Given that ± one standard deviation covers 68% of a normal distribution, the results suggest that 68% of the readings fall within the sensor accuracy. Similarly, considering ± two standard deviations suggests that 95% of the readings are within a difference of 1 μm. The validation tests demonstrate that the sub-press is capable of measuring to an accuracy of at worst 1 μm with potential to measure even smaller displacements.

3.3 Compliance Effects and Estimation

Machine compliance presents significant challenges when testing small specimens under compression, as detailed in Section 2.9.1. There are two types of compliance referred to in this dissertation, i.e. global compliance, referring to the compliance of the testing machines and fixtures, and local compliance referring to the deformation of the platens in the vicinity of the specimen.

3.3.1 Inconsistent Global Compliance

Kalidindi *et al*. [116] highlighted that large testing machines not only introduce compliance issues but also display non-linear compliance behaviour. In fact, they claim that the compliance factor varies across different materials. This was attributed to the inherent non-linearity of machine compliance, where non-sample displacement depends on the applied load in a non-linear manner. Through extensive mechanical testing across a range of materials, Kalidindi *et al*. [116] demonstrated the importance of characterizing this non-linear compliance relationship to achieve accurate and reliable measurements. Daras *et al*. [94], however, demonstrated that the base sub-press successfully eliminates these global compliance effects.

3.3.2 Localised Platen Deformation

As discussed in Section 2.9.1, in addition to the global compliance of larger test machines and fixtures, local compliance of the test platens themselves can also impact compression test accuracy. Augat *et al*. [117] argued that systematic

errors in strain measurements stem from measuring strain across the machine platens rather than directly on the specimen. Furthermore, Odgaard & Linde [107] noted that strain is concentrated near the boundaries of specimens compared to the central region, potentially leading to an overestimation of average strain and, consequently, an underestimation of modulus.

The aforementioned localised deformations can be explained with reference to analytical solutions provided by Timoshenko & Goodier [118], who considered the surface deflection of a semi-infinite solid subjected to a uniform load q distributed over a circular area with radius a. The deflection at the boundary of the loaded circle is:

$$w_{r=a} = \frac{4(1-\nu^2)qa}{\pi E} \tag{3.1}$$

where w is the deflection; r is the radial distance from the centre of the circle; a is the radius of the circle; ν is the Poison's ratio; q is the load per unit area on the segment and E is the Young's modulus. Similarly the maximum deflection, which occurs at the centre of the circle, is given by:

$$w_{\max} = \frac{2(1-\nu^2)qa}{E} \tag{3.2}$$

From the preceding equations it is clear that the deflections beneath the uniformly loaded circular area are not uniform, with the maximum deflection at the centre being 57% greater than that at the edge.

Timoshenko & Goodier [118] also examined the example of a rigid die shaped as a circular cylinder that is pressed against the plane boundary of a semi-infinite elastic solid. In this situation, the displacement remains uniform across the circular base of the die. However, the pressure distribution is not uniform, and its intensity can be expressed as:

$$q = \frac{P}{2\pi a\sqrt{a^2 - r^2}} \tag{3.3}$$

where P is the total load on the die, a the radius of the die and r the distance from the centre of the circle on which the pressure acts.

This pressure distribution is clearly non-uniform, with the minimum pressure occurring at the centre ($r = 0$), where it is equal to half the average pressure across the circular contact area. At the boundary of the contact area ($r = a$), the pressure theoretically approaches infinity. In practical scenarios, material yielding will occur along the boundary, however, this yielding is localised and does not significantly influence the pressure distribution at points located some distance from the edge of the circle. The displacement of the die can be described by the following equation:

$$w = \frac{P(1 - \nu^2)}{2aE} \tag{3.4}$$

In practical compression tests, a specimen acts neither as a rigid die, nor does it provide a uniform pressure, but would behave somewhere in between these two extremes. What is clear, however, is that deflection and pressure at the interface between a specimen and a flat platen are not uniform, with concentrated loads occurring along the face edge of the specimen, which confirms the aforementioned work of Odgaard & Linde [107]. Furthermore, if a specimen is stiff enough, the localised loading at the face edge can cause initial yielding at the face edge that progresses inward with further deformation. This progressive yielding explains the so-called 'take-up' behaviour typically observed at the start of compression tests. In addition, progressive yielding will smear the elastic region of the stress-strain curve, thus further degrading the assessment of the apparent modulus.

3.3.3 Platen Compliance Assessment

In light of the preceding discussion, the sub-press, which has been shown to effectively eliminate the global compliance issues associated with the UTM [94], introduces its own compliance factor due to local platen deformation. To the author's knowledge, and after an extensive literature review, there does not appear to be a published experimental methodology to assess the local compliance of a set of platens.

To address the aforementioned, the following procedure is proposed to estimate the local compliance of the sub-press. The procedure is based on a series on experiments on two sets of specimens with the same diameter but different height-to-diameter ratios, i.e. (1:1 and 2:1). In an ideal scenario, where the sub-press would exhibit perfect rigidity and zero machine compliance, the tall (2:1) specimens, being twice the height of the short (1:1) specimens, would theoretically possess exactly half the stiffness of the short specimens. However, the measured stiffness ratio is affected by the sub-press compliance, because the tall specimen is less sensitive to it than the short specimen. The tall specimens experience greater deflection, rendering the additional deflection from the sub-press (which is the same for both the tall and the short specimens) less significant in comparison to its total deflection. The effect on the apparent stiffness of the shorter specimens is thus more pronounced. As as a result, the taller specimens should exhibit a stiffness slightly greater than half that of the shorter specimens. This is demonstrated with sample calculations in Appendix A. Using this stiffness ratio, the sub-press compliance can be inferred by simultaneously solving:

$$\left(\frac{\delta}{F}\right)_1 = \frac{1}{k_{\text{sp}}} + \frac{1}{k_s} \tag{3.5}$$

$$\left(\frac{\delta}{F}\right)_2 = \frac{1}{k_{\text{sp}}} + \frac{1}{\frac{1}{2}k_s} \tag{3.6}$$

where the symbol δ denotes the measured combined deformation; F is the measured force; k_{sp} is the stiffness of the sub-press and platens and k_{s} is the stiffness of the specimen. Note that this procedure does not require stiffness of the specimen to be known. It is only required that specimens have consistent properties. In fact, repeating this procedure with materials that span the domain of interest is well advised.

For the work described in subsequent sections, a large number of PMMA and 1050 Al compression specimens were machined from single rods of each material. These two materials were chosen as the elastic moduli encompass the range of expected apparent moduli of cortical bone. All the specimens had a diameter of 5 mm to ensure the same contact area. Half of the specimens from each material had a height of 5 mm (resulting in a 1:1 height-to-diameter ratio) and the other half had

a height of 10 mm (resulting in a 2:1 height-to-diameter ratio). This was done to assess the stiffness ratio between the two specimen geometries and thus the local deformations between the specimens and the sub-press, for each platen variation. A smaller amount of compression specimens were also machined from 6000 series Al to assess the performance of the sub-press with harder materials.

3.3.4 Flat Platens

Figures 3.7 and 3.8 shows a typical stress vs strain and force vs deflection plot for PMMA and Al using the unmodified sub-press i.e. flat platens. Table 3.1 shows the average apparent modulus and stiffness results for a total of 24 compression tests i.e. 6 tall and 6 short PMMA and Al specimens.

Table 3.1 *Comparison of the apparent material properties for different specimen geometries for Al and PMMA, respectively, using the unmodified sub-press.*

Material Property	**Specimen Geometry**	**1050 Al**	**PMMA**
Apparent Average Modulus [GPa]	**Tall**	7.59 (SD: 4.24)	3.45 (SD: 0.17)
	Short	3.72 (SD: 1.13)	3.02 (SD: 0.45)
Apparent Average Stiffness, k [kN/mm]	**Tall**	14.92	6.77
	Short	14.63	11.86
k_{tall}/k_{short}		1.02	0.57

For the PMMA, the short specimens had an average apparent modulus of 3.02 GPa with a standard deviation of 0.45 GPa which corresponds to an average stiffness of 11.86 kN/mm, whereas the tall specimens had an average apparent modulus of 3.45 GPa with a standard deviation of 0.17 GPa which corresponds to an average stiffness of 6.77 kN/mm. This resulted in a stiffness ratio of 0.57, which is in the anticipated range, i.e. 0.51 t0 0.66 as set out in Appendix A.

For the Al, the short specimens had an average apparent modulus of 3.72 GPa with a standard deviation of 1.13 GPa which corresponds to an average stiffness of 14.63 kN/mm. Additionally, the tall specimens had an average apparent modulus of 7.59 GPa with a standard deviation of 4.24 GPa which corresponds to an average stiffness of 14.92 kN/mm. This resulted in a stiffness ratio of just over one, which

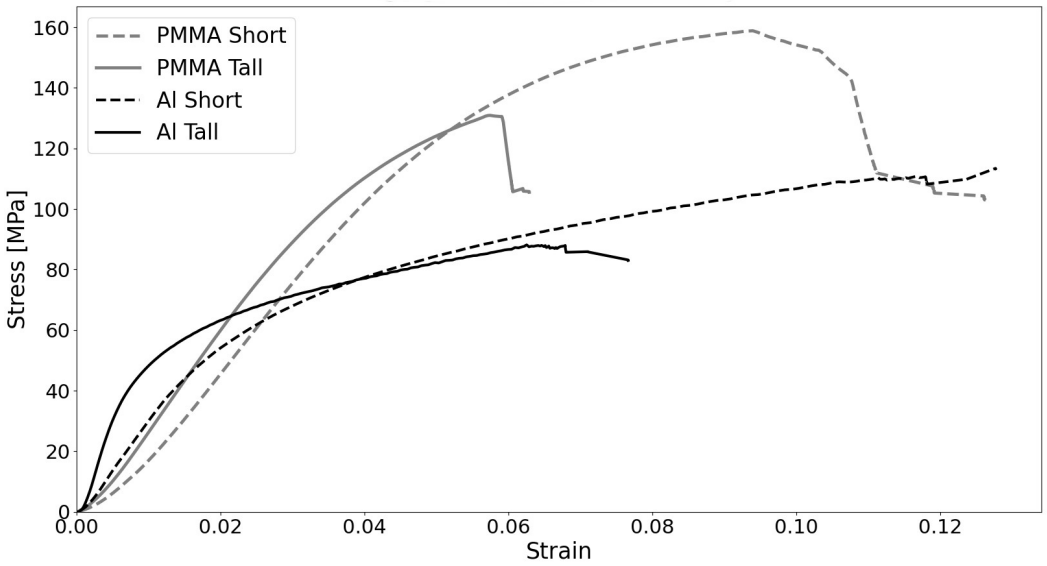

Figure 3.7 A representative stress-strain curve for the base sub-press.

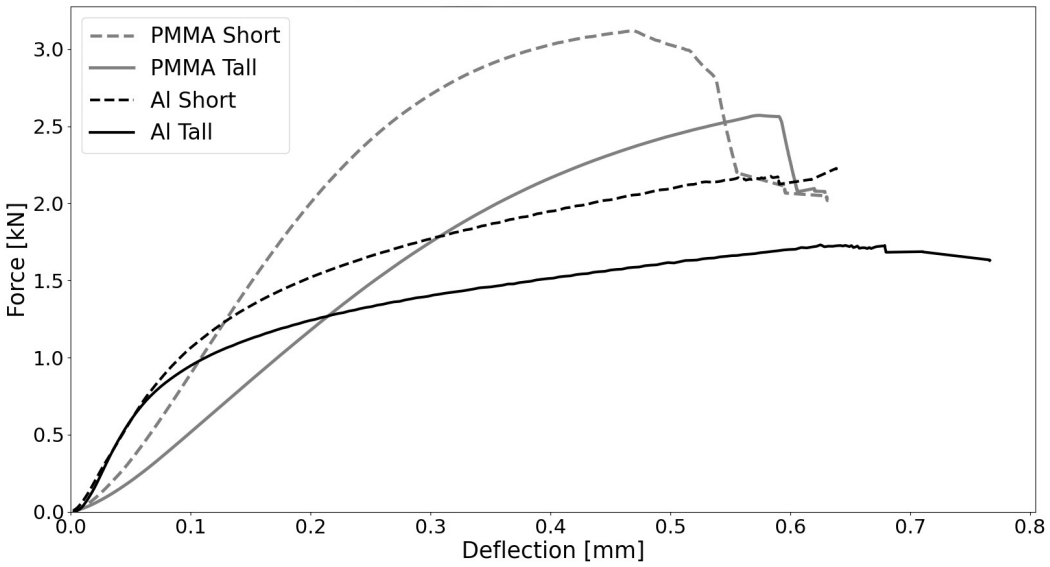

Figure 3.8 A representative force-deflection curve for the base sub-press.

is well above the expected range as evident in the force-deflection curve, shown in Figure 3.8, where the tall Al specimen is clearly as stiff as the short Al specimen.

While an apparent modulus in the range of 3.02 GPa to 3.45 GPa is reasonable for PMMA, the values of 3.72 GPa and 7.59 GPa for the Al specimens are clearly erroneous. This indicates that local platen compliance has a large effect for the Al specimens.

The compliance of the sub-press can be approximated as two springs in series where its stiffness can be calculated as the sum of the local deformation of the two platen faces and the uniform deformation of the plunger and base between the Hall-effect sensors and the base threads. The total deformation can be approximated as:

$$\delta_{sp} = \frac{F}{k_{sp}} = \frac{2F(1-\nu^2)}{dE} + \frac{2FL}{\left(\frac{\pi}{4}D^2E\right)} \tag{3.7}$$

where the first term estimates the local deformation of the platens, which can be approximated using the aforementioned 'rigid die' indentation solution of Timoshenko & Goodier [118] given in 3.4 and the second term estimates the uniform deformation of the plunger and base [119]. The symbol δ denotes the measured combined deformation; F is the measured force; ν is the Poisson's ratio of the sub-press; d is the diameter of the specimen; E is the elastic modulus of stainless steel; L is the combined active length of the plunger and the base and D is the diameter of the plunger and base.

When applying Equations 3.5 and 3.6 to the results in Table 3.1, the results were inconsistent with the platen stiffness estimate obtained from Equation 3.7. It became apparent that the apparent modulus values were not accurate enough. In paricular, the values for Al are unrealistic and give counter-intuitive results. It is postulated that the large error in the stiffness ratio for the Al is indicative of non-uniform deformation in the Al specimen. The Al specimen is stiff enough to cause sufficient localised elastic deformation in the platens such that the face edge of the specimen is more highly loaded than the centre. As postulated in Section 3.3.2, progressive yielding occurs at the edge and progresses inward with further deformation, which smears the elastic region of the stress-strain curve and results in an erroneous reading of the apparent modulus. This is evident in Figure 3.7 where the Al curve has a less clear linear portion when compared to the PMMA

curve. Consequently, the inferred compliance of the sub-press with the flat platens was not used, as the abnormal behaviour indicated that the sub-press compliance could not be accurately determined in this configuration. In fact, it is this result that inspired the development of the modified platens.

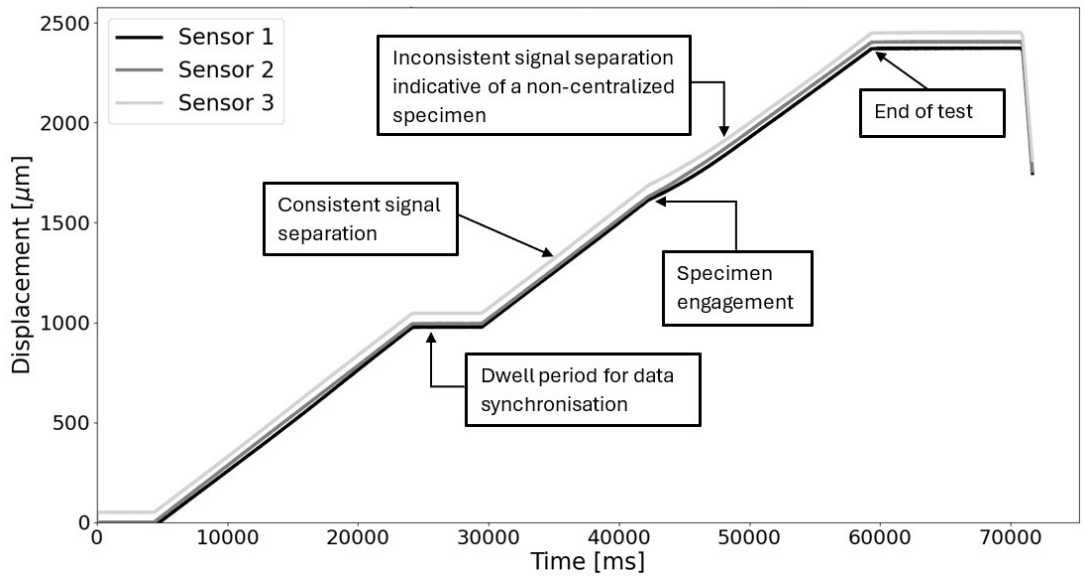

Figure 3.9 A representative displacement-time curve for the base sub-press.

Finally, the results show that the measuring system is sensitive enough to detect if the position of the specimen is not perfectly centred on the platens. This is illustrated in Figure 3.9, which shows that the three sensor reading remain parallel, i.e. record identical deflection, until the platen impact the specimen, whereupon they diverge. This is indicative of a slight tilt of the plunger due to an offset specimen. This further underscores the importance and effectiveness of the 3-sensor set-up.

3.3.5 Conical Frustum Platens

The application of the conical frustum platens improved the compression test results. Figure 3.10 demonstrates a reduction in the smeared elastic region compared to the flat platens, although some take-up behaviour is still evident and Figure 3.11 displays the correct stiffness behaviour for both PMMA and Al. Thus, the stress-strain curves now show a clearer linear portion for both materials, and the force-deflection curves indicate, as expected, that the tall specimens are less stiff than the short specimens for both PMMA and Al. Furthermore, Figure 3.12 illustrates an improvement in specimen placement, i.e. the three sensor traces do not diverge after contact with the specimen. The improved specimen placement is due to the reduced radius of the specimen platform, which facilitates more accurate centring of the specimen on the platens. Table 3.2 shows the average apparent modulus and stiffness results for another 24 compression tests using the conical frustum platens.

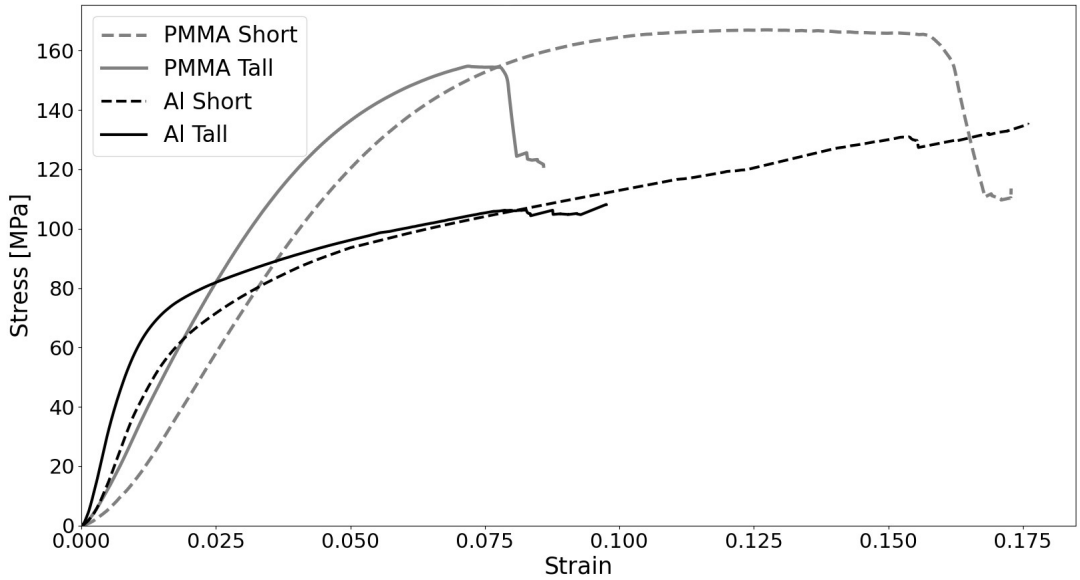

Figure 3.10 A representative stress-strain curve for the conical frustum platens.

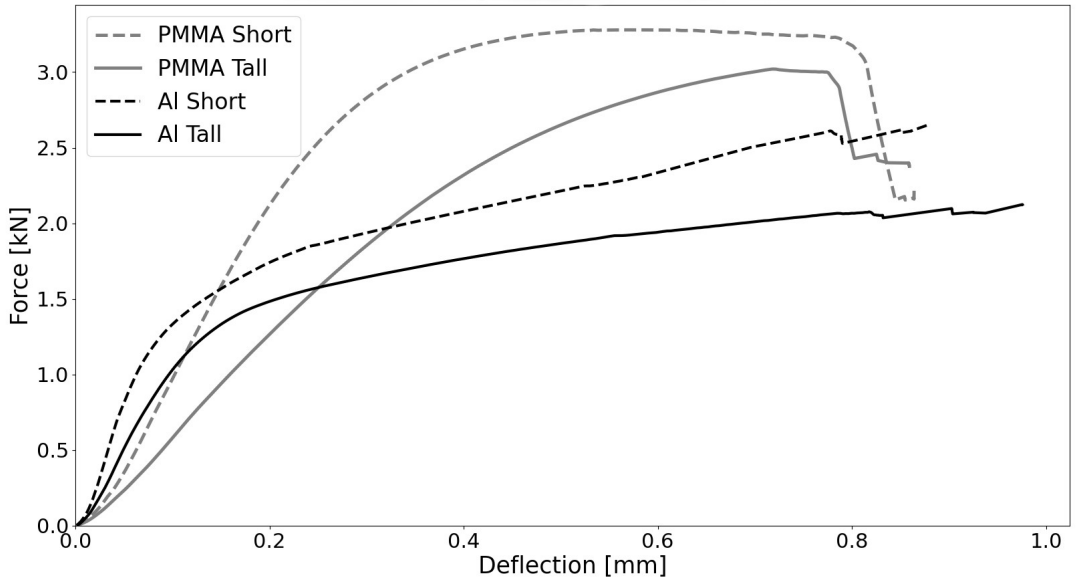

Figure 3.11 A representative force-deflection curve for the conical frustum platens.

Table 3.2 *Comparison of the apparent material properties for different specimen geometries for Al and PMMA, respectively, using the conical frustum platens.*

Material Property	**Specimen Geometry**	**1050 Al**	**PMMA**
Apparent Average Modulus [GPa]	**Tall**	7.14 (SD: 1.95)	3.76 (SD: 0.17)
	Short	6.24 (SD: 1.84)	3.24 (SD: 0.24)
Apparent Average Stiffness, k [kN/mm]	**Tall**	14.02	7.39
	Short	24.49	12.73
k_{tall}/k_{short}		0.57	0.58

For the PMMA, the short specimens had an average apparent modulus of 3.24 GPa with a standard deviation of 0.24 GPa which corresponds to an average stiffness of 12.73 kN/mm, whereas the tall specimens had an average apparent modulus of 3.76 GPa with a standard deviation of 0.17 GPa which corresponds to an average stiffness of 7.39 kN/mm. Although the results from the modified sub-press are

slightly higher than from the unmodified sub-press, it resulted in a stiffness ratio of 0.58, which is well within the acceptable range.

For the Al, the short specimens had an average apparent modulus of 6.24 GPa with a standard deviation of 1.84 GPa which corresponds to an average stiffness of 24.49 kN/mm, whereas the tall specimens had an average apparent modulus of 7.14 GPa with a standard deviation of 1.95 GPa which corresponds to an average stiffness of 14 kN/mm. This resulted in a stiffness ratio of 0.57, which is now in the expected range, demonstrating the effectiveness of the sub-press modification in reducing the non-uniform loading on the Al specimens. The apparent modulus readings for the Al specimens, however, are still substantially too low (compared to an industry standard of 71 GPa for 1050 Al [120]), indicating that the modifications to the sub-press does not eliminate the non-uniform loading completely and that the sub-press has significant compliance effects on the Al specimens. The sub-press compliance thus has to be calculated and accounted for.

Equation 3.7 was used to estimate the deformation of the sub-press for both the PMMA and Al tests. Despite the angled design, the conical frustum platens are sufficiently flat for this estimation to remain applicable, while the slope is still steep enough to effectively reduce the progressive yielding seen with the flat platens.

The analytically estimated compliance of the sub-press, using Equation 3.7, resulted in a stiffness of 305 kN/mm, which is in the same order of magnitude as the stiffness of the Al specimens at 280 kN/mm, which, in turn, implies that the effect of compliance should be significant. By contrast, the stiffness of the PMMA specimens is 10 kN/mm, which is an order of magnitude less than the estimated stiffness of the sub-press. The compliance of the sub-press should thus have a far less significant effect on the PMMA specimens. However, it should be noted that several simplifying assumptions were made, such as the platens being completely flat, further work is thus needed to refine this estimate.

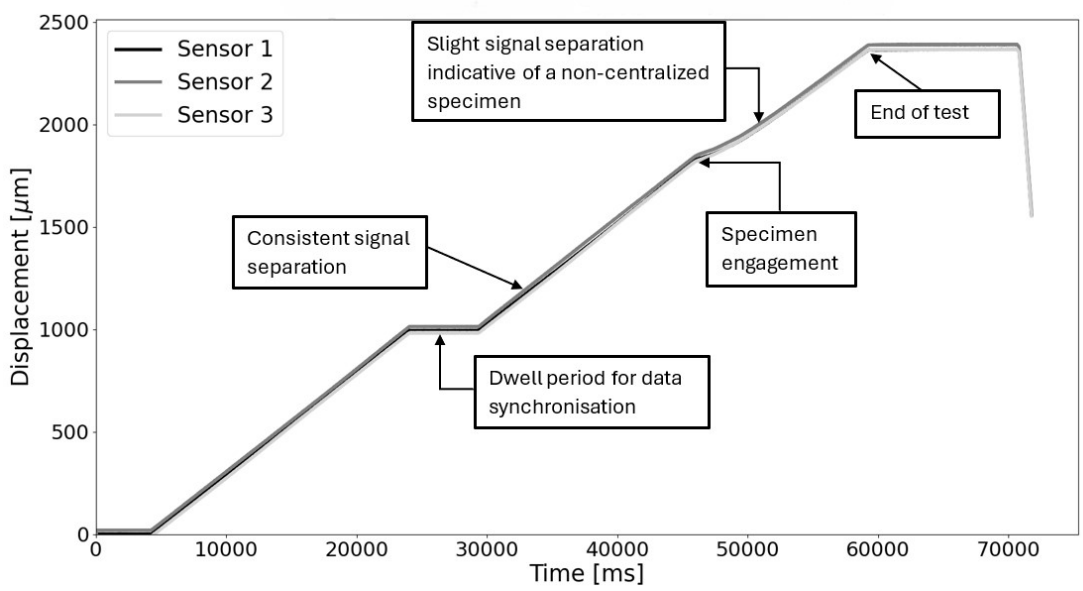

Figure 3.12 A representative displacement-time curve for the conical frustum platens.

The stiffness of the sub-press can now be accounted for in the calculated specimen stiffnesses and the true moduli can be calculated as:

$$E = \frac{|k_{spec} - k_{sp}| \cdot h}{\pi r^2} \tag{3.8}$$

where E is the true elastic modulus for the specimen; k_{spec} is the measured apparent stiffness of the specimen; k_{sp} is the estimated stiffness of the sub-press; h is the height of the specimen and r is the radius of the specimen.

The inferred true modulus values, after the sub-press compliance has been accounted for, are 3.85 GPa for the PMMA and 74.8 GPa for the Al. It is thus clear that the local deformation of the sub-press when testing stiffer materials is of significance whereas it has little to no effect on more compliant materials such as the PMMA.

3.3.6 Hyperbolic Frustum Platens

The compression tests were repeated using the hyperbolic frustum platens, but this time a stronger Al (6000 series) was used to assess its performance. These tests demonstrated further reductions in non-uniform loading, take-up behaviour, and improved specimen placement, as illustrated in Figures 3.13 to 3.15. The stress-strain curve now exhibits a better-defined linear portion with virtually no take-up behaviour. The force-deflection curves confirm that the tall specimens are less stiff than the short specimens for both PMMA and 6000 series Al, as expected. Additionally, the displacement-time curve for the sub-press measurement system indicates precise specimen centring, with all three sensors tracking closely together, thanks to the reduced specimen stage diameter matching that of the specimen itself. However, it is important to note that positioning the specimen within the sub-press remains challenging due to the small size of the stage.

Table 3.3 presents the average apparent modulus and stiffness results from 24 compression tests using the hyperbolic frustum platens. For the PMMA, the short specimens had an average apparent modulus of 3.04 GPa with a standard deviation of 0.93 GPa which corresponds to an average apparent stiffness of 11.93 kN/mm, whereas the tall specimens had an average apparent modulus of 3.24 GPa with a standard deviation of 0.13 GPa which corresponds to an average apparent stiffness of 6.36 kN/mm, closely agreeing with the results of both the flat and conical platens.

Table 3.3 *Comparison of the apparent material properties for different specimen geometries for Al and PMMA, respectively, using the hyperbolic frustum platens.*

Material Property	**Specimen Geometry**	**6000 Al**	**PMMA**
Apparent Average Modulus [GPa]	**Tall**	49.23 (SD: 1.13)	3.24 (SD: 0.13)
	Short	35.65 (SD: 1.6)	3.04 (SD: 0.93)
Apparent Average Stiffness, k [kN/mm]	**Tall**	96.67	6.36
	Short	139.98	11.93
k_{tall}/k_{short}		0.69	0.53

For the 6000 series Al, the short specimens had an average apparent modulus of 35.65 GPa with a standard deviation of 1.6 GPa corresponding to an average

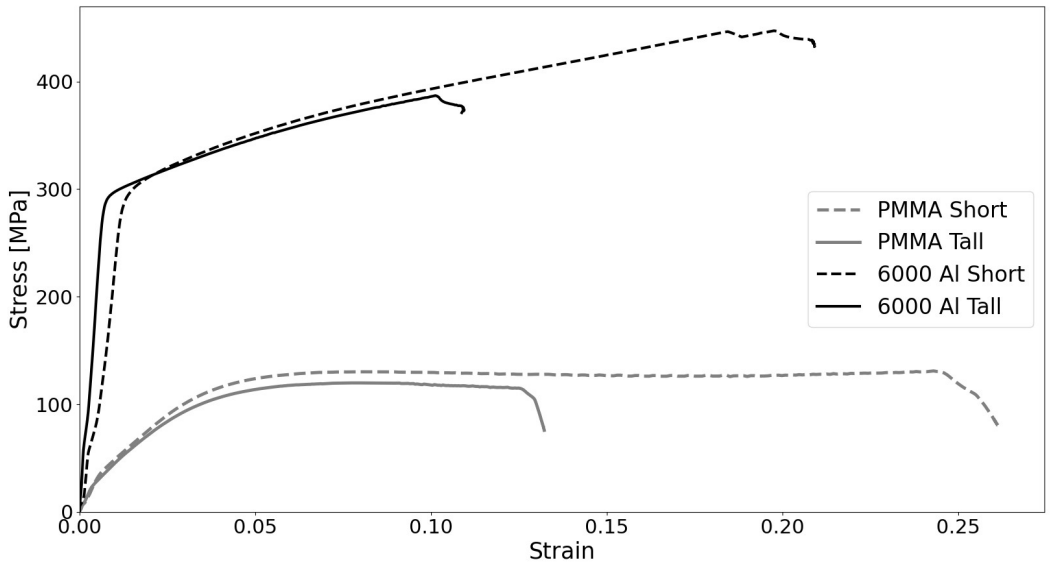

Figure 3.13 A representative stress-strain curve for the hyperbolic frustum platens.

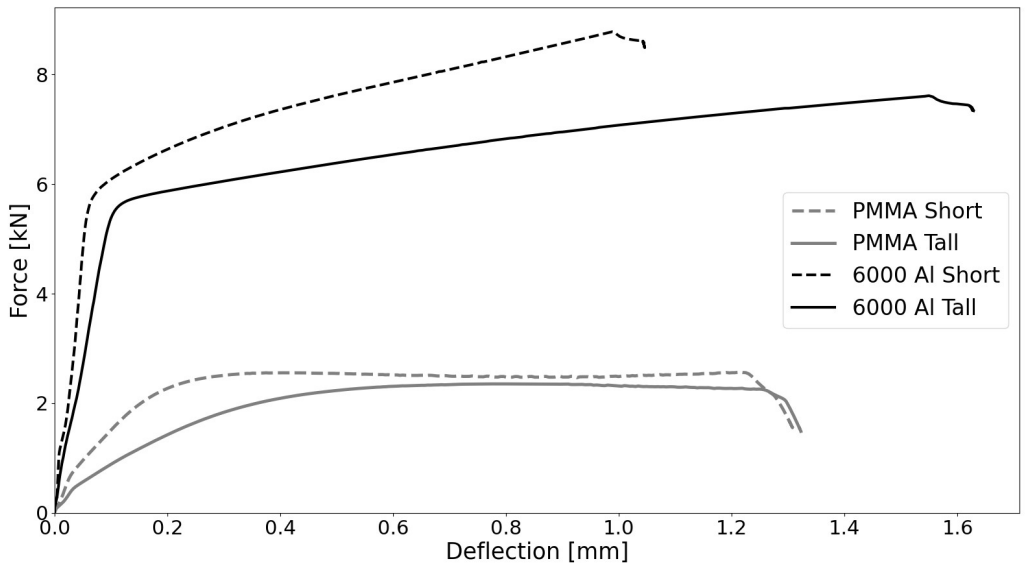

Figure 3.14 A representative force-deflection curve for the hyperbolic frustum platens.

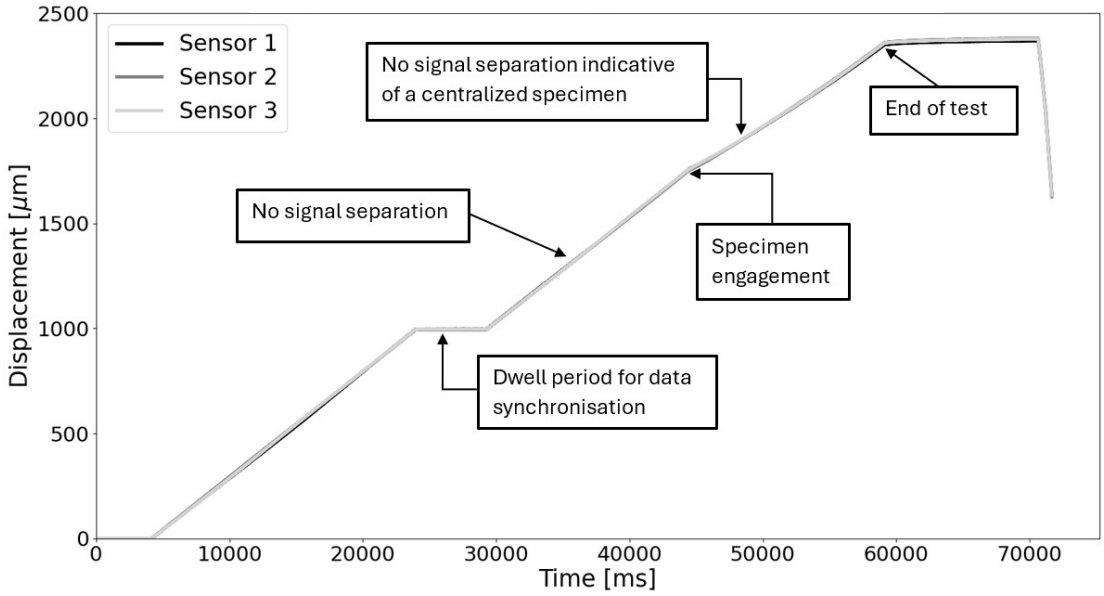

Figure 3.15 A representative displacement-time curve for the hyperbolic frustum platens.

apparent stiffness of 139.98 kN/mm and the tall specimens had an average apparent modulus of 49.23 GPa with a standard deviation of 1.13 GPa corresponding to an average apparent stiffness of 96.67 kN/mm, resulting in a stiffness ratio of 0.69, which is slightly higher than with the flat and conical platen variations, but within the expected range of 0.513 to 0.71 as set out in Appendix A. The hyperbolic frustum platens not only achieve the expected stiffness ratio but also demonstrate an improvement in the measured moduli, highlighting the effectiveness of these platens in mitigating non-uniform loading.

Equation 3.7 was extended by adding a third term to include the specimen stage and thus account for the hyperbolic frustum:

$$\delta_{sp} = \frac{F}{k_{sp}} = \frac{2F(1-\nu^2)}{dE} + \frac{2FL}{\left(\frac{\pi}{4}D^2E\right)} + \frac{2Fh}{\left(\frac{\pi}{4}d^2E\right)} \tag{3.9}$$

where the symbol δ denotes the measured combined deformation; F is the measured force; ν is the Poisson's ratio of the sub-press; d is the diameter of the specimen and the specimen stage; E is the elastic modulus of stainless steel; L is the combined active length of the plunger and base; D is the diameter of the base and plunger and h is the height of the specimen stage.

This extended equation was utilized to estimate the deformation of the modified sub-press with the hyperbolic frustum platens for both PMMA and 6000 series Al tests, in the same manner as for the conical frustum platens. The newly estimated compliance of the sub-press indicated a stiffness of 201 kN/mm, which is lower than that of the conical frustum platens but remains within the same order of magnitude as the stiffness of the 1050 Al specimens at 280 kN/mm. It is, however, an order of magnitude greater than the stiffness of the PMMA specimens, which stands at 10 kN/mm. Consequently, the compliance of the sub-press is expected to still have a more pronounced effect on Al specimens than on the PMMA specimens.

The stiffness of the sub-press can now be factored into the calculated specimen stiffnesses, allowing for the accurate determination of the true moduli using Equation 3.8, just as was done with the conical frustum platens. The inferred true modulus values, after the new estimated sub-press compliance has been accounted for, are 3.5 GPa for the PMMA, which is comparable to the conical frustum and multi-machine tests, and 79.6 GPa for the 6000 series Al, which is slightly higher than the values for the 1000 series Al.

Figure 3.16 depicts a "platen-on-platen" (PoP) test, which was conducted without a specimen to directly measure the stiffness of the sub-press. This test yielded a sub-press stiffness of 198 kN/mm, closely aligning with the newly estimated sub-press compliance. These findings highlight the importance of considering the specimen platform as an additional spring in series, rather than combining it with the plunger or base of the sub-press. Additionally, while this no-specimen test with this platen configuration provides an accurate measurement of compliance,

it remains crucial to account for the specimen influence due to local deformations and Hertzian stresses on the platens resulting from specimen contact, potentially explaining the slight difference in the estimated and measured stiffness of the sub-press. The raw data from the UTM for the no-specimen tests reveals not only a lack of repeatability but also a smeared elastic region and an extended take-up portion, resulting in significantly lower values compared to the sub-press. This inconsistency would have led to an average apparent stiffness of just 16.17 kN/mm, significantly lower than that obtained from the sub-press.

Using the stiffness ratio of the two different specimen geometries, the sub-press compliance was inferred using the experimental data obtained from the hyperbolic frustum platen tests with 6000 series Al, as described in Section 3.3.3. Solving for equations 3.5 and 3.6 simultaneously, the stiffnesses of the short and tall specimens could be calculated and the machine compliance could be accounted for. This analysis resulted in an inferred sub-press compliance of 95 kN/mm for the PMMA and 150 kN/mm for the Al. All of these compliances (analytical, inferred and measured/PoP) are within a standard deviation of 65 kN/mm of one another. These results confirm that the sub-press is an effective tool for accurately measur-

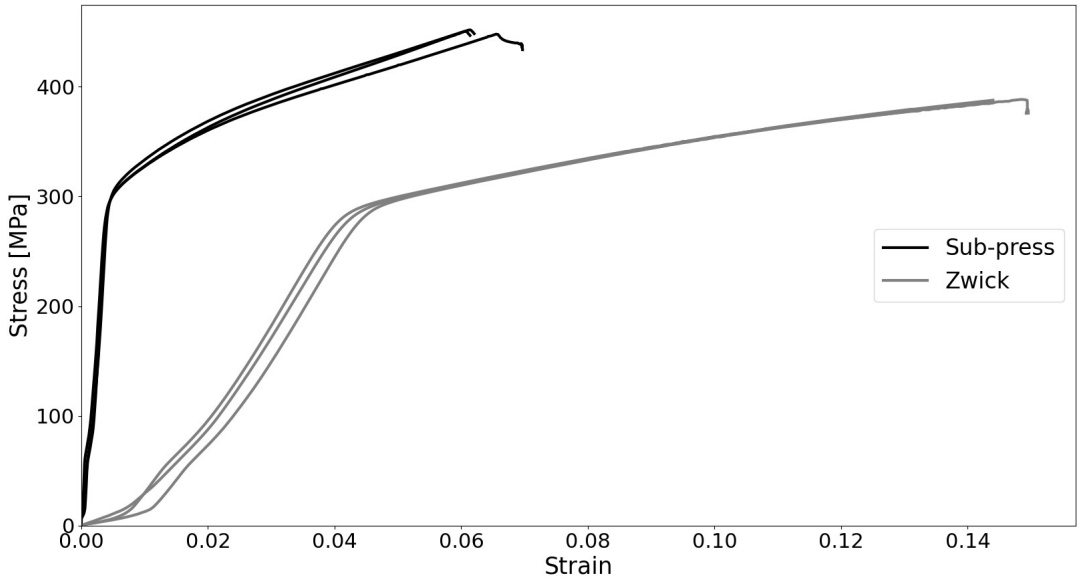

Figure 3.16 An average stress-strain curve for three PoP tests.

ing modulus in small specimens, whether composed of soft or hard materials and that its compliance can be successfully accounted for.

3.4 Multi-Machine Standard Material Tests

While the demonstration of the accuracy of a sub-press should be specimen independent, it is also useful to use standard materials with known elastic moduli to evaluate the operation of the sub-press. To this end, a multi-test approach was taken i.e. using three different standard testing techniques and apparatuses to characterise two standard materials. These tests were conducted by N. Daras [121], but not reported in detail. The principle of this approach is that, while any one of the techniques may provide an erroneous result, the possibility that all three techniques would provide near identical incorrect results is highly unlikely. These tests were conducted on PMMA and Al specimens as these two materials are known to have elastic moduli that encompass the range of expected elastic moduli for cortical bone [1]. Additionally, being synthetic and processed materials, it was anticipated that the specimens would behave in a consistent manner, therefore making them a reliable baseline to validate the operation of the sub-press.

These tests consisted of wave speed tests, tensile tests and quasi-static 3-point bending tests. A 2 m long 20 mm diameter rod of PMMA and another of Al were obtained for these tests. These rods were used as received for the wave speed tests and all the specimens used in the tensile tests and quasi-static 3-point bending tests were machined from the respective rods subsequent to the wave speed tests. Therefore, it is reasonable to expect that the respective results should all correlate. All specimen machining and preparation were conducted using a milling machine or a lathe. Further details of how the specimens were prepared are described in Section 3.5.1.

For the wave speed tests, shown in Figure 3.17, the rods were strain gauged in the centre and a short stress pulse, generated by the striker of a Hopkinson Pressure Bar (HPB), was captured as it propagated in the bar. Significant pulse shaping was applied to reduce dispersion and attenuation. This is shown in Figure 3.18.

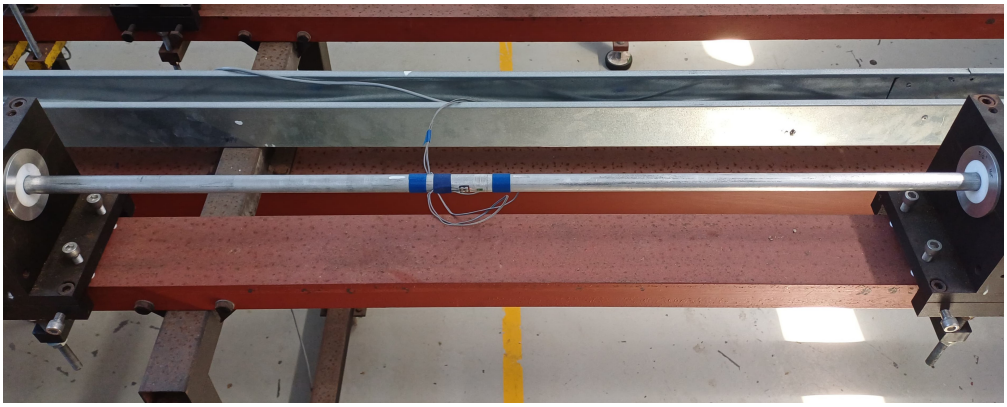

Figure 3.17 A 2m long Al rod fixed in a SHPB set-up for wave-speed tests.

From the measured wave speed and density, the modulus could be calculated using simple stress wave theory:

$$c = x_{\mathrm{w}} \left(\frac{v_{\mathrm{w}}}{2} \right) \tag{3.10}$$

$$E = \rho c^2 \tag{3.11}$$

where the symbol c is the material speed of sound in m/s; x_{w} is the distance the wave had to travel along the HPB in mm; v_{w} is the wave speed in ms; E is the modulus in GPa and ρ is the density in kg/m^3. The results of four tests per material showed an average modulus of 3.85 GPa within a range of 3.81 GPa to 3.88 GPa for the PMMA and an average modulus of 75.15 GPa within a range of 74.9 GPa to 75.4 GPa for the Al.

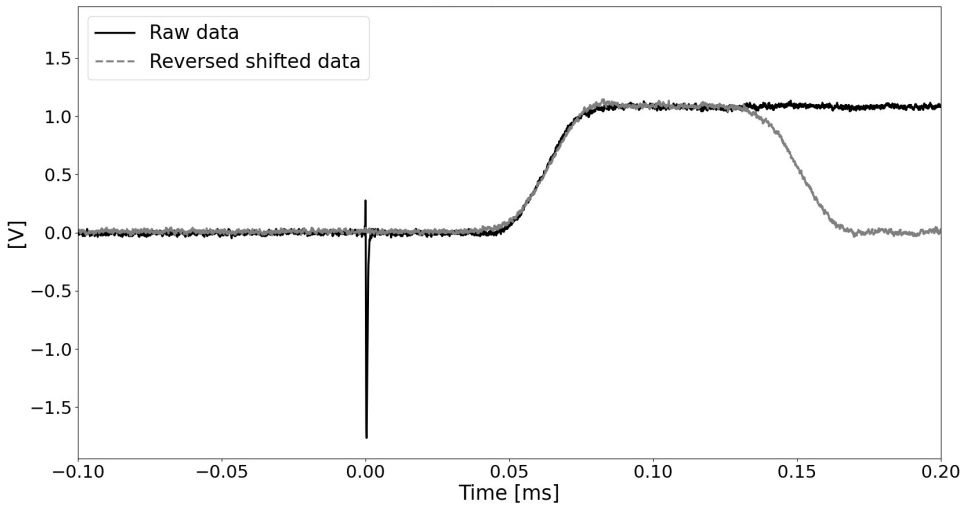

Figure 3.18 A plot of the stress pulse and reversed reflective wave for a wave-speed test on Al, after pulse shaping has been applied.

The tensile tests involved using the Zwick UTM in a tensile configuration, as shown in Figure 3.19, but using a visual extensometre to measure displacement directly on long thin specimens with a cross section of 5 mm x 5 mm and a length of 400 mm, cut from the original rods. The results of two tests for each material showed an average modulus of 3.98 GPa and 73.61 GPa for the PMMA and Al, respectively.

The quasi-static 3-point bending tests were performed on an Instron 3365 UTM, shown in Figure 3.20). These tests required machine compliance correction to account for the compliance of the UTM and the test fixtures. This was done through two test series with the first series using a single bending specimen with a cross section of 5 mm x 5 mm and 40 mm length, and the second series using two bending specimens placed alongside each other.

Similarly to the sub-press in Section 3.3, if machine compliance were non-existent, the single specimen test would theoretically exhibit exactly half the stiffness of the double specimen test. However, since machine compliance is present and the same for both single and double specimen test, both the specimen and machine stiffness

can be obtained from the equations:

$$\left(\frac{\delta}{F}\right)_1 = \frac{1}{k_{\text{UTM}}} + \frac{1}{k_s} \tag{3.12}$$

$$\left(\frac{\delta}{F}\right)_2 = \frac{1}{k_{\text{UTM}}} + \frac{1}{2k_s} \tag{3.13}$$

where the symbol δ denotes the measured combined deformation; F is the measured force; k_{UTM} is the stiffness of the Instron universal testing machine and k_{s} is the stiffness of a single specimen.

Solving for equations 3.12 and 3.13 simultaneously, the stiffness of the machine was calculated as 102.88 kN/mm and was then accounted for. This resulted in an average modulus of 3.24 GPa with a standard deviation of 0.093 GPa for the PMMA, and 74.78 GPa with a standard deviation of 0.996 GPa for the Al.

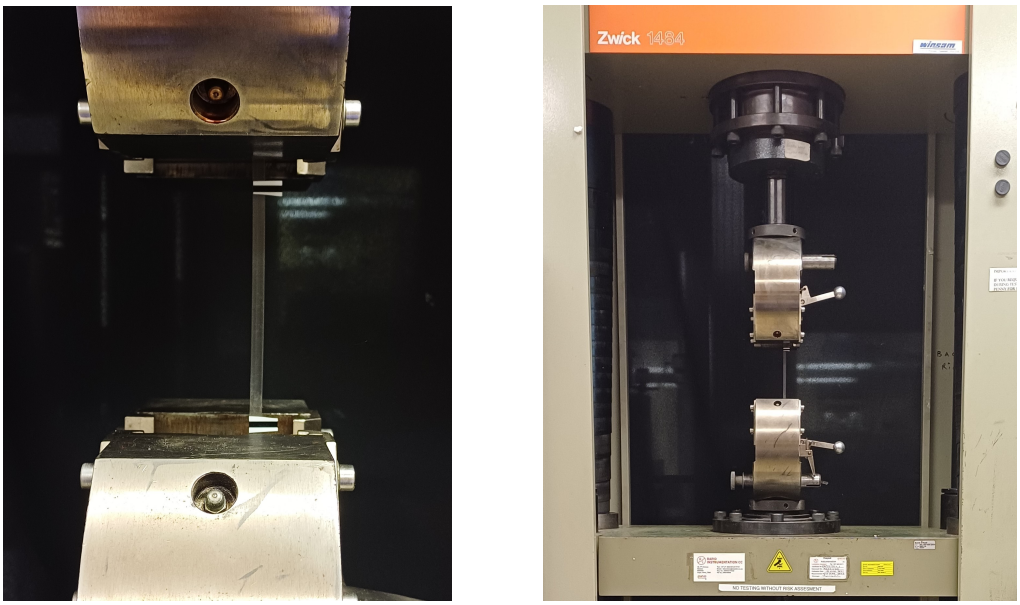

(a) **(b)**

Figure 3.19 A tensile test set-up with (a) A close-up of a PMMA tensile specimen in the UTM grips and marked with horizontal lines for the VE and (b) A view of the UTM in a tensile configuration with a PMMA tensile specimen clamped in the UTM grips.

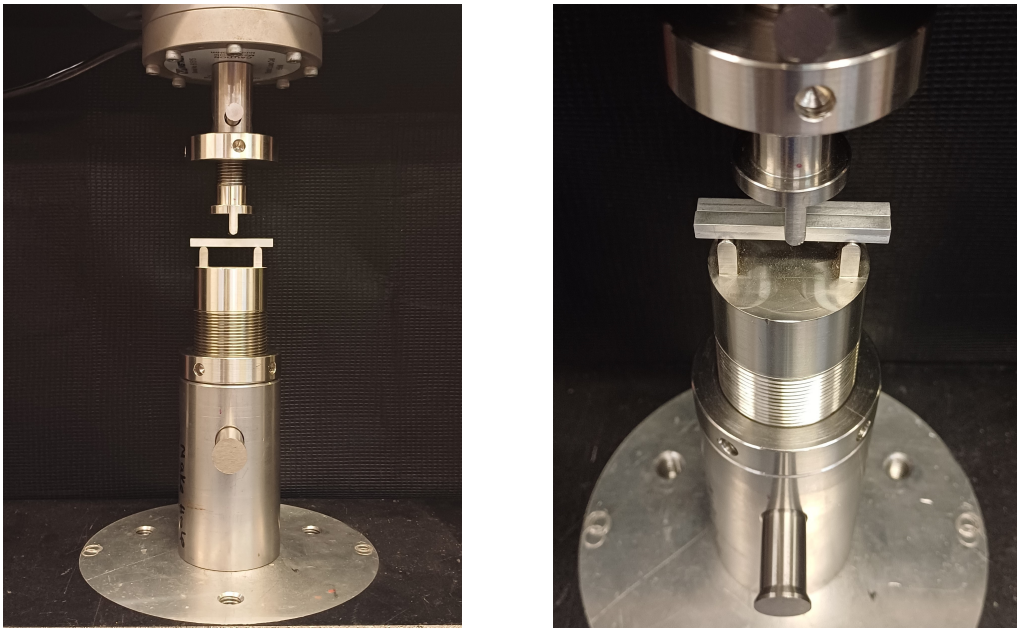

(a) **(b)**

Figure 3.20 A 3-point bending test set-up with (a) A single Al 3-point bending specimen on the Instron 3-point bending test set-up and (b) A double Al 3-point bending specimen on the Instron 3-point bending test set-up.

The close agreement of these three distinct testing techniques, shown in Figure 3.21, strongly suggests that the modulus of the PMMA and Al specimens are well characterized and can be used as reference materials to assess results obtained from the sub-press. Furthermore, the results from the QS sub-press tests are also in close agreement with the multi-machine test results especially the wave-speed tests. The specimens required for the multi-machine tests are also much larger than the specimens used with the sub-press, meaning more material is required for these testing methods, which is not always a viable option.

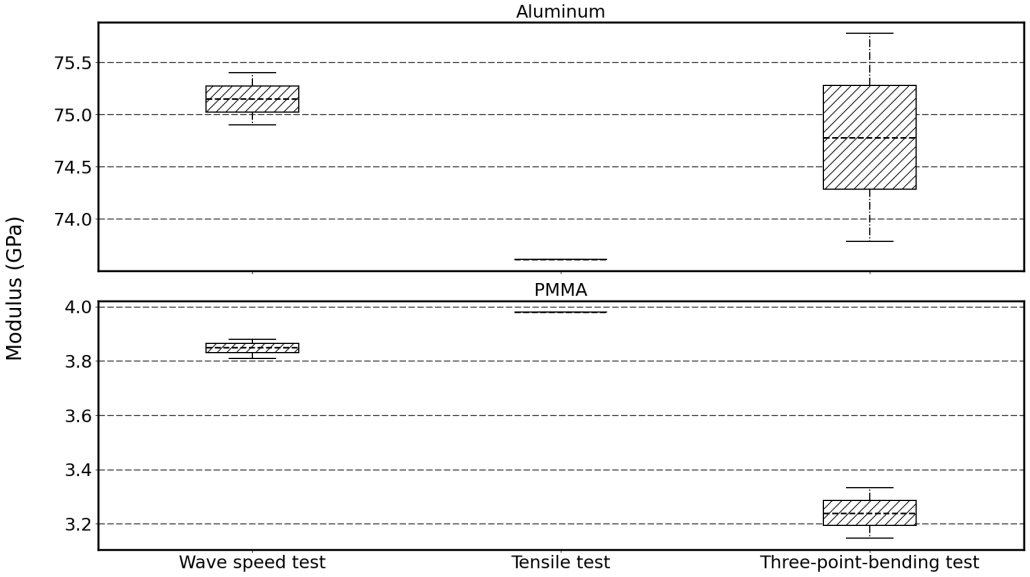

Figure 3.21 A box-and-whisker plot for the three different testing methods. Note the tensile test results consist of only two tests for each material.

3.5 Bone Specimen Preparation

There are numerous factors can effect the response of bone to stress, as is evident in literature (Section 2.2). For this study, it was imperative to reduce the number of variables that could contribute to differentiating bone properties, as much as possible. All bone was thus sourced from the same place and on the same day. Bovine bone was chosen as it was readily available in the given location and time-frame. Bovine bone has also been shown to yield greater specimen sizes due to a thicker cortical layer, ultimately yielding more consistent results. Fresh[1] femurs from adult bovine were sourced and collected directly from Bill Riley Meat in Brooklyn, Cape Town. Each bovine femur was selected by hand by the researcher from a bin of femurs. The femurs were chosen based on the thickness of the cortical layer and overall size of the femur, with preference given to the largest and thickest bones. Since these bones were from food animals, they were free of illnesses and were slaughter for production purposes. As the bones used in this study were merely a by-product of the food industry, no further ethical clearance

[1]Bone material that has an age of less than 24 hours post-mortem, and has never been frozen as a whole bone or specimen.

was required (ethical clearance forms can be seen in Appendix D). The precise age and the sex of the donor animals from which the bones were sources, is unknown.

For this study, a height-to-diameter ratio of 2:1 was used to remain as close as possible to rigid plastic standards [91, 92] as mentioned in Section 2.6, but still maximise the number of specimens retrieved from a single donor bone.

3.5.1 Specimen Machining and Storage

For the degradation study, three fresh cow femurs were obtained, one for each round of testing: 1. fresh; 2. one month in storage; and 3. three months in storage. This timeline was selected based on a logarithmic scale from day 0 to six months, following a similar approach to Daras [121], as it provides a broader representation compared to evenly spaced time intervals. One femur was worked with at a time to prevent inadvertent mislabelling. Any extra meat or membrane from the bone's exterior was scraped off using a utility knife. From bone one, the proximal, medial and distal sections, shown in Figure 3.22, were cut using a table saw to form medallions as shown in Figure 3.23a. After removal of the bone marrow, the hollowed-out bone medallions were halved and machined into sectors: anterior lateral; anterior medial; posterior lateral and posterior medial, shown in Figure 3.22, to form longitudinal strips as shown in Figures 3.23b and 3.23c.

A belt sander was then used to roughly grind down each of these strips into a more symmetrically shape. This was done to ensure that the bone would remain firmly in the chuck of the lathe, as shown in Figure 3.23d, for additional machining and to ensure that the bone would not wobble from being held off-centre when being turned. Using a lathe, these bone strips were formed into smooth cylinders. Once cylindrical, a small piece was cut off at the appropriate length to form a single bone specimen. All the specimens had a slight protrusion on one face from the sectioning process. To get rid of this protrusion, the affected face was sanded with fine grit sandpaper. The mass, length and diameter of each specimen was recorded using a Sartorious Analytical Lab Balance Scale with a readability of 0.1 mg and a Micro-Tec Dial-150 Vernier Caliper with a 0–150 mm range and a 0.01 mm resolution. Each specimen was kept in saline in a clear specimen container, depicted in Figure 3.24, and was labelled according to the specimen designation shown in Figure 3.25.

Two 5 mm diameter by 10 mm length specimens were machined from each sector of bone one (anterior lateral; anterior medial; posterior lateral and posterior medial) totalling in 24 specimens per whole bone. Bones two and three were cut in half, through the medial section. The proximal half of bones two and three were machined in a similar fashion to bone one (totalling in 12 5 mm x 10 mm specimens each) whereas the distal halves were kept whole and were wrapped in sterile, saline-soaked gauze and placed in individual, labelled plastic bags. As mentioned in Section 2.7, it is advised against using PBS for long-term storage below freezing temperatures, thus a normal saline solution (9% NaCl) was used instead. The 'heads' of the distal halves were kept attached to indicate the orientation of the bone for later machining. The specimens from bone one were tested on the same day as whole bones were acquired and machined, i.e. within 24hours of slaughter. The specimens and whole halves from bones two and three were taken to the wet lab in the Blast Impact and Survivability Research Unit (BISRU) and placed into

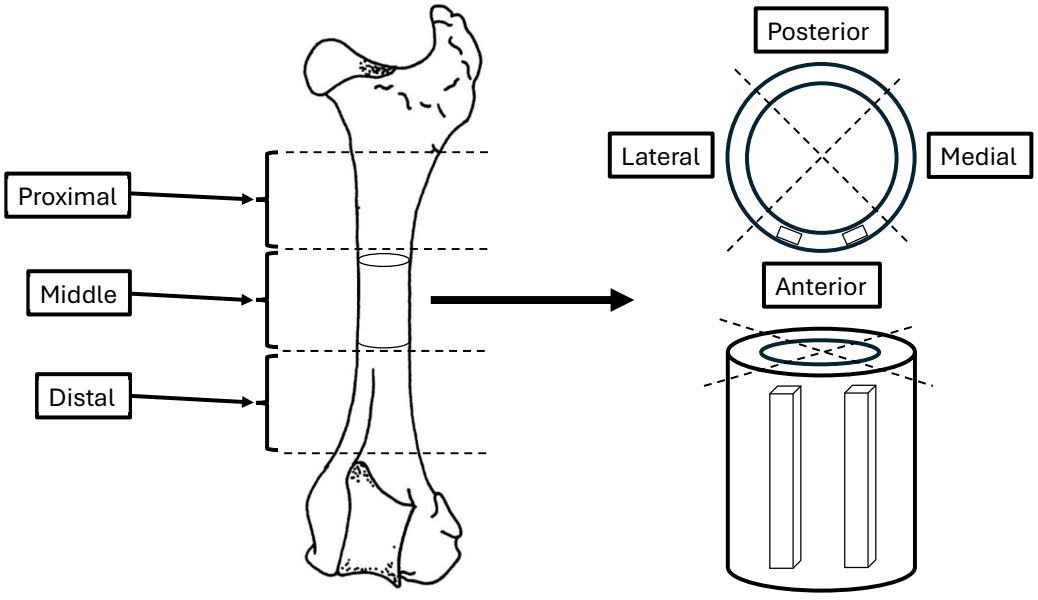

Figure 3.22 A schematic showing the location naming convention of specimens from a bovine femur.

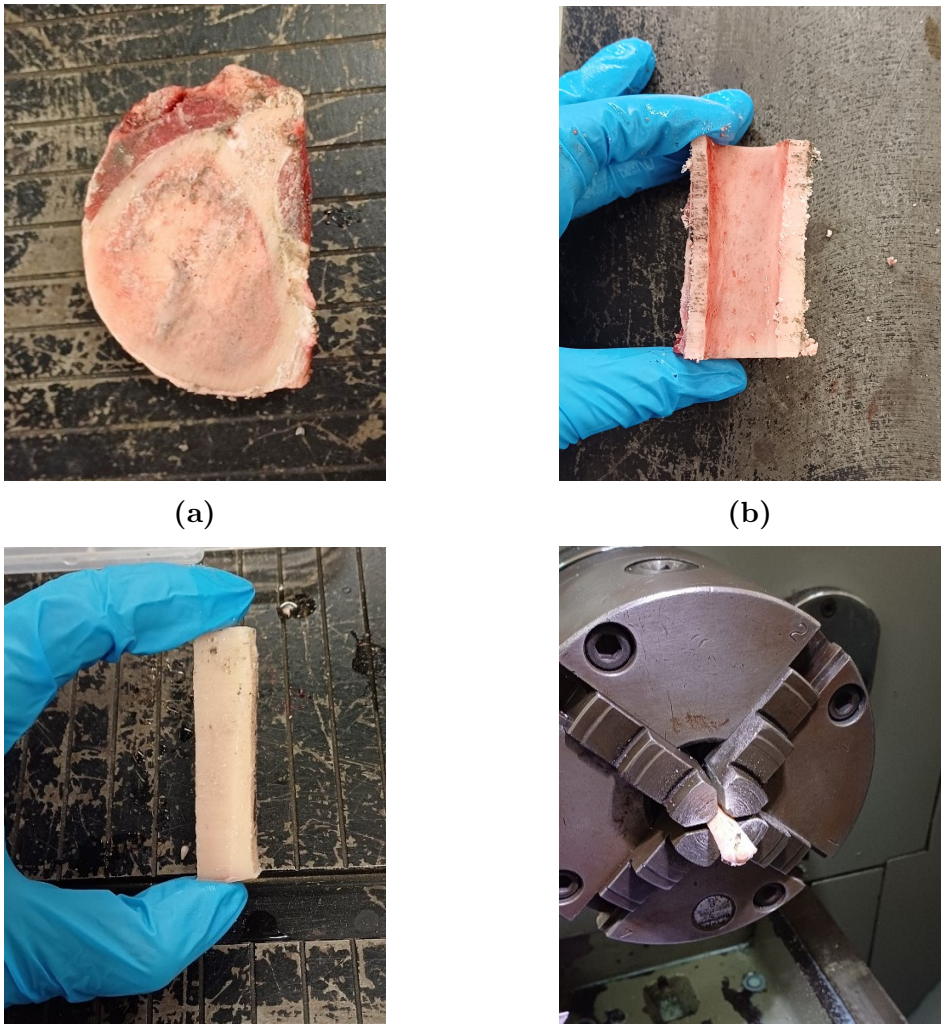

(a) **(b)**

(c) **(d)**

Figure 3.23 Bovine cortical bone specimen preparation with (a) A bone medallion machined from the medial section of a bovine femur, (b) The halved, hollowed-out bone medallion, (c) A longitudinal bone strip machined from the anterior lateral sector of the hollowed-out bone medallion and (d) The bone strip secured in the chuck of the lathe.

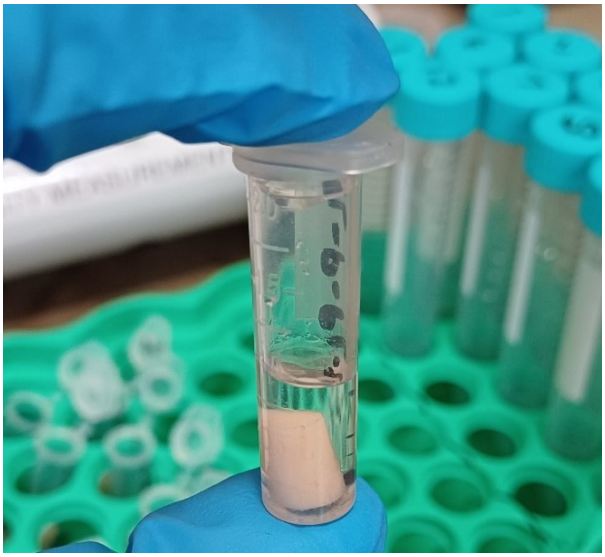

Figure 3.24 A bone specimen in saline in a clear, labelled specimen container.

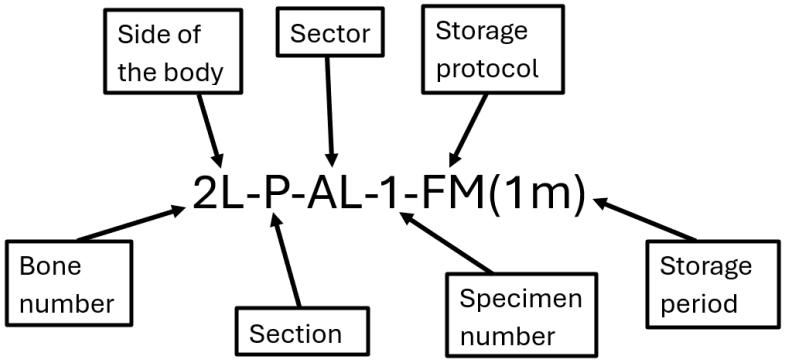

Figure 3.25 An example of the designation for a specimen taken from bone number two (which was taken from the left side of the body), from the proximal section and anterior lateral sector, specimen number one of two, frozen first as a whole bone and then machined (freeze-machine) and was stored for one month.

the bio-freezer, where they were kept frozen at -32°C to be machined and/or tested at a later date, to allow for the assessment of degradation of the material properties of bone due to longer storage times and to assess whether these properties degrade differently with different storage methods (specimen storage vs whole-bone stor-

age). Special care was given to label each bone and specimen correctly throughout the entire machining process.

The whole halves of bones two and three were machined at a later time (after 1 month in storage and after 3 months in storage, respectively). The whole half of each bone was taken out of the freezer on each of the respective testing days and allowed to thaw completely before machining. The same machining process was followed as on the first day (two 5 mm diameter by 10 mm length specimens from each sector of the bone).

3.6 Quasi-Static Testing

Quasi-static testing, was done in two series i.e. to assess degradation of the mechanical properties of cortical bone after long-term storage and to assess the machine compliance of the sub-press. The experimental set-up, testing procedures and data processing required to extract the compressive strengths and apparent modulus from a specimen are described in the subsequent subsections.

3.6.1 Experimental Setup

A Zwick 1484 UTM, located in the UCT's Centre for Materials Engineering (CME), was utilized for both series of quasi-static tests. The UTM was configured with a 10kN load cell for compression testing. The plunger of the sub-press was threaded in to the 10kN load cell and the base of the sub-press was secured to the base plate of the UTM using two M8 bolts. The Arduino micro-controller was then connected to the sensors in the sub-press and to a laptop using a data cable.

3.6.2 Testing Procedure

The flat platen variation of the sub-press (or the unmodified sub-press) was shown in Section 3.3.4 to be effective for low-modulus materials like PMMA. Given that bone has a similar stiffness to PMMA, it was concluded that the flat platen variation of the sub-press would be sufficient for the degradation study. Tests took place in three rounds i.e. 1. fresh; 2. after one month in storage; and 3. after three months in storage. For round one the fresh specimens were tested on the same day of collection and machining. Each specimen was removed from the saline

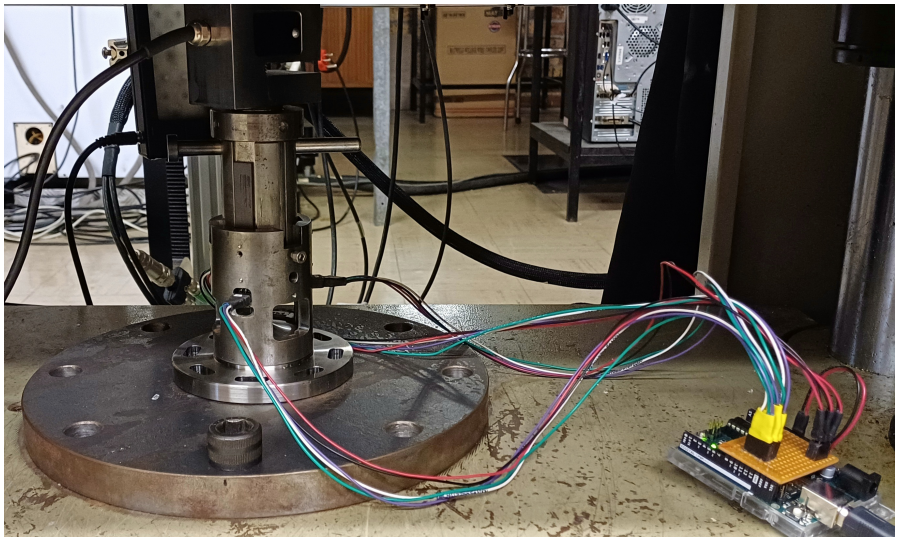

Figure 3.26 Experimental set-up of the sub-press set up inside the Zwick UTM with the data lead cables connecting the sensors to the micro-controller.

solution, and any excess saline clinging to the specimen was removed by dabbing gently with paper towel. The specimen was then placed face down (so that the cylinder stood upright) in to the sub-press (using tweezers) centred on the stage of the base. The upper testing platform of the UTM was manually lowered until the bottom of the plunger almost touched the upper face of the specimen (this was done to reduce the amount of time needed before the test started, and to prevent a sudden stress increase when the testing surface suddenly comes into contact with the specimen) and the UTM cross-head absolute was set at this point so that the cross-head could return to that position after each test. To make sure the specimen was not being pre-loaded, the computer's digital readout was monitored closely. For rounds two and three of the degradation tests, the frozen machined specimens and whole bones were removed from the freezer and allowed to thaw on each of the respective testing days. The whole bones were machined as described in Section 3.5.1 and the same testing procedures were used as in round one.

For the sub-press compliance tests the same testing procedure was followed as for the degradation study. The testing procedure also remained mostly the same regardless of specimen material or geometry, or which sub-press platen variation

was used, the UTM cross-head absolute, however, had to be reset between different specimen geometries or if a different sub-press platen variation was used.

Compression tests were performed at a strain rate of 0.01 s^{-1} for both series of testing and data acquisition rates for the cross-head displacement and the sub-press displacement were set to 100 Hz. The main focus was on the elastic portion of the material response, hence the test was terminated when the specimens started to exhibit non-elastic behaviour. To ensure the testing conditions remain exactly the same for each round of tests, all the specimens from each round were tested on a single day.

3.6.3 Data Processing

This section reviews the processes applied to the data gathered from the quasi-static testing. It discussed the analysis of the raw stress strain data to obtain modulus and UCS for the PMMA, Al and bone tests as well as the log-normal analysis that was applied to the cortical bone data post-processing to account for any skewness. This is shown in more detail in Appendix B and C.

3.6.3.1 Stress-Strain Analysis

Upon completion of daily tests, data from the UTM were exported as a CSV files and saved along with sub-press data collected from the hall effect sensors and magnetic strips via an Arduino micro-controller. These files are stored in a folder labelled with the test series name and date. A Python script was used for data processing. First, the script prompts the user to select the UTM test data file and choose a specific specimen for analysis. It then generates a displacement versus time plot for the selected specimen. The user manually selects six points on this plot, and the nearest data rows are identified. Straight lines are fitted between these points to capture key transitions, and the times of these transitions are calculated based on the intersection of the fitted lines.

Next, the data is truncated to remove irrelevant sections before the datum, and displacement, force, and time values are zeroed for further analysis. The script interpolates the data at regular intervals (0.1 seconds) to create a consistent time series. Verification plots of displacement and force versus time are generated to ensure accuracy. A similar process is applied to sub-press data, where displacement

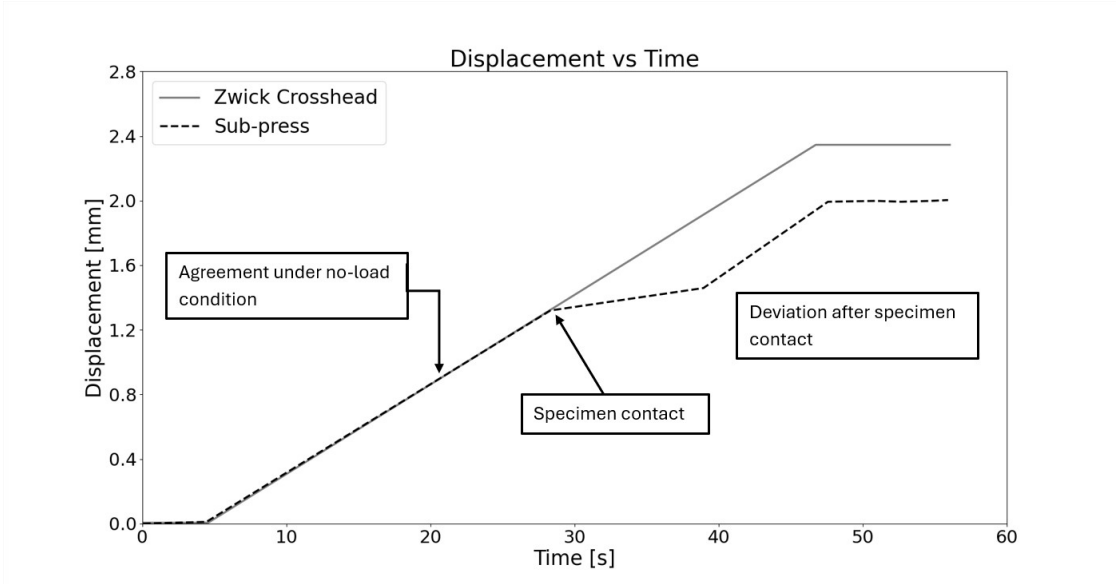

Figure 3.27 Comparison of typical sub-press (–) and UTM cross-head (—) displacement vs time data for a bovine cortical bone test.

values are smoothed and converted from μm to mm. The UTM and sub-press data are then synchronized and combined into a single dataset.

These combined UTM and sub-press displacement vs time plots revealed a significant deviation between the sub-press displacement data and the UTM cross-head data, as shown in Figure 3.27. During no-load conditions, before the plunger impacted the specimen, the sub-press and cross-head displacement-time data were essentially identical, differing by less than two microns. This no-load phase established a datum for synchronizing sub-press displacement data with the force data from the testing machine software, preventing specimen pre-loading.

Following this, the script calculates stress and strain values based on user-provided specimen dimensions (diameter, height, and weight). The calculated stress and strain data are added to the combined dataset. Finally, a stress-strain and strain rate plot is generated and a gradient calculation of the elastic portion is made to determine the modulus. The results are exported as a CSV file for further analysis.

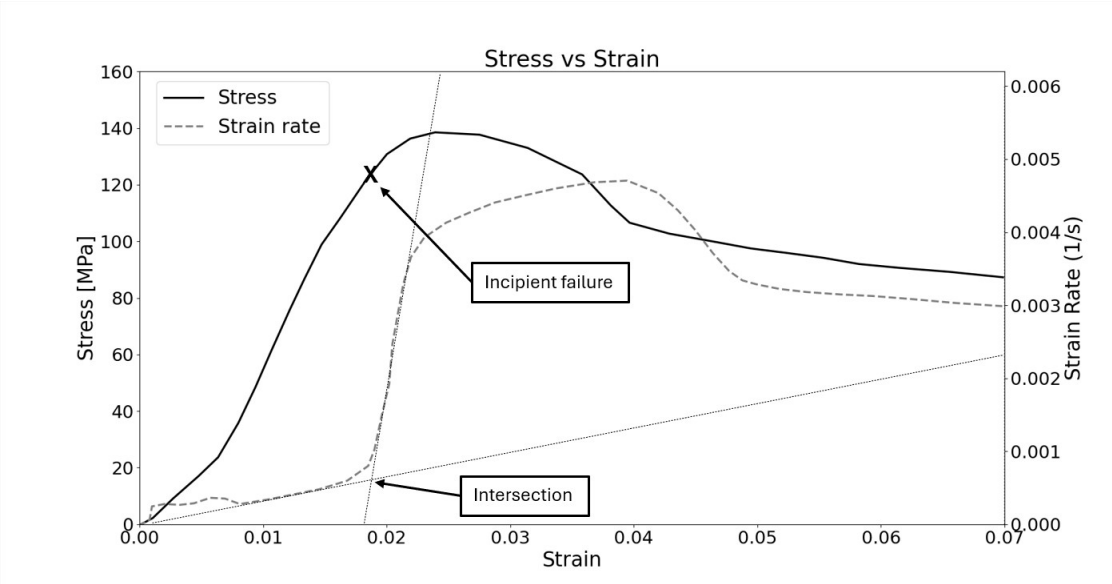

Figure 3.28 A typical stress and strain rate vs strain plot for a bone specimen.

The stress-strain and strain rate curve, shown in Figure 3.28, revealed that the actual strain rate was lower than the 0.01 s^{-1} set by the UTM until after specimen failure. The sharp increase in strain rate near maximum stress indicated the point of incipient failure, which is crucial for accurate material characterization. The point of incipient failure of a specimen is identified using two linear fits on the stress-strain and strain rate plot. The first linear fit is generated over the region of the strain rate plot where the specimen is deforming at a near constant strain rate. This can be seen by the initial flat portion of the strain rate data. The second linear fit is generated over the region of rapid increase in strain rate. This is interpreted as the region wherein the elastic energy built up during the take-up in machine compliance is being released as the specimen begins to lose structural integrity and cannot offer any resistance to the cross-head. It is interesting to note that there is no perceptible deviation in the stress vs strain curve at this point, i.e. without a detailed strain rate history the point of incipient failure is undetectable.

3.6.3.2 Log-normal Analysis

To analyse data sets exhibiting skewed distributions, a three-parameter log-normal distribution was employed [122, 123, 124, 125]. This approach assumes that the logarithm of the data, combined with a constant parameter (λ), follows a normal distribution. For positively skewed data, the transformation is given by:

$$Y = \ln(X - \lambda) \tag{3.14}$$

where X represents the original data, and λ is a threshold parameter chosen by the data analyst to ensure the logarithmic transformation is valid.

The mean, median, and mode of the original data X can be computed from the transformed data Y using the following equations [122, 123, 124, 125]:

$$\text{Mean}(X) = \lambda + \exp(\mu + \frac{\theta^2}{2}) \tag{3.15}$$

$$\text{Median}(X) = \lambda + \exp(\mu) \tag{3.16}$$

$$\text{Mode}(X) = \lambda + \exp(\mu - \theta^2) \tag{3.17}$$

where μ is the mean of the logarithmic values, and θ^2 is the variance.

For negatively skewed data, where values cluster around an upper bound, the transformation becomes:

$$Y = \ln(\lambda - X) \tag{3.18}$$

This leads to the following modified equations for the mean, median, and mode:

$$\text{Mean}(X) = \lambda - \exp(\mu + \frac{\theta^2}{2}) \tag{3.19}$$

$$\text{Median}(X) = \lambda - \exp(\mu) \tag{3.20}$$

$$\text{Mode}(X) = \lambda - \exp(\mu - \theta^2) \tag{3.21}$$

For each data set, λ was assigned a value two units larger than the minimum value to avoid invalid logarithmic calculations. The logarithmic transformation was then performed, and the skewness of the log values was minimised using a skewness analysis and a goal-seek function in Microsoft Excel. Once the log values were optimised, μ and θ were calculated as the mean and standard deviation of the logarithmic set, respectively. These values were then used to compute the mean, median, and mode in the original data frame.

This method allowed for a more accurate representation of the skewed data compared to assuming a standard normal distribution.

Chapter 4

Experimental Results

This section contains the results after all data processing for all QS tests from the degradation study, with special interest in the apparent modulus and maximum compressive strength.

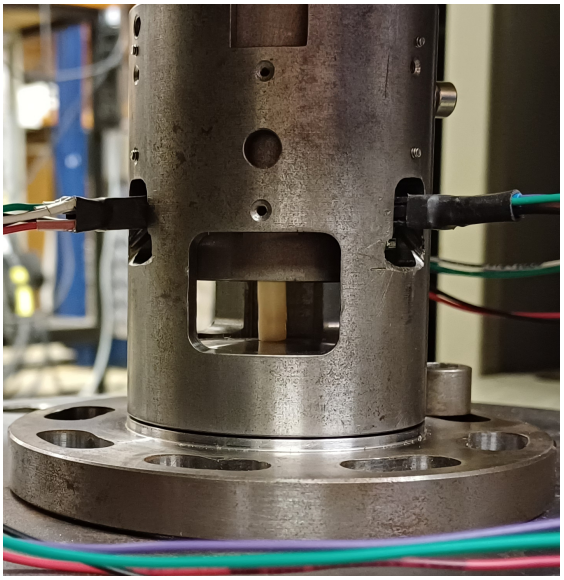

Figure 4.1 A bovine cortical bone specimen placed on the specimen stage in the sub-press.

4.1 Degradation Study

For this study, two storage protocols were followed namely "machine-freeze" (MF), i.e. specimen storage and "freeze-machine" (FM), i.e. whole-bone storage as discussed in Section 3.5. For both these protocols, specimens were tested fresh, after one month (1m) and after three months (3m). For the purpose of this dissertation, the term 'fresh' refers to bone material that has an age of less than 24 hours post-mortem, and has never been frozen as a whole bone or specimen.

The fresh bone showed an average apparent modulus of 12.86 GPa with a standard deviation of 0.66 GPa and an average ultimate compressive strength (UCS) of 175.17 MPa with a standard deviation of 7.8 MPa. Figure 4.2 shows the raw data from 24 compression tests. A representative test was selected from the dataset based on which specimen most closely aligned with the mean modulus calculated through the log-normal analysis described in Section 3.6.3. Figure displays the adjusted data with take-up removed, offering a clearer representation of the low scatter in results. Notably, the representative curve originates from the raw data

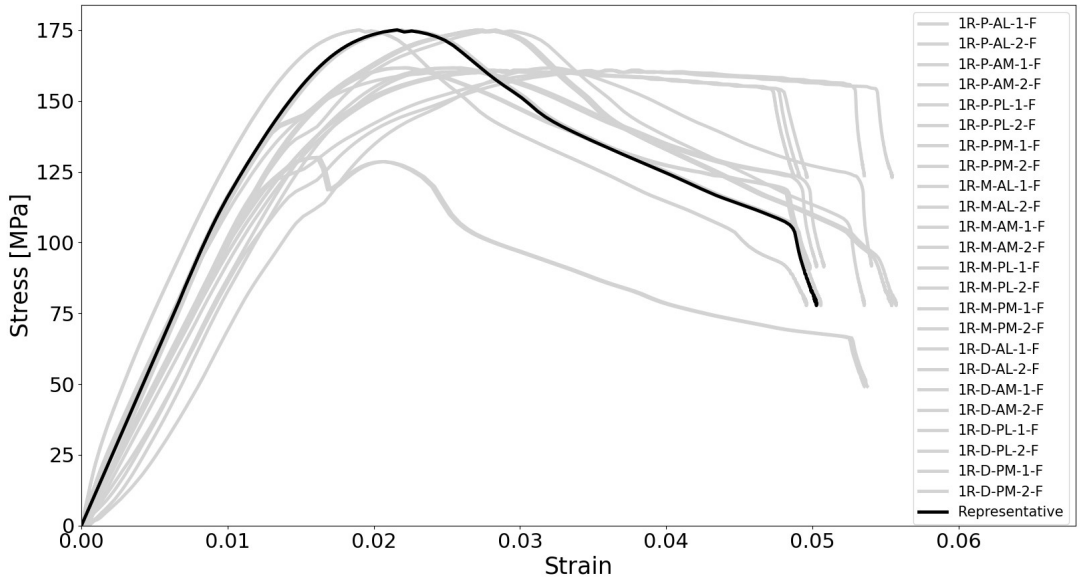

Figure 4.2 A raw stress-strain plot for 24 fresh bovine cortical bone specimens, with a representative curve superimposed.

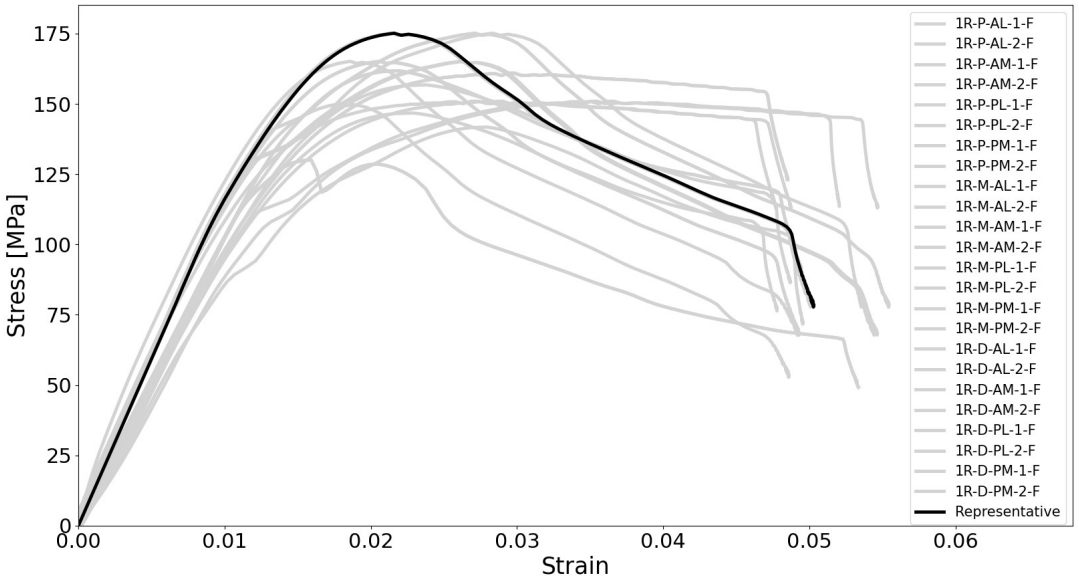

Figure 4.3 The shifted stress-strain plot for 24 fresh bovine cortical bone specimens, with a representative curve superimposed.

of an actual test, illustrating that, with precise specimen machining, preparation, and perfect centring on the lower platen, a distinct elastic region with no visible take-up can indeed be achieved.

The results after one month in storage showed an average apparent modulus of 9.98 GPa with a standard deviation of 1.18 GPa for the MF specimens as shown in Figure 4.4 and 10.46 GPa with a standard deviation of 1.8 GPa for the FM specimens as shown in Figure 4.5, indicating a better preservation of apparent modulus with whole-bone storage than with specimen storage, but still a noticeable decline in apparent modulus from fresh to one month. The results, also showed a slight decrease in UCS from fresh to one month in storage with the MF specimens having an average UCS of 159.8 MPa and the FM specimens having an average UCS of 164.8 MPa, with a standard deviation of 9.78 MPa and 14.8 MPa, respectively. In the later tests, as the specimen preparation process was practiced and refined, a noticeable reduction in scatter was observed in the raw data plots.

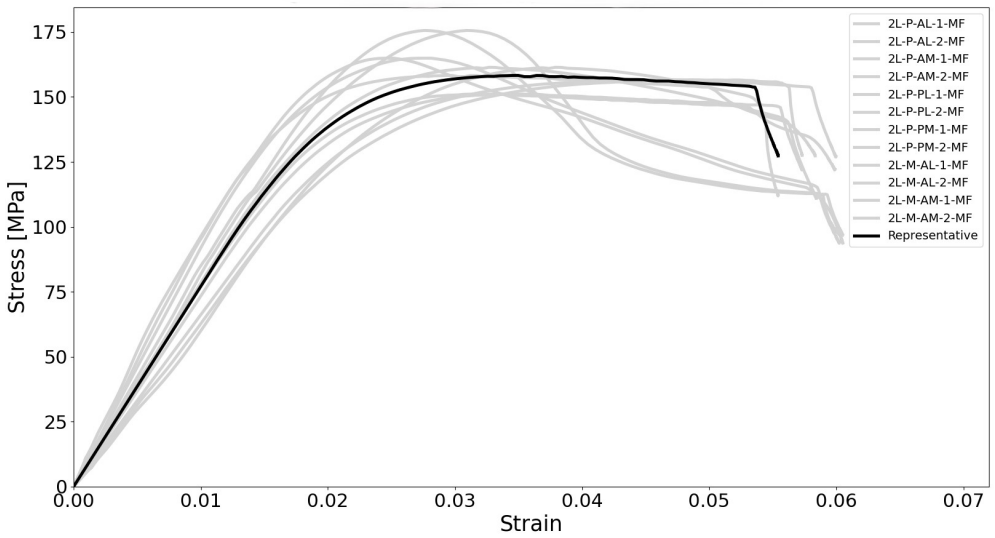

Figure 4.4 A raw stress-strain plot for 12 MF bovine cortical bone specimens after one month in storage, with a representative curve superimposed.

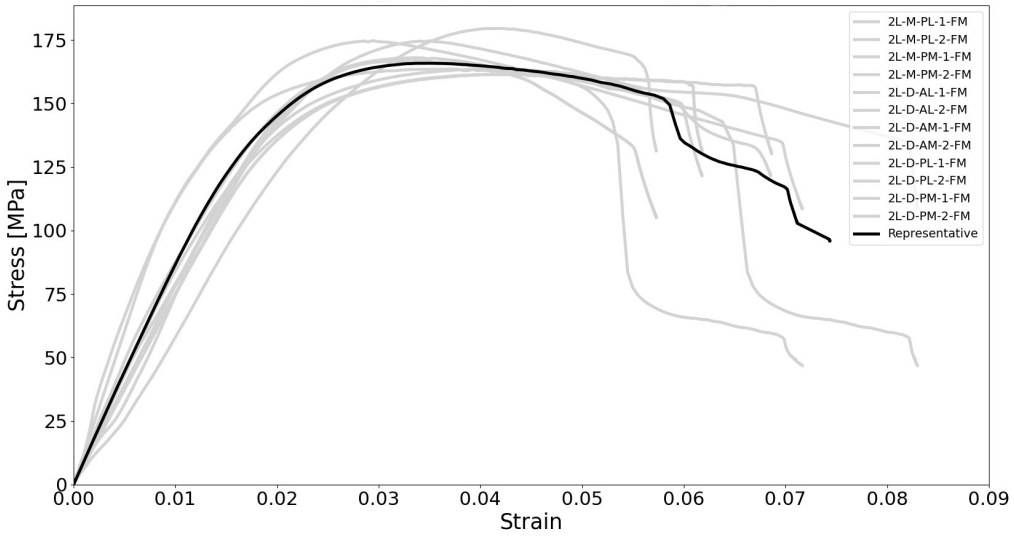

Figure 4.5 A raw stress-strain plot for 12 FM bovine cortical bone specimens after one month in storage, with a representative curve superimposed.

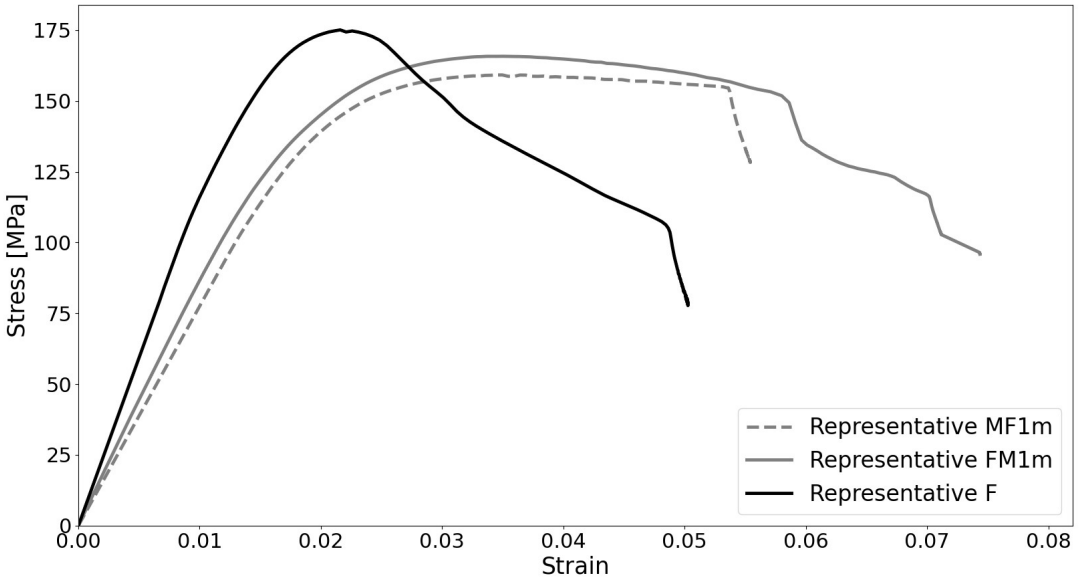

Figure 4.6 A comparison of the F and 1m results.

Specimens tested after 3 months in storage resulted in an apparent modulus of 6.42 GPa for the MF specimens as shown in Figure 4.7, with a standard deviation of 2.24 GPa and an apparent modulus of 7.22 for the FM specimens as shown in Figure 4.8, with a standard deviation of 2.30 GPa, approximately half the apparent modulus of the fresh bone, regardless of storage protocol. The UCS of the specimens stored for three months, however, increased from fresh and 1m with an average UCS of 192.2 MPa for the MF specimens with a standard deviation of 27.5 MPa and and average UCS of 199.5 MPa for the FM specimens with a standard deviation of 23.9 MPa. The large standard deviation in the average apparent modulus and average UCS for the 3m specimens compared to the fresh and 1m specimens, also indicates that long-term freezing not only affects the mechanical properties of bone, but also causes more variability within these properties [5]. Figure 4.9 shows the average stress vs strain plots for the MF and FM specimens

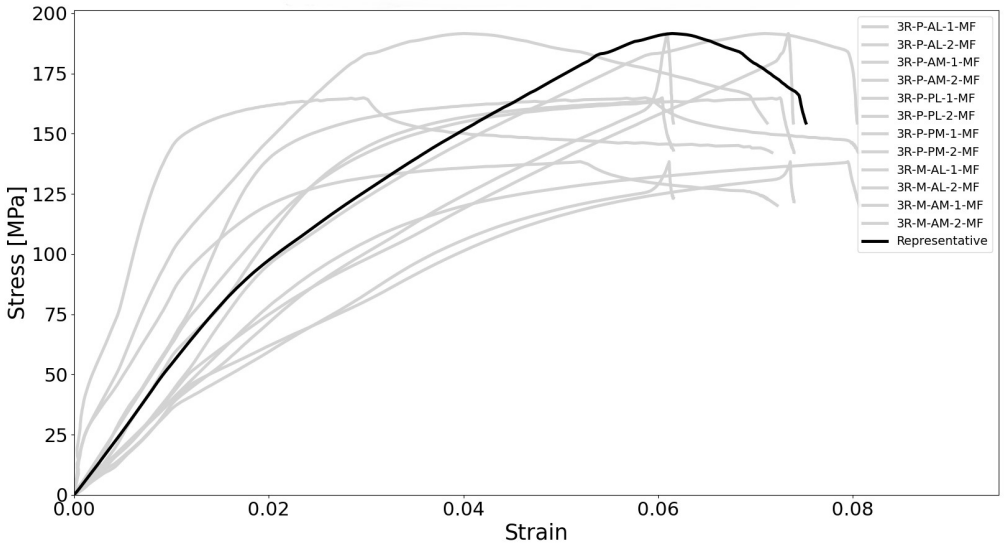

Figure 4.7 A raw stress vs strain plot for 12 MF bovine cortical bone specimens after three months in storage, with a representative curve superimposed.

Figure 4.10 shows the apparent moduli for the fresh specimens, with both normal and log-normal distributions displayed. The histogram shows that the data is lightly skewed to the left. As can be seen in Figures 4.10, a normal distribution (in grey) does not accurately represent the peak in the data. A log-normal distribution (in black) allows for the trailing values to be represented without allowing them to detract from the concentration of data at the higher end of the spectrum. It is important to note, however that as storage time progresses (from fresh to 1m to 3m), the normal distribution and log-normal distribution become closer, i.e. the 3-parameter log-normal analysis, as described in section 3.6.3, effectively reverts to a normal analysis if the original data is not skewed. Appendix C shows the normal and log-normal distributions for the other test series.

The apparent specimen density, showed little change over time, regardless of storage protocol with an average apparent density of 1.729 g/cm^3 for fresh specimens, an average apparent density of 1.801 g/cm^3 and 1.699 g/cm^3 for MF1m and FM1m specimens, respectively and finally an average apparent density of 1.799 g/cm^3 for MF3m specimens and 1.800 g/cm^3 for FM3m specimens.

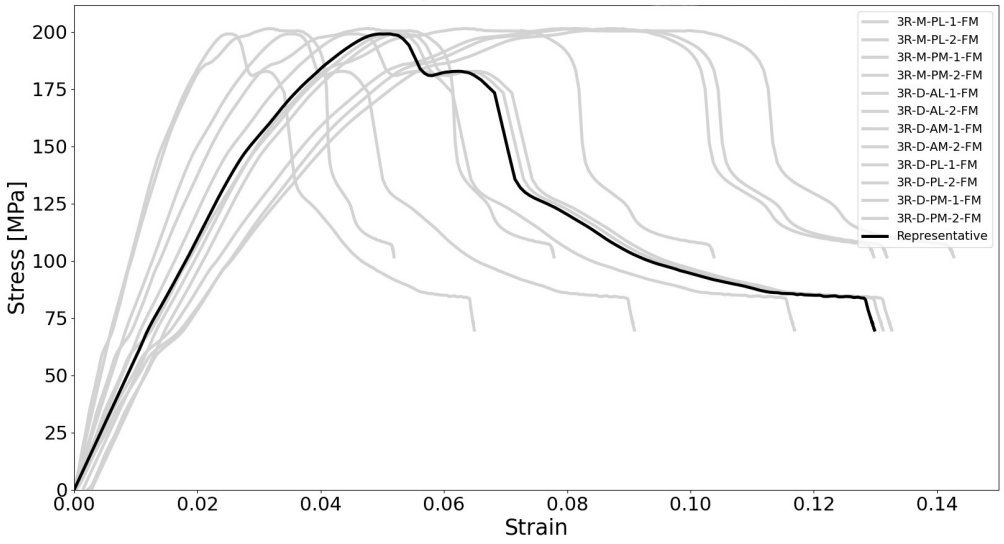

Figure 4.8 A raw stress vs strain plot for 12 FM bovine cortical bone specimens after three months in storage, with a representative curve superimposed.

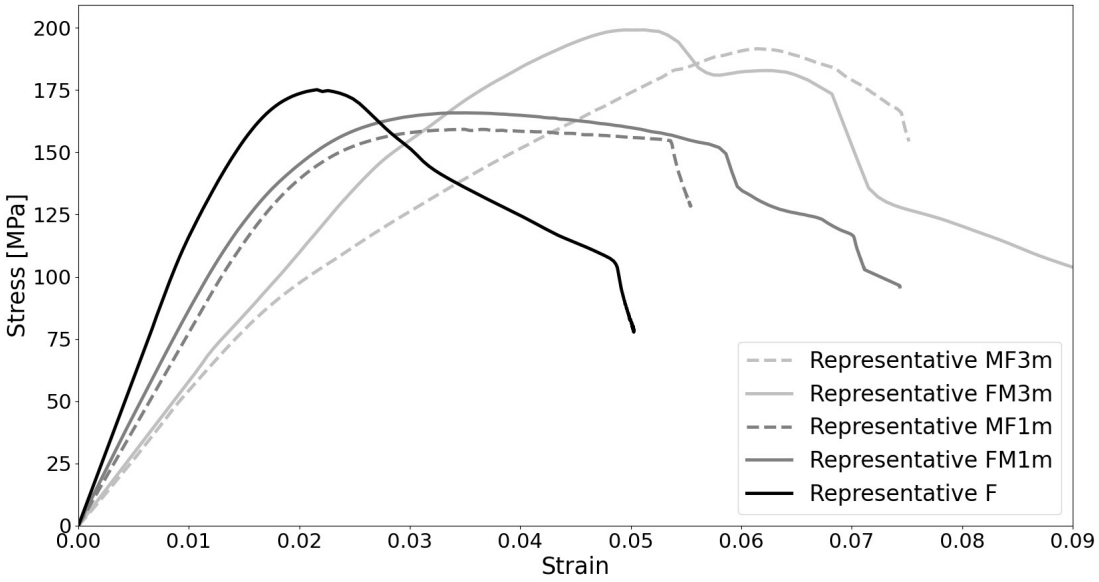

Figure 4.9 A comparison of the F, 1m and 3m results.

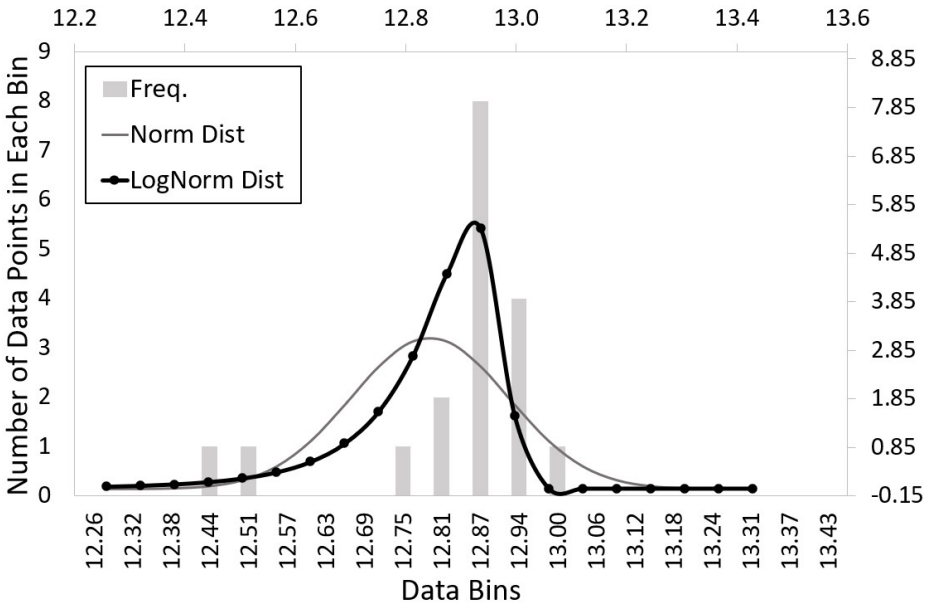

Figure 4.10 Apparent moduli for fresh specimens, with both normal and log-normal distributions displayed. The bottom and left axis represent the original data set whereas the top and right axis are continuous and represent the log transformed data.

Figure 4.11 shows a scatter plot of the apparent modulus values for each test series over time with the mode (obtained from the log-normal analysis) superimposed in black. The fresh results show very little scatter whereas the scatter increases for the one month and 3 month tests, with the 3 month results showing the most scatter. The slight horizontal offset in data points is merely for clarity, all specimens in a test series was tested on a single day.

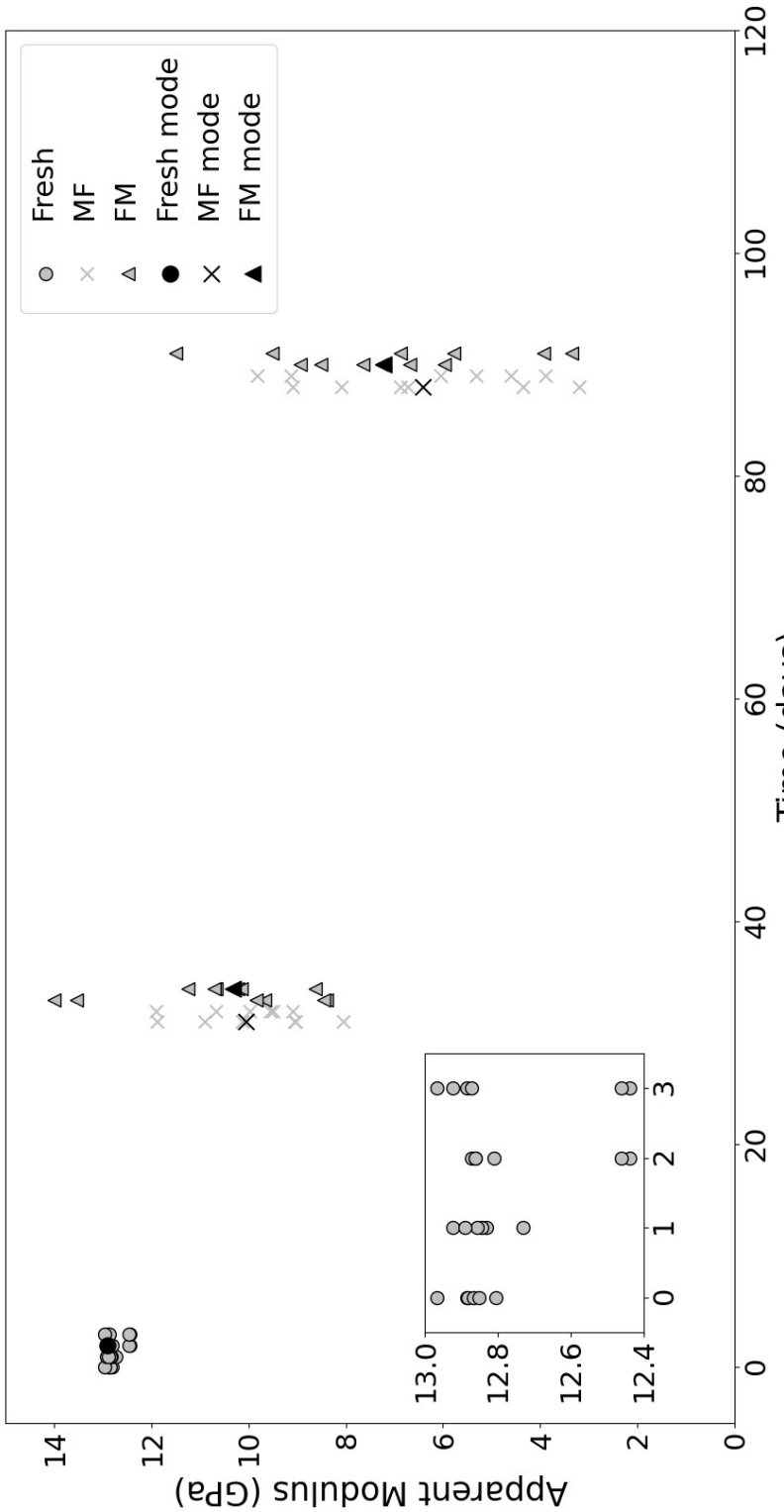

Figure 4.11 A scatter plot of the apparent moduli vs time for the different test series with a zoomed inset showing the scatter of the fresh results.The slight horizontal offset in data points is merely for clarity and all specimens in a test series were in fact tested on a single day.

4.1.1 Failure Modes

Three modes of failure were observed in the specimens post-testing and is shown in Figure 4.12. The fresh specimens failed by shear, but remained intact. The 1m specimens split straight down the middle of the specimen in the longitudinal direction and most of the specimens remained intact, although some split apart completely (this was mostly observed with the MF specimens). The 3m specimens simply crumbled apart from the top face of the specimen, downwards, regardless of storage protocol. These failure modes were consistent for all specimens depending on the test cycle (fresh, 1m, 3m).

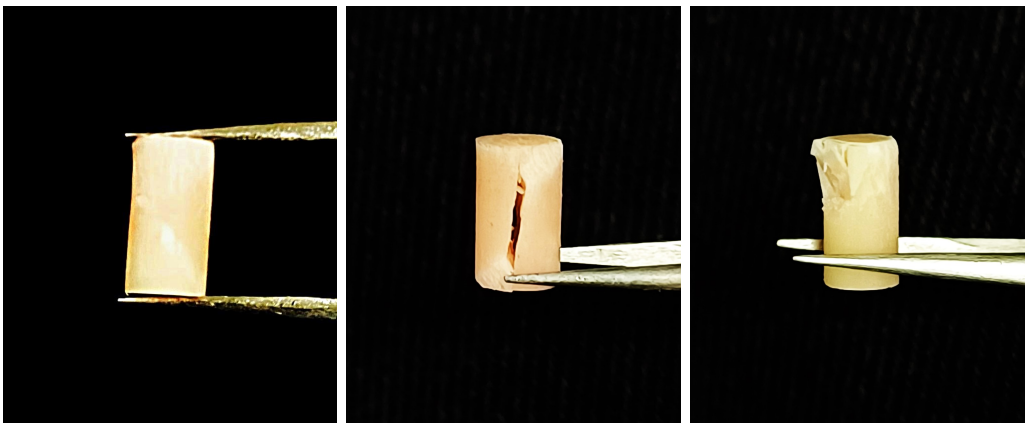

(a) **(b)** **(c)**

Figure 4.12 The different failure modes of bovine cortical bone specimens with (a) A fresh specimen after failure, (b) A 1m specimen after failure and (c) A 3m specimen after failure.

Chapter 5

Discussion

The focus of this section is on interpreting the results of this study in relation to the objectives. The primary aim was to study degradation in storage. The aim was pursued firstly, through a thorough literature review which led to the identification the primary objective, i.e. to assess two different storage protocols ("machine-freeze" (MF) and "freeze-machine"(FM)) in the preservation of the mechanical properties of bovine cortical bone in long-term storage. This, in turn, led to the secondary objective, i.e. validating the sub-press accuracy, which led to a tertiary objective, i.e. investigate local platen compliance with three distinct platen variations.

This section will provide an analysis of the results, beginning with a short summary of literature findings, followed by the validation of sub-press accuracy, the estimation of the sub-press compliance and assessment of the sub-press platen variations, and concluding with the findings from the degradation study. Key observations regarding the consistency, variability, and failure modes will also be discussed in relation to the existing literature, highlighting the implications for bio-mechanical testing and the overall significance of the findings.

5.1 Findings from Literature

This section explores a comprehensive review of the literature on a variety of topics, from bone structural properties across species to the effects of storage and

testing methods on bone response. Ultimately, these studies provide essential insights for understanding bone mechanics, the impact of specimen handling, and the experimental limitations that influence mechanical property assessments.

5.1.1 Factors That Influence Modulus and Other Mechanical Properties

When investigating the bone structure in different species, Brits *et al*. [24] found juvenile and adult human bone to have distinct properties and placed them in separate categories. The adult human bone displayed a mixture of primary vascular longitudinal bone along with dense and uneven Haversian bone. The osteons were either dispersed or closely packed, depending on their density. By contrast, the adolescent human bone primarily displayed uneven Haversian bone, along with sporadic secondary osteons and sizeable Haversian canals. This implies that the age of the person whose bone specimens were used may have a discernible impact on the micro-structure present.

It was also found that there are conflicting reports on the micro-structural organisation of ostrich bone. Spatz *et al*. [27] found ostrich cortical bone to be primarily fibrolamellar with minimal Haversian bone present by, which is consistent with the description provided by Castanet *et al*. [30]. By contrast, Currey [19] reports that ostriches frequently have substantial Haversian bone present. This discrepancy may be due in part to the fact that Spatz *et al*. [27] were basing their observations solely on the leg bones of the ostrich, and Castanet *et al*. [30] were basing their observations on long bones from the hind limb, whereas it is unclear where in the skeleton of the ostrich Currey's [19] specimens came from. Both groups relied solely on the leg bones of the ostrich for their observations. Furthermore, within a single species, the way in which the femur bears load will affect the specific micro-structures present [31]. As each species will stand and move in a different way, it makes sense that the load, and hence the micro-structure, will vary across species.

When investigating the effect of donor age on the mechanical response of bone, Martin & Atkinson [34] found that the material strength of bone actually increases initially up to the age of about 30, after which the strength starts to decline. Martin & Atkinson [34] attributed this to the fact that bone does not initially form as secondary osteons, but as primary bone, which becomes secondary bone

through remodelling as an individual ages. This implies that remodelling will gradually increase the porosity in the bone and number of cement lines present, but that this process takes time, as is demonstrated in this rise and fall of material strength.

Augat & Schorlemmer [32] found that the overall porosity of cortical bone increases with every remodelling of the tissue, due to the fact that not all of the previously removed material is fully replaced, indicating that bone becomes more porous as a result of this modification. Moreover, as an individual ages, there is more time for micro-damage to occur and accumulate, due to repeated loading of the bone [32, 37]. This suggests that the accumulation of micro-damage over time weakens the bone. This is supported by a study reported by Hui *et al*. [38], which revealed an increase in fracture occurrence in bones from older individuals. It should be emphasized that this specific study [38] combines information on fractures in the shafts of long bones with fractures in areas such as the head of the femur. It is important to note that this presents information on a combination of cortical and cancellous bone, with no clear way to separate out the response of the cortical bone specifically.

Ebbesen *et al*. [33], who specifically examined the mineral composition of trabecular bone, observed that trabecular bone has a lower bone mineral density as it ages. This may indicate that it is the cancellous bone that becomes weaker and the cortical bone fractures because it does not have enough support. As opposed to this, Currey *et al*. [35] found that mineral content increases with age. However, they [35] did find that toughness decreases with age, which concurs with the other studies mentioned. One possible cause for this difference in conclusion is the way each researcher assessed mineral content. Similar to Currey *et al*. [35] a study performed on porcine bone by Feng & Jasiuk [39] showed age-related changes in the structure and chemical composition of cortical bone and that mineral content and mineral-to-organic-ratio increased with age. This indicates that mineral content increased towards adulthood and thus implies that children's bones are weaker, but tougher.

While investigating the effect of micro-structural variations on bone response, Ebacher *et al*. [69] conducted a study of the failure of human cortical bone under compression. They observed that longitudinal specimens showed the development of cracks that were oblique to the osteonal direction and occasionally even had a

step-like appearance. Many uncracked fibril bundles remained connected across the crack as it mostly followed the circumference of the circular lamellae surrounding the osteons. The crack was found to consist of many small micro-cracks, as well as displaying evidence of some small crack interaction with present canaliculi, which are defined as tiny canals between natural bone cavities, although cracks were much more sensitive to the Haversian canals themselves and to osteocyte lacunae, which are defined as small cavities in the bone [69]. This highlights the significance of bone's highly hierarchical structure in terms of how it responds to stress, especially when it comes to controlled cracking that permits significant inelastic strain before macroscopic failure.

5.1.2 Post-mortem Age and Storage Protocols

The post-mortem age of bone specimens significantly influences their mechanical properties, as shown by studies by Lee & Jasiuk [5], Welgemoed [36], and Daras *et al*. [41]. These studies examined changes in the mechanical response of bone after extended storage, with each noting a reduction in properties like Young's modulus and ultimate strength over time. Lee & Jasiuk [5] observed diminished mechanical properties in porcine bone after one to five years of freezer storage, hypothesizing that ice crystal formation and enzyme activity cause structural degradation. Welgemoed [36] similarly identified reductions in apparent modulus in long-term frozen femurs, with less variation in compressive strength. Daras *et al*. [41] found severe degradation in cortical bone after six months regardless of storage method, and suggested that specimen storage durations of under one week are required to yield data representative of in-vivo properties. Collectively, these findings underline that long-term freezing can obscure correlations between porosity and bone mechanics, limiting the predictability of mechanical properties in aged bone specimens.

The storage conditions of bone specimens, such as the choice of storage solution, temperature, and duration, can significantly affect the mechanical properties measured during testing. Alcohol-glycerine storage, for instance, tends to enhance Young's modulus while reducing plastic energy absorption, likely due to water loss from the bone matrix, which can be reversed by rehydration in saline [95, 96]. Specimens stored in saline and frozen retain visco-plastic behaviour, closely mirroring fresh bone properties, whereas alcohol-stored specimens appear brittle. Studies

using formalin, such as those by Van Haaren *et al* . [2], found some preservation of mechanical properties; however, extended storage periods (e.g., eight weeks) led to changes in Young's modulus and ultimate strain [4]. Freezing, particularly below -20°C, generally preserves bone structure but can still result in degradation due to enzyme activity and crystal formation within the matrix [73, 5].

Recent protocols comparing refrigerated and frozen storage found that freezing whole bones before machining better maintains mechanical properties over time, although degradation increases significantly beyond six months regardless of the method [41]. Lee & Jasiuk [5] further observed that long-term freezing at -20°C weakens bone structure and diminishes the correlation between porosity and mechanical properties like Young's modulus[5]. Overall, choosing appropriate storage protocols is crucial to maintain bone integrity, with saline storage and short-term freezing providing better property retention than alternatives.

An extensive review of the literature revealed no clear definition of what constitutes "fresh" bone in testing, nor any consensus among researchers on this term.

5.1.3 Compression Testing and Machine Compliance

Quasi-static compression tests are essential for understanding the mechanical behaviour of a material under compressive loads, particularly for biological materials like bone. These tests utilize a universal testing machine (UTM), where the traditional gripping jaws are replaced by anvils or platens, applying force to specimens typically shaped as cubes or cylinders [104]. While the primary outcome of compression testing is the measurement of compressive strength, it can also provide insights into the material's plastic behaviour [105].

Strain measurement during these tests can be done through various techniques, including machine cross-head displacement, strain extensometers, and strain gauges. However, using cross-head displacement can introduce significant errors due to machine compliance (the inherent flexibility of the testing apparatus) which may lead to inaccurate strain readings, especially in small bone specimens [6]. The use of extensometers requires large specimen sizes due to technical difficulties with securing the arms of the extensometer on the surface of small or irregularly shaped specimens [126]. The typically slippery and smooth surfaces of fresh bone specimens further exacerbate these fixation difficulties. There may also be transverse

pre-loading on the specimen, causing damage to the specimen, as a result of attaching contact-type extensometers [127]. The use of strain gauges also pose a challenge as installation of these devices can be difficult when dealing with bone material in terms of specimen surface preparation and choice of adhesive. A common source of error lies in the bonding of the gauge to the test specimen and insufficient specimen surface preparation [128]. Another technique for strain measurement is digital image correlation (DIC), an optical, non-contact technique for measuring displacement. The surface is usually painted or sprayed to produce a high contrast speckle pattern. DIC works by tracking the pixels of serial digital photographs taken of the painted surface at different stages of deformation. However, limitations arise with using acrylic paint for surface preparation, such as paint not sticking to wet, biological specimens or penetrating into the pores of specimens which could then potentially carrying applied loads or obstruct marrow flow, and thus could affect mechanical behaviour [129]. Optical techniques are also negatively affected if testing is done in an enclosed chamber, e.g. to control the temperature, or in a fluid, e.g. to mimic in-situ conditions.

The correction of testing machine compliance is seldom reported. Zhao *et al*. [7] published a review paper examining 177 papers, including 20 studies directly analysing compression testing techniques to improve accuracy, found that only 12 of these studies applied a machine compliance correction and just one study [106] provided specific details on the compliance correction algorithm. Determining global machine compliance typically involves driving the platens together with no specimen, but this can introduce variability due to a given machine's inconsistent loading behaviour [106]. Furthermore, local compliance errors in strain measurement have been highlighted in studies, where strain was recorded across machine platens rather than directly on the specimen, leading to significant discrepancies in the results [32]. Given that strain often concentrates around the edges of specimens, this can lead to an overestimation of average strain and, consequently, an underestimation of the material's modulus[108, 107, 109].

For bone testing, particularly with small specimens, accounting for machine compliance is vital due to the necessity of obtaining precise modulus values for biomechanical modelling [45]. The biological variability of bone properties across different regions necessitates the extraction of multiple specimens from a single donor, as large or whole bone samples may not yield consistent material characteristics

[88, 89]. This approach not only allows for more accurate representation of in-vivo conditions but also addresses the challenge of drying out, which could alter the mechanical properties of the bone [90]. Thus, the ability to conduct a high volume of tests on small bone specimens within a limited time frame is paramount for ensuring valid mechanical property assessments.

Thus, where relative values are sought, traditional cross-head displacement measurement of strain could be sufficient and is quick and simple to implement. It also places fewest restrictions on the specimen, with no need for large-sized specimens or surface preparation to facilitate attachment of extensometers or strain gauges. Although the effect of machine compliance must be corrected for. If absolute values are of interest in the study and large specimens/samples are available, then extensometers can be used to improve the accuracy of strain measurement. If localized strain changes are of interest to the researcher, strain gauges can be used. Digital image correlation is a method that would be most useful in studies interested in full-field strain measurements (e.g. whole bone fracture analysis) [130]. Further studies using DIC on ex-vivo bone samples are required before reliability of this method can be assessed. The sub-press can do all of this without any (or at least most) of the limitations listed above.

The reviewed literature reveals that bone structure and properties are heavily influenced by factors such as species, age, storage conditions, and testing methodologies. Variations in micro-structural organization and mineral composition not only indicate differences across species but also reflect the role of remodelling and ageing in the evolution of bone strength. Additionally, the impact of specimen preparation and strain measurement techniques highlights the importance of refining experimental methods to obtain accurate mechanical data. This collective knowledge underscores the need for continued research, particularly in adopting precise testing techniques to better capture the mechanical behaviour of bone and support accurate biomechanical modelling.

5.2 Sub-press Accuracy Validation

The sub-press accuracy validation tests offer a thorough assessment of the capability of the sub-press measurement system, i.e. three hall effect sensor, magnetic multi-pole strip pairs, to accurately measure displacements to the desired reso-

lution of one micron. Daras *et al*. [94] emphasized the importance of precise machining and design considerations, allowing the sub-press to provide a highly accurate and repeatable compression testing environment. By designing the base sub-press such that critical parts, particularly the platen and mating surfaces, could be machined on a lathe in a single operation, the study minimized the risk of non-concentricity. This ensures parallelism between the upper and lower platens and pure axial compression on specimens. The bottom face of the sleeve, perpendicular to the plunger's axis, also serves as an ideal datum, supporting the use of the sub-press for high-accuracy displacement measurements.

To validate the accuracy of displacement measurements, a Mitutoyo depth micrometer, with a 10 μm resolution, and a Nikon microscope were used in a controlled set-up. The use of a custom mounting fixture allowed for precise control and measurement of incremental 10 μm displacements. Importantly, while incremental adjustments aimed for exact 10 μm steps, minor deviations occurred due to manual adjustments. Image processing software was used to correct for these deviations, ensuring that the true displacement of each increment was accurately measured down to 0.1 μm. This high level of precision highlights the capability of the sub-press, especially when taking into account the resolution limitations of the manual micrometer.

Results across ten repetitions indicated that the sub-press could consistently measure incremental displacements with an average deviation of only 0.051 μm and a standard deviation of 0.466 μm. This minimal deviation underscores the reliability of the sub-press and its agreement with the micrometer readings, supporting its sensitivity to detect and measure even sub-micron displacements. The data suggests that 68% of measurements fall within one standard deviation of the true displacement, indicating high accuracy within the range of the sensor resolution. Extending this to two standard deviations, 95% of measurements are within 1 μm of the intended displacement, demonstrating the capability of the measurement system to measure displacements with precision up to 1 μm, even if the actual resolution extends slightly beyond this threshold.

The precision achieved in this commissioning test strongly supports the suitability of the sub-press for accurately assessing small bone specimen deformation under controlled axial compression, reinforcing its applicability in highly sensitive mechanical testing contexts. This conclusion is further supported by Figure 3.27,

where, under a no-load condition, it is evident that the sub-press (the dashed line) records the same displacement-time data as the UTM cross-head (the solid line) to within two micron. Given the scale of the load frame, this level of agreement is satisfactory. However, when the plunger makes contact with the specimen, the UTM continues to record linear displacement-time data, while the sub-press is able to record the take-up in compliance of the load frame.

5.3 Sub-press Compliance Estimation

The machine compliance tests aimed to assess the actual material properties of PMMA and Al specimens, specifically focusing on modulus and stiffness for different specimen geometries. The stiffness ratio between tall and short specimens was used as a measure to evaluate the sub-press compliance. According to the theoretical expectation, the stiffness of the tall specimens should be slightly more than half that of the short specimens.

The results for PMMA specimens using the unmodified sub-press aligned well with the theoretical expectations. The calculated stiffness ratio of 0.57 falls within the predicted range, suggesting that the machine compliance did not significantly affect the results for PMMA. The slight discrepancy in the apparent modulus values between the short and tall specimens could be attributed to experimental variations or slight inconsistencies in specimen preparation. However, the consistent trend in stiffness values supports the theoretical expectation that the tall specimens, being double the height, should exhibit roughly half the stiffness of the short specimens.

In contrast to the PMMA specimens, the Al specimens presented more interesting results. The tall specimens had a significantly higher average apparent modulus than the short specimens with a large standard deviation. The resulting stiffness ratio of just over 1 greatly exceeded the expected value of 0.5, indicating a deviation from the anticipated behaviour. This unexpected stiffness ratio suggests that factors such as the sub-press compliance or specimen alignment may have played a more significant role in the Al tests compared to the PMMA tests. In particular, the lack of a clear elastic region in the stress-strain curve for Al, as seen in 3.7 further supports the theory that the Al specimens are not deforming uniformly. Additionally, the divergent displacement-time plots (Figure 3.9) for the

three sensors indicate that specimen misalignment has a large effect on measured results, further highlighting the importance of the three-sensor configuration.

For tests using the conical frustum platens, the results from the PMMA specimens showed a slight increase in apparent modulus and corresponding stiffness values from the flat platen results. Notwithstanding these higher values, the stiffness ratio remained within the acceptable range at 0.58.

By contrast, both the short and tall Al specimens showed improved apparent moduli and corresponding stiffness values, although they were still not sufficiently close to the expected values. However, the resulting stiffness ratio of 0.57 aligns with the expected theoretical value, suggesting that the modified sub-press, with its conical frustum profile improved the accuracy of the tests and allows for a correction factor to be determined and used.

Using Equation 3.7, the compliance of the sub-press was estimated, revealing a calculated stiffness of 305 kN/mm, which is comparable to the stiffness of 280 kN/mm of the Al specimens. This suggests that the sub-press compliance effects are significant. Conversely, the sub-press stiffness is an order of magnitude more than the stiffness of the PMMA specimens of 10 kN/mm, explaining the far less significant impact on the measurements. By incorporating the compliance of the sub-press into the calculations, the inferred true moduli were calculated as 3.85 GPa for PMMA and 74.80 GPa for Al. These values are in good agreement with those obtained from multi-machine test series and are practically identical to the wave speed tests (3.85 GPa for PMMA and 75.15 GPa for Al). The improvement of the displacement-time plots of the three sensor outputs compared to that of the flat platens, shows the significance of reducing the specimen platform in aiding with specimen alignment.

For tests using the hyperbolic frustum platens, the results from the PMMA specimens showed a slight decrease in apparent modulus and corresponding stiffness values from the conical frustum platen results but produced the best stiffness ratio out of the 3 platen variations at 0.53.

The harder Al (6000 series) yielded a stiffness ratio of 0.69, which is slightly higher than with the flat and conical platen variations, but still within an acceptable range, demonstrating the effectiveness of the hyperbolic frustum in achieving the expected stiffness ratio and improving the measured moduli, thereby indicating a

reduction in non-uniform loading. Both the PMMA and Al tests show virtually no take-up in the stress-strain curves, which strongly indicates that uniform loading has been achieved.

Using Equation 3.9, the compliance of the sub-press with hyperbolic frustum platens was estimated, revealing a calculated stiffness of 201 kN/mm, which is again comparable to the stiffness of the 1050 Al specimens themselves at 280 kN/mm and an order of magnitude more than the stiffness of the PMMA specimens at 10 kN/mm, indicating a far more significant impact on the Al measurements than on the PMMA measurements, similar to the first estimation from the conical frustum platens. By incorporating the new compliance estimation of the sub-press into the calculations, the inferred true moduli were calculated as 3.5 GPa for PMMA and 79.6 GPa for the 6000 series Al. These values are in good agreement with those obtained from multi-machine test series. The near-identical displacement-time plots (Figure 3.15) of the three sensor outputs further emphasise the importance of the reduced specimen platform for specimen alignment.

A "platen-on-platen" (PoP) test measured the sub-press stiffness at 198 kN/mm, closely matching the new estimated compliance. This highlights the importance of taking the specimen platform into account when estimating the sub-press compliance analytically. While the test accurately measures the stiffness of the sub-press, accounting for the specimen influence is still crucial, as local deformations and Hertzian stresses may explain minor differences between estimated and measured stiffness. The raw data from the UTM no-specimen tests highlighted issues of repeatability, a smeared elastic region, and an extended take-up portion, which would have resulted in a significantly lower apparent stiffness of 16.17 kN/mm, underscoring the limitations of this method compared to the sub-press.

By analysing the stiffness ratio of two specimen geometries during the hyperbolic frustum platen tests with 6000 series Al, the sub-press compliance was inferred to be 95 kN/mm for the PMMA and 150 kN/mm for the Al, which is within a standard deviation of 65 kN/mm of the PoP measurement and the analytical estimate. This confirms that the sub-press is effective for accurately measuring modulus in small specimens, whether soft or hard and that its compliance can be reliably accounted for.

The consistency of the apparent material properties and stiffness ratios for PMMA across all sub-press platen variations reinforces the reliability of the testing set-up for this material. However, the variability in the Al results highlights the need for different sub-press platen variations for different applications. The close agreement between the analytical, measured and inferred sub-press compliance strongly supports the accuracy of the determined sub-press stiffness. The 6000 series Al tests demonstrate that the sub-press is well-suited for testing stiffer materials, provided the appropriate platen is used and compliance is properly accounted for.

There are thus three platen variations tailored for different applications: the flat platen is ideal for analysing plastic behaviour; the conical frustum platen is suitable for reducing non-uniform loading and achieving accurate modulus measurements with minimal compliance correction, while maintaining an overall compliance similar to that of the flat platens, and the hyperbolic frustum platen is optimal for achieving near-perfect uniform loading with no take-up behaviour, though it requires accounting for additional compliance.

Overall, these results underscore the importance of machine compliance correction in material property testing and demonstrate the effectiveness of specific sub-press modifications in achieving more accurate measurements.

5.4 Degradation Study

Within the broader aim of developing improved bone specimen curation protocols, the primary objective of this study was to investigate the effects of two storage protocols namely “machine-freeze” (MF) and “freeze-machine” (FM) on the mechanical properties of bovine cortical bone over time. The results from fresh, i.e., less than 24 hours post-mortem and without prior freezing, one-month (1m), and three-month (3m) storage periods, were compared. The primary metrics evaluated were the apparent modulus and ultimate compressive strength (UCS), which are crucial indicators of bone apparent modulus and strength.

The fresh bone specimens showed an average apparent modulus of 12.81 GPa, representing the benchmark for bone tested at this strain rate and under optimal conditions [1]. The UCS of 175.17 MPa, however is lower than reported in other studies [41, 36]. The relatively low standard deviations (0.66 GPa for modulus and 7.80 MPa for UCS) and relatively small variation between the tests, in general,

compared to the stored specimens, suggest consistency in these properties among fresh bone samples, implying minimal variability in mechanical performance when bones are tested soon after collection.

After one month of storage, both storage protocols exhibited a decline in apparent modulus, with MF specimens showing an average of 9.98 GPa and FM specimens showing 10.46 GPa. This reduction demonstrates the degenerative effect of storage on bone apparent modulus. However, the results suggest that whole-bone storage (FM) preserved the apparent modulus slightly better than specimen storage (MF), possibly due to less exposure to environmental fluctuations or mechanical processing during storage. Despite this better preservation of apparent modulus in the FM protocol, the decline in modulus from fresh to one month was notable, indicating that even whole-bone storage could not fully prevent changes in mechanical properties. In terms of UCS, the values decreased slightly after one month of storage, with MF specimens at 159.80 MPa and FM specimens at 164.80 MPa. The fact that UCS remained relatively high after one month, especially in the FM group, suggests that bone strength is somewhat more resistant to early degenerative effects of freezing compared to its apparent modulus. The standard deviations were higher for the FM group (14.80 MPa), however, pointing to increased variability in this storage protocol or perhaps increased sensitivity to machining damage, though the general trends remained consistent.

The three-month storage results reveal a more drastic reduction in apparent modulus. The MF specimens had an average modulus of 6.42 GPa, while the FM specimens showed 7.22 GPa. These values are approximately half of those observed in fresh bone, underscoring the significant decline in apparent modulus over extended storage periods. While FM specimens still performed slightly better than MF specimens in terms of modulus, both protocols exhibited a substantial decline, indicating that long-term freezing severely compromises bone apparent modulus regardless of the storage method. Interestingly, the UCS for both MF and FM specimens increased after three months, reaching 192.20 MPa and 199.50 MPa, respectively. This increase in UCS with prolonged storage, coupled with the higher standard deviations (27.50 MPa for MF and 23.90 MPa for FM), may indicate that freezing alters the deformation mechanisms of bone, making it more brittle but also more resistant to compressive failure until it reaches a critical strain point. The large standard deviations in both modulus and UCS after three months sug-

gest that freezing induces greater variability in mechanical behaviour, perhaps due to inconsistencies in ice crystal formation within the bone matrix or other microstructural changes [5]. It should also be noted that it was increasingly difficult to machine the FM3m specimens as parts of the bone chipped off during machining due to the brittle nature of the bone.

Figure 4.11 shows no significant difference in apparent modulus degradation or scatter between the two storage protocols ("machine-freeze" and "freeze-machine"). The minimal scatter in the apparent modulus values across the 24 fresh specimens, irrespective of bone region, strongly suggests that accurate modulus measurement is achievable when strict testing and specimen preparation protocols are consistently applied. This consistency implies that bone region alone does not introduce substantial variability in modulus values, as evidenced by the fresh data. The increased scatter observed in the results from specimens stored for one and three months, however, indicates that variability is likely due to the storage protocol rather than the testing apparatus, procedure, or bone region. Since all tests in this study were conducted using identical equipment, methods, and by the same researcher, storage protocol appears to be the primary factor influencing the observed variability in modulus measurements. Furthermore,the apparent density of specimens did not change significantly over time, regardless of storage protocol, with an average difference of 0.06 g/cm^3 between fresh and stored specimens.

The observed failure modes further support the hypothesis that freezing impacts bone mechanics over time. Fresh specimens primarily failed by shear but remained intact, whereas one-month specimens split longitudinally, with some staying together and others separating completely. By three months, the specimens exhibited brittle, crumbly failure, consistent with the reduced modulus and increased UCS. This transition from shear to brittle failure could be linked to the combined effects of water loss, freezing-induced micro-fractures, and overall reduction in bone toughness.

The increasing scatter in the apparent modulus values over time reiterates the hypothesis that freezing introduces variability in how bones respond to mechanical loads [5]. In conclusion, while both storage protocols led to declines in bone apparent modulus, the FM protocol appeared to better preserve the mechanical properties of cortical bone over time compared to the MF protocol. However, neither method prevented significant degradation, particularly after three months.

The increase in UCS after three months, coupled with the observed brittle failure modes, suggests that long-term freezing fundamentally alters the mechanical properties of bone, making it more susceptible to catastrophic failure while maintaining compressive strength up to a certain threshold. These findings underscore the importance of considering the duration and method of bone storage in bio-mechanical testing to ensure accurate, representative results.

Chapter 6

Conclusions & Recommendations

6.1 Conclusions

This research includes a thorough literature review which led to the assessment of two different storage protocols ("machine-freeze" (MF) and "freeze-machine"(FM)) in the preservation of the mechanical properties of bovine cortical bone in long-term storage. The design, calibration, and application of a micron-accurate sub-press for testing the mechanical properties of small cortical bone specimens through the use of novel platen modifications was explored and local platen compliance was investigated.

6.1.1 Findings from Literature

The literature review provides a well-rounded examination of the variables affecting bone mechanics, from species-specific structural differences to methodological considerations in mechanical testing. Species-specific structural differences, such as the presence and arrangement of osteons, reflect evolutionary adaptations to varying loading demands, while within-species studies highlight the profound effects of ageing and remodelling on bone strength and resilience. The mechanical response of bone is sensitive to storage methods, with long-term freezing and preservation protocols introducing potential degradations that alter measured properties and complicate the interpretation of results. Furthermore, the review underscores the critical role of measurement techniques in biomechanical testing. Techniques like

extensometers, strain gauges, and digital image correlation each offer unique advantages but come with limitations in precision, particularly for small or irregular specimens.

Given these challenges, implementing highly accurate, compliance-corrected methods, such as strain measurement directly on specimens and non-contact approaches, can significantly improve data fidelity. Emerging tools like the sub-press, which minimize traditional strain measurement limitations, may provide the precision needed for small-scale specimens without compromising accuracy. Overall, this review emphasizes the importance of standardizing and optimizing experimental approaches to capture the true mechanical behaviour of bone, informing the development of more reliable biomechanical models and fostering a deeper understanding of bone mechanics across various contexts.

6.1.2 Sub-press Accuracy Validation

The accuracy validation of the sub-press confirms its capability to measure submicron displacements with high reliability, making it a robust tool for precise mechanical testing. By ensuring parallelism and concentricity through careful machining and design, this sub-press set-up offers an exceptionally stable platform for displacement measurements. The use of a Mitutoyo depth micrometer and Nikon microscope, combined with image processing software, validated incremental displacements with remarkable precision, achieving an average deviation of only 0.051 μm across tests. This minor difference, alongside a standard deviation of 0.466 μm, underscores the sensitivity of the sub-press system, with 95% of measurements within 1 μm accuracy. Furthermore, the consistency observed between the sub-press and UTM cross-head readings under no-load conditions and the sub-press's ability to detect load frame compliance upon specimen contact highlight its superior resolution. These findings validate the sub-press as a suitable instrument for assessing the minute deformations of small bone specimens, essential for accurate biomechanical testing and modelling.

6.1.3 Sub-press Compliance Estimation

This study demonstrates that machine compliance correction is critical to accurately measure material properties, particularly when testing specimens of varying

stiffness. The three sub-press platen designs provide distinct advantages depending on the application and material properties: the flat platen excels in plasticity-focused tests, the conical frustum platen enhances modulus accuracy with minimal compliance adjustments, and the hyperbolic frustum platen achieves the highest degree of uniform loading, making it ideal for higher-stiffness materials like the 6000 series Al.

The results show that while PMMA tests consistently aligned with theoretical stiffness ratios across all platen types, Al specimens displayed higher sensitivity to machine compliance and alignment, underscoring the need for platen-specific modifications when testing stiffer materials. The successful matching of estimated and measured compliance values further supports the reliability of the modified sub-press set-up.

Ultimately, the findings emphasize that accounting for machine compliance, through tailored platens, enhances the precision of modulus measurements across a range of materials, thereby improving the reliability and applicability of the testing methodology for both compliant and stiff specimens.

6.1.4 Degradation Study

The comparison of fresh and stored bone specimens offered insights into how storage affects bone elasticity and strength. Fresh bone specimens served as a baseline, demonstrating consistent mechanical properties with an apparent modulus of 12.81 GPa and ultimate compressive strength (UCS) of 175.17 MPa. These results, obtained less than 24 hours post-mortem and without prior freezing, highlight the optimal conditions for assessing cortical bone. The low standard deviations in modulus and UCS among fresh specimens indicate minimal variability in bone mechanics when tested under controlled conditions. However, one-month storage introduced notable degradation, with MF specimens averaging a modulus of 9.98 GPa and FM specimens at 10.46 GPa, indicating that freezing induces early-stage reduction in elasticity. The FM protocol preserved bone elasticity slightly better than MF. UCS values, though moderately reduced, showed greater resilience to early degradation, suggesting that bone strength may be less affected than elasticity in the initial stages of storage. Three-month storage results revealed a substantial reduction in elasticity, with both MF and FM protocols yield-

ing apparent modulus values approximately half that of fresh bone. Interestingly, UCS increased after prolonged freezing, with MF reaching 192.20 MPa and FM 199.50 MPa. This rise in UCS, accompanied by a shift to brittle failure modes, suggests that extended freezing introduces structural changes, such as ice crystal formation or collagen matrix alterations, which reduce bone toughness but increase its resistance to compressive failure until a critical strain threshold. The increased scatter in both modulus and UCS, especially after three months, reflects the variability introduced by freezing and the complex interaction between bone micro-structure and storage conditions.

The findings on apparent density in this study showed minimal change over time, suggesting that observed mechanical degradation stems from micro-structural rather than compositional alterations. Moreover, the low scatter observed in fresh specimen data suggests that the variability in bone mechanical properties reported in the literature may be influenced more by differences in storage protocols than by bone region. Additional factors contributing to this scatter likely include inconsistencies in testing apparatus, uncorrected machine compliance, and variations in specimen preparation protocols.

In summary, while the FM protocol demonstrated marginally better preservation of mechanical properties, both MF and FM storage protocols resulted in significant degradation of bone elasticity over time. This aligns with the findings of Daras *et al*. [41], who reported severe cortical bone degradation after six months, irrespective of the storage method, and recommended that storage durations be limited to less than one week to obtain data representative of in-vivo properties. The findings underscore that long-term freezing alters the deformation mechanisms of bone, contributing to increased brittleness, greater variability in mechanical response, and higher susceptibility to catastrophic failure under compressive loads. These results have practical implications for specimen handling and storage in biomechanics, stressing the importance of protocol selection and storage duration to maintain the integrity of biomechanical assessments.

This work contributes to the broader field of bone mechanics by combining novel instrumentation, rigorous testing, and careful consideration of storage impacts, ultimately providing an accurate, repeatable and robust means of assessing bone properties and aiding in the development of standardized storage and testing protocols for biomaterials.

6.2 Recommendations

6.2.1 Long-term Storage of Whole Bones

For future research and practical applications, it is recommended to prioritize storing whole bones over small specimens, particularly for durations up to one month. Whole-bone storage appears to better maintain the mechanical integrity of bone, helping preserve mechanical properties that are representative of fresh, in-vivo conditions. It is generally advised, however, to avoid storing bones in any form for longer than a month if accurate representation of fresh bone behaviour is desired, as storage beyond this period results in considerable deviation from the original mechanical properties.

Further research is needed to investigate the underlying mechanisms of storage-induced degradation. The current literature does not widely recognize storage-induced degradation as a significant issue, and there is a notable gap in research on this topic. While a detailed investigation of degradation mechanisms would be valuable, such work would require extensive research efforts. Future studies should consider exploring these mechanisms using advanced analytical techniques such as imaging and compositional analysis to better understand how storage conditions influence mechanical property changes.

6.2.2 Multi-Species Degradation Study

A comprehensive investigation into the degradation behaviour of cortical bone across multiple species would provide valuable insights, especially given the ethical limitations around obtaining fresh human bone samples. By characterizing the degradation patterns in a variety of species, researchers may establish generalized behaviour that can reasonably infer degradation trends in human bones. This cross-species comparison would be particularly useful if a broad set of species can demonstrate similar degradation responses, suggesting that the findings could potentially be extrapolated to human bone.

While this study focused on bovine bone due to its availability and thick cortical layer, previous research, including the work of Welgemoed [36], has identified degradation trends across multiple species, including mammals, primates, birds,

and reptiles. These studies suggest that degradation may follow a universal trend, although further research is required to confirm whether human cortical bone exhibits the same behaviour. If future studies establish a consistent degradation pattern across species, it may be possible to use existing human cortical bone datasets to estimate mechanical property changes at earlier post-mortem time points.

6.2.3 Failure Modes of Bone Specimens

This study identified three distinct failure modes associated with bone degradation. To better understand these modes, a focused investigation at the micro-structural level is recommended, potentially aligning with a multi-species study. This approach could help determine whether failure patterns observed here are consistent across different species or if there are unique aspects to each, ultimately aiding in better characterization of bone fragility and resilience as influenced by storage and degradation.

6.2.4 Quasi-Static Compression Testing

To enhance the accuracy of quasi-static compression testing for bone specimens, it is recommended to use the sub-press with the flat platens for analysing the plastic behaviour of materials. If an accurate measurement of modulus and uniform load distribution is required, the hyperbolic frustum platens are recommended, as this platen variation minimizes compliance and take-up issues. Local machine compliance, however, should be accounted for in all tests to ensure accurate modulus measurements. Additionally, testing bone specimens in a saline bath could better replicate in-vivo conditions, allowing for more physiologically relevant mechanical responses and improving the translational value of the findings to real-world applications.

6.2.5 Future Testing Considerations

The experimental conditions in this study were carefully chosen to ensure a reliable and repeatable testing methodology. Key factors such as fresh versus frozen bone at different degradation states, whole bone versus machined specimens, and quasi-static testing were considered. Future research should explore additional ex-

perimental conditions to better characterize bone degradation. Potential avenues include testing under different strain rates, multi-species comparisons, randomizing specimen extraction sites within a bone, and conducting tests in a liquid environment at physiological temperatures. Additionally, factors such as species, age, and sex variations could influence degradation behaviour and should be considered in future studies.

All tests in this study were conducted at room temperature in a controlled laboratory environment. While environmental temperature effects on mechanical properties were discussed in the literature review, future research should consider testing under different temperature conditions, including at body temperature, to better replicate in-vivo conditions.

6.2.6 Numerical Work

A dedicated numerical study focusing on the deformations of the sub-press, particularly around specimen-platen interaction, is recommended to further validate the findings from this dissertation. Modelling the localised deformations for each platen type would yield detailed insights into how these deformations influence strain measurement accuracy and possibly confirm the hypothesised progressive yielding of specimens. Such work could enhance understanding of machine compliance and loading dynamics.

A key recommendation for future work is to apply finite element analysis (FEA) to optimize platen design. While this study primarily focused on establishing a robust experimental foundation and assessing platen performance, refining platen shape and curvature could improve accuracy, especially in addressing edge effects and localized yielding. FEA simulations could be used to model stress distributions at the platen-specimen interface, identifying regions susceptible to localized yielding. This analysis would provide a more precise understanding of platen design and its effects on strain measurement accuracy.

Transitioning from linear modulus calculations to non-linear constitutive models is also recommended to expand the applicability of the findings to broader biomechanical contexts. Non-linear models are particularly valuable for capturing the full stress-strain response of bone, especially as it approaches failure. However, this study focused on the elastic behaviour of bone, which is more relevant for small-

scale mechanical characterization and comparative analysis of different storage protocols. Future work could incorporate non-linear models to capture post-yield behaviour and fracture mechanics, enhancing the broader applicability of these findings, particularly in scenarios involving progressive damage and failure.

References

[1] T. P. Johnson, S. Socrate & M. C. Boyce, "A viscoelastic, viscoplastic model of cortical bone valid at low and high strain rates", *Acta Biomaterialia*, vol. 6, no. 10, (2010), pp. 4073–4080.

[2] E. H. van Haaren, B. C. van der Zwaard, A. J. van der Veen, I. C. Heyligers, P. I. Wuisman & T. H. Smit, "Effect of long-term preservation on the mechanical properties of cortical bone in goats", *Acta orthopaedica*, vol. 79, no. 5, (2008), pp. 708–716.

[3] E. Sedlin & C. Hirsch, "Factors affecting the determination of the physical properties of femoral cortical bone", *Acta Orthopaedica*, vol. 37, no. 1, (1966), pp. 29–48.

[4] C. Ohman, E. DallAra, M. Baleani, S. V. S. Jan & M. Viceconti, "The effects of embalming using a 4 percent formalin solution on the compressive mechanical properties of human cortical bone", *Clinical biomechanics*, vol. 23, no. 10, (2008), pp. 1294–1298.

[5] W. Lee & I. Jasiuk, "Effects of freeze-thaw and micro-computed tomography irradiation on structure-property relations of porcine trabecular bone", *Journal of Biomechanics*, vol. 47, (2014), pp. 1495–1498.

[6] N. H. Hart, S. Nimphius, T. Rantalainen, A. Ireland, A. Siafarikas & R. U. Newton, "Mechanical basis of bone strength: influence of bone material", *Journal of Musculoskeletal and Neuronal Interactions*, vol. 17, no. 3, (2017), pp. 114–139.

[7] S. Zhao, M. Arnold, S. Ma, R. Abel, J. Cobb, U. Hansen & O. Boughton, "Standardizing compression testing for measuring the stiffness of human bone", *Bone Joint Research*, vol. 7, no. 8, (2018), pp. 524–538.

[8] B. Clarke, "Normal bone anatomy and physiology", *Clinical journal of the American Society of Nephrology*, vol. 3, no. 3, (2008), pp. S131–S139.

[9] Health Jade, "Long bone anatomy", 2019, URL `https://healthjade.net/wp-content/uploads/2019/03/Long-bone-anatomy.jpg`, [Online; accessed May 23, 2023].

[10] M. Monier-Faugere, C. Langub & H. Malluche, "Bone biopsies: A modern approach", in: "Metabolic Bone Disease and Clinically Related Disorders", chap. 8, pp. 237–280, Academic Press, 3 edn., 1998.

[11] R. K. Fuchs, S. J. Warden & C. H. Turner, "Bone anatomy, physiology and adaptation to mechanical loading.", in: "Bone Repair Biomaterials.", , editors J. A. Planell, S. M. Best, D. Lacroix & A. Merolli, chap. 2, pp. 25–68, Woodhead Publishing., 2009.

[12] L. M. Biga, S. Bronson, S. Dawson, A. Harwell & et al., "Anatomy & physiology: Bone structure", URL `https://opentextbc.ca/anatomyandphysiology/chapter/6-3-bone-structure/`, [Online; accessed May 23, 2023].

[13] The fi

brolamellar smoking gun, URL `http://reptilis.net/2007/07/04/the-{\@@par}brolamellar-smoking-gun/`, [Online; accessed July 18, 2023].

[14] L. M. Biga, S. Bronson, S. Dawson, A. Harwell & et al., "Anatomy & physiology: Bone formation and development", URL `https://opentextbc.ca/anatomyandphysiology/chapter/6-4-bone-formation-and-development`, [Online; accessed May 23, 2023].

[15] K. S. Davison, K. Siminoski, J. Adachi, D. A. Hanley, D. Goltzman, A. B. Hodsman, R. Josse, S. Kaiser, W. P. Olszynski & A. Papaioannou, "Bone

strength: the whole is greater than the sum of its parts", *Seminars in arthritis and rheumatism*, vol. 36, (2006), pp. 22–31.

[16] M. L. Bouxsein, "Bone quality: where do we go from here?", *Osteoporosis International*, vol. 14, no. 5, (2003), pp. 118–127.

[17] S. Weiner, W. Traub & H. D. Wagner, "Lamellar bone: structure-function relations", *Journal of Structural Biology*, vol. 126, no. 3, (1999), pp. 241–255.

[18] K. Padian & E. T. Lamm, *Bone histology of fossil tetrapods: advancing methods, analysis, and interpretation*, Univ of California Press, 2013.

[19] J. D. Currey, "The many adaptations of bone", *Journal of Biomechanics*, vol. 36, no. 10, (2003), pp. 1487–1495.

[20] P. Rowe, A. Koller & S. Sharma, *Physiology, Bone Remodeling.*, Treasure Island (FL): StatPearls Publishing, [Updated 2023 Mar 17], URL `https://www.ncbi.nlm.nih.gov/books/NBK499863/`.

[21] T. Wright & W. Hayes, "Tensile testing of bone over a wide range of strain rates: effects of strain rate, microstructure and density", *Medical and Biological Engineering*, vol. 14, no. 6, (1976), pp. 671–680.

[22] J. D. Currey, "The effects of strain rate, reconstruction and mineral content on some mechanical properties of bovine bone", *Journal of Biomechanics*, vol. 8, no. 1, (1975), pp. 81–86.

[23] J. L. Katz, H. S. Yoon, S. Lipson, R. Maharidge, A. Meunier & P. Christel, "The effects of remodeling on the elastic properties of bone", *Calcified Tissue International*, vol. 36, no. 1, (1984), pp. S31–S36.

[24] D. Brits, M. Steyn, E. Noelle & et al., "A histomorphological analysis of human and non-human femora", *International journal of legal medicine*, vol. 128, no. 2, (2014), pp. 369–377.

[25] M. Martiniakova, B. Grosskopf, R. Omelka, K. Dammers, M. Vondrkov & M. Bauerov, "Histological study of compact bone tissue in some mammals: a method for species determination", *International Journal of Osteoarchaeology*, vol. 17, no. 1, (2007), pp. 82–90.

[26] D. H. Enlow, "An evaluation of the use of bone histology in forensic medicine and anthropology", *Berlin, Heidelberg: Springer Berlin Heidelberg*, pp. 93–112.

[27] H. C. Spatz, E. O'Leary & J. F. Vincent, "Young's moduli and shear moduli in cortical bone", *Proceedings of the Royal Society of London B: Biological Sciences*, vol. 263, no. 1368, (1996), pp. 287–294.

[28] S. Gourion-Arsiquaud, J. C. Burket, L. M. Havill, E. DiCarlo, S. B. Doty, R. Mendelsohn, M. C. van der Meulen & A. L. Boskey, "Spatial variation in osteonal bone properties relative to tissue and animal age", *Journal of Bone and Mineral Research*, vol. 24, no. 7, (2009), pp. 1271–1281.

[29] A. R. Tumarkin-Deratzian, "Fibrolamellar bone in wild adult alligator mississippiensis", *Journal of Herpetology*, vol. 41, no. 2, (2007), pp. 341–345.

[30] J. Castanet, K. C. Rogers, J. Cubo & J. Jacques-Boisard, "Periosteal bone growth rates in extant ratites (ostrich and emu) implications for assessing growth in dinosaurs", *Comptes Rendus de l'Academie des sciences-Series III-Sciences de la Vie*, vol. 323, no. 6, (2000), pp. 543–550.

[31] A. A. Abdel-Wahab, K. Alam & V. V. Silberschmidt, "Analysis of anisotropic viscoelastoplastic properties of cortical bone tissues", *Journal of the Mechanical Behavior of Biomedical Materials*, vol. 4, no. 5, (2011), pp. 807–820.

[32] P. Augat & S. Schorlemmer, "The role of cortical bone and its microstructure in bone strength", *Age and ageing*, vol. 35, no. 2, (2006), pp. ii27–ii31.

[33] E. N. Ebbesen, J. S. Thomsen, H. Beck-Nielsen, H. J. Nepper-Rasmussen & L. Mosekilde, "Age-and gender-related differences in vertebral bone mass, density, and strength", *Journal of Bone and Mineral Research*, vol. 14, no. 8, (1999), pp. 1394–1403.

[34] R. B. Martin & P. J. Atkinson, "Age and sex-related changes in the structure and strength of the human femoral shaft", *Journal of Biomechanics*, vol. 10, no. 4, (1977), pp. 223–231.

[35] J. D. Currey, K. Brear & P. Zioupos, "The effects of ageing and changes in mineral content in degrading the toughness of human femora", *Journal of biomechanics*, vol. 29, no. 2, (1996), pp. 257–260.

[36] Lee-Anne Welgemoed, *An experimental investigation of interspecies variation in mechanical properties of cortical bone*, M.Sc thesis, the University of Cape Town, Cape Town, 2018.

[37] D. Carter & W. C. Hayes, "Compact bone fatigue damage in residual strength and stiffness", *Journal of Biomechanics*, vol. 10, no. 5, (1977), pp. 325–337.

[38] S. L. Hui, C. W. Slemenda & C. C. Johnston Jr, "Age and bone mass as predictors of fracture in a prospective study", *Journal of Clinical Investigation*, vol. 81, no. 6, (1988), pp. 1804–1809.

[39] L. Feng & I. Jasiuk, "Multi-scale characterization of swine femoral cortical bone", *Journal of Biomechanics*, vol. 10.

[40] J. P. Berteau, C. Baron, M. Pithioux, F. Launay, P. Chabrand & P. Lasaygues, "In vitro ultrasonic and mechanic characterization of the modulus of elasticity of children cortical bone", *Ultrasonics*, vol. 54, no. 5, (2014), pp. 1270–1276.

[41] N. Daras, T. J. Cloete & G. N. Nurick, "Degradation of the mechanical properties of cortical bone due to long duration storage", *Journal of Mechanical Behavior of Biomedical Materials*, vol. 157.

[42] Z. Wu, T. C. Ovaert & G. L. Niebur, "Viscoelastic properties of human cortical bone tissue depend on gender and elastic modulus", *Journal of Orthopaedic Research*, vol. 30, no. 5, (2012), pp. 693–699.

[43] T. Crenshaw, E. Peo, A. Lewis, B. Moser & D. Olson, "Influence of age, sex and calcium and phosphorus levels on the mechanical properties of various bones in swine", *Journal of Animal Science*, vol. 52, no. 6, (1981), pp. 1319–1329.

[44] JOHANNA W. LAMPE & CHERYL L. ROCK, "Chapter 10 - biomarkers and biological indicators of change", in: "Nutrition in the Prevention

and Treatment of Disease", , editors ANN M. COULSTON, CHERYL L. ROCK & ELAINE R. MONSEN, pp. 139–153, Academic Press, San Diego, 2001, URL https://www.sciencedirect.com/science/article/pii/B978012193155150012X.

[45] J. D. Currey, "Tensile yield in compact bone is determined by strain, postyield behaviour by mineral content", *Journal of Biomechanics*, vol. 37, no. 4, (2004), pp. 549–556.

[46] J. Currey, "Comparative mechanical properties and histology of bone", *American Zoologist*, vol. 24, no. 1, (1984), pp. 5–12.

[47] E. Novitskaya, P.-Y. Chen, S. Lee, A. Castro-Cese na, G. Hirata, V. A. Lubarda & J. McKittrick, "Anisotropy in the compressive mechanical properties of bovine cortical bone and the mineral and protein constituents", *Acta Biomaterialia*, vol. 7, no. 8, (2011), pp. 3170–3177.

[48] R. Crowninshield & M. Pope, "The response of compact bone in tension at various strain rates", *Annals of Biomedical Engineering*, vol. 2, no. 2, (1974), pp. 217–225.

[49] R. R. Adharapurapu, F. Jiang & K. S. Vecchio, "Dynamic fracture of bovine bone", *Materials Science and Engineering: C*, vol. 26, no. 8, (2006), pp. 1325–1332.

[50] D. T. Reilly & A. H. Burstein, "The elastic and ultimate properties of compact bone tissue", *Journal of Biomechanics*, vol. 8, no. 6, (1975), pp. 393–405.

[51] R. Allena & C. Cluzel, "Identification of anisotropic tensile strength of cortical bone using brazilian test", *Journal of the Mechanical Behavior of Biomedical Materials*, vol. 38, (2014), pp. 134–142.

[52] S. Li, E. Demirci & V. V. Silberschmidt, "Variability and anisotropy of mechanical behavior of cortical bone in tension and compression", 2013, URL https://doi.org/10.1016/j.jmbbm.2013.02.021, [Online; accessed July 24, 2023].

[53] B. Sanborn, C. Gunnarsson, M. Foster, P. Moy & T. Weerasooriya, "Effect of loading rate and orientation on the compressive response of human cortical bone", Tech. rep., DTIC Document, 2014.

[54] Q. Grimal, S. Haupert, D. Mitton, L. Vastel & P. Laugier, "Assessment of cortical bone elasticity and strength: mechanical testing and ultrasound provide complementary data", *Medical Engineering and Physics*, vol. 31, no. 9, (2009), pp. 1140–1147.

[55] F. G. Evans & M. Lebow, "Regional differences in some of the physical properties of the human femur", *Journal of Applied Physiology*, vol. 3, no. 9, (1951), pp. 563–572.

[56] M. M. Barak, J. D. Currey, S. Weiner & R. Shahar, "Are tensile and compressive young's moduli of compact bone different?", *Journal of the Mechanical Behavior of Biomedical Materials*, vol. 2, no. 1, (2009), pp. 51–60.

[57] D. B. Burr, M. B. Schafer & R. G. Frederickson, "Composition of the cement line and its possible mechanical role as a local interface in human compact bone", *Journal of Biomechanics*, vol. 21, no. 11, (1988), pp. 939–945.

[58] J. D. Currey, "The effect of porosity and mineral content on the young's modulus of elasticity of compact bone", *Journal of Biomechanics*, vol. 21, no. 2, (1988), pp. 131–139.

[59] R. Amprino, "Investigations on some physical properties of bone tissue", *Acta Anat.*, vol. 34, (1958), pp. 161–186.

[60] P. E. Riches, N. M. Everitt, A. R. Heggie & D. S. McNally, "Microhardness anisotropy of lamellar bone", *J. Biomech.*, vol. 30, (1997), pp. 1059–1061.

[61] V. Ziv, H. D. Wagner & S. Weiner, "Microstructure-microhardness relations in parallel-fibered and lamellar bone", *Bone*, vol. 18, (1996), pp. 417–428.

[62] D. Liu, V. Ziv, H. D. Wagner & S. Weiner, "Mechanical properties-structure relations of parallel fibered and lamellar bone: In-plane anisotropy", *Am. Acad. Orthopaedic Surgeons*.

[63] S. Lees & E. A. Page, "A study of some properties of mineralized turkey leg tendon", *Connect Tissue Res.*, vol. 28, (1992), pp. 263–287.

[64] W. Bonfield & M. D. Grynpas, "Anisotropy of the young's modulus of bone", *Nature*, vol. 270, (1977), pp. 453–454.

[65] C. H. Turner, A. Chandran & R. M. V. Pidaparti, "The anisotropy of osteonal bone and its ultrastructural implications", *Bone*, vol. 17, (1995), pp. 85–89.

[66] D. Liu, H. D. Wagner & S. Weiner, "Bending and fracture of compact circumferential and osteonal lamellar bone of the baboon tibia", *J. Mater. Sci. Mater. Med.*

[67] A. A. Abdel-Wahab, A. R. Maligno & V. V. Silberschmidt, "Micro-scale modelling of bovine cortical bone fracture: Analysis of crack propagation and microstructure using x-fem", *Computational Materials Science*, vol. 52, no.1, (2012), pp. 128–135.

[68] V. Ebacher, C. Tang, H. McKay, T. R. Oxland, P. Guy & R. Wang, "Strain redistribution and cracking behavior of human bone during bending", *Bone*, vol. 40, no. 5, (2007), pp. 1265–1275.

[69] V. Ebacher, P. Guy, T. R. Oxland & R. Wang, "Sub-lamellar microcracking and roles of canaliculi in human cortical bone", *Acta Biomaterialia*, vol. 8, no. 3, (2012), pp. 1093–1100.

[70] C. V. Rampersadh, L. Welgemoed & T. J. Cloete, "A multispecies investigation of the strain rate sensitivity of the modulus of cortical bone", *DYMAT*.

[71] T. J. Cloete, G. Paul & E. B. Ismail, "Hopkinson bar techniques for the intermediate strain rate testing of bovine cortical bone", *Philosophical Transactions of the Royal Society A: Mathematical, Physical and Engineering Sciences*, vol. 372, no. 2015.

[72] U. Zapata, K. Metzger, Q. Wang, R. M. Elsey, C. F. Ross & P. C. Dechow, "Material properties of mandibular cortical bone in the american alligator, alligator mississippiensis", *Bone*, vol. 46, no. 3, (2010), pp. 860–867.

[73] J. Moreno & F. Forriol, "Effects of preservation on the mechanical strength and chemical composition of cortical bone: an experimental study in sheep femora", *Biomaterials*, vol. 23, no. 12, (2002), pp. 2615–2619.

[74] Q. Wang, D. S. Strait & P. C. Dechow, "A comparison of cortical elastic properties in the craniofacial skeletons of three primate species and its relevance to the study of human evolution", *Journal of Human Evolution*, vol. 51, no. 4, (2006), pp. 375–382.

[75] P. C. Dechow & W. L. Hylander, "Elastic properties and masticatory bone stress in the macaque mandible", *American Journal of Physical Anthropology*, vol. 112, no. 4, (2000), pp. 553–574.

[76] A. Parish, W. Chen & T. Weerasooriya, "High strain-rate tensile behavior of pig bones", *http://dx.doi.org/10.1051/dymat/2009128*.

[77] A. R. Ayagara & R. Hambli, "On dynamic behavior of bone: Experimental and numerical study of porcine ribs subjected to impact loads in dynamic three-point bending tests.", *Journal of the Mechanical Behavior of Biomedical Materials*, vol. 98, (2019), pp. 336–347.

[78] K. L. Reed & T. D. Brown, "Elastic modulus and strength of emu cortical bone", *The Iowa Orthopaedic Journal*, vol. 21, (2001), pp. 53–57.

[79] H. Yamada & F. G. Evans, *Strength of biological materials*, Williams and Wilkins, 1970.

[80] A. R. Cuff, J. A. Bright & E. J. Rayfield, "Validation experiments on finite element models of an ostrich (struthio camelus) cranium", *PeerJ*, vol. 3, (2015), p. e1294.

[81] A. Casinos & J. Cubo, "Avian long bones, flight and bipedalism", *Comparative Biochemistry and Physiology Part A: Molecular and Integrative Physiology*, vol. 131, no. 1, (2001), pp. 159–167.

[82] D. R. Carter & W. C. Hayes, "Bone compressive strength: the influence of density and strain rate", *Science*, vol. 194, no. 1, (1976), pp. 174–1176.

[83] G. Evans, J. Behiri, L. Vaughan & W. Bonfield, "The response of equine cortical bone to loading at strain rates experienced in vivo by the galloping horse", *Equine Veterinary Journal*, vol. 24, no. 2, (1992), pp. 125–128.

[84] J. McElhaney & E. F. Byars, "Dynamic response of biological materials", *ASME*.

[85] G. Paul, *The strain rate dependent properties of bovine cortical bone*, M.Sc thesis, University of Cape Town, 2014.

[86] R. M. Kulin, F. Jiang & K. S. Vecchio, "Effects of age and loading rate on equine cortical bone failure", *Journal of the Mechanical Behavior of Biomedical Materials*, vol. 4, no. 1, (2011), pp. 57–75.

[87] A. Van der Westhuizen, *The strain rate dependent mechanical properties and modelling of bovine cortical bone in compression*, Ph.D. thesis, University of Cape Town, 2008.

[88] D. C. Wirtz, N. Schiffers, R. Frost, T. Pandorf, W. Weichert & K. Radermacher, "Critical evaluation of known bone material properties to realize anisotropic fe-simulation of the proximal femur", *Journal of Biomechanics*, vol. 33, no. 10, (2000), pp. 1325–1330.

[89] J. Y. Rho, Y. Tsui & G. M. Pharr, "Elastic properties of human cortical and trabecular lamellar bone measured by nanoindentation", *Biomaterials*, vol. 18, no. 20, (1997), pp. 1325–1330.

[90] J. S. Nyman, A. Roy, X. Shen, R. L. Acuna, J. H. Tyler & X. Wang, "The influence of water removal on the strength and toughness of cortical bone", *J Biomech*, vol. 39, no. 5, (2006), pp. 931–938.

[91] ASTM D695-23, "Standard test method for compressive properties of rigid plastics", (2023).

[92] ISO 604:2002, "Plastics - determination of compressive properties", (2002).

[93] J. H. McElhaney, "Dynamic response of bone and muscle tissue", *Journal of Applied Physiology*, vol. 21, no. 4, (1966), pp. 1231–1236.

[94] N. Daras, G. Nurick & T. Cloete, "A novel quasi-static compression test set-up with micron order accuracy for small specimens", *Journal of the Brazilian Society of Mechanical Sciences and Engineering*, vol. 46, no. 466, (2024), pp. 2–10.

[95] U. Stefan, B. Michael & S. Werner, "Effects of three different preservation methods on the mechanical properties of human and bovine cortical bone", *Bone*, vol. 47, no. 6, (2010), pp. 1048–1053.

[96] P. Lucksanasombool, W. Higgs, R. Higgs & M. Swain, "Fracture toughness of bovine bone: influence of orientation and storage media", *Biomaterials*, vol. 22, no. 23, (2001), pp. 3127–3132.

[97] J. C. Goh, E. J. Ang & K. Bose, "Effect of preservation medium on the mechanical properties of cat bones", *Acta Orthopaedica Scandinavica*, vol. 60, no. 4, (1989), pp. 465–467.

[98] B. Kaye, C. Randall, D. Walsh & P. Hansma, "The effects of freezing on the mechanical properties of bone", *The Open Bone Journal*, vol. 4, no. 1.

[99] G. Gómez, *Crystallization-related PH Changes During Freezing of Sodium Phosphate Buffer Solutions*, University of Michigan, 1995, URL `https://books.google.co.za/books?id=XUNtAAAAMAAJ`.

[100] K Pikal-Cleland, N Rodríguez-Hornedo, G Amidon & J Carpenter, "Protein denaturation during freezing and thawing in phosphate buffer systems: Monomeric and tetrameric β-galactosidase", *Archives of biochemistry and biophysics*, vol. 384, (2001), pp. 398–406.

[101] P Kolhe, E Amend & S Singh, "Impact of freezing on ph of buffered solutions and consequences for monoclonal antibody aggregation", *Biotechnology progress*, vol. 26, (2009), pp. 727–33.

[102] D. Hasson & R. Armstrong, "A ductile-to-brittle transition in bone?", *Journal of Materials Science*, vol. 9, no. 7, (1974), pp. 1165–1170.

[103] J. Smith & R. Walmsley, "Factors affecting the elasticity of bone", *Journal of Anatomy*, vol. 93, no. 4, (1959), pp. 503–523.

[104] A. Shrivastava, "Plastic properties and testing", in: "Introduction to Plastics Engineering", pp. 49–110, William Andrew Publishing, 2018.

[105] C. Plummer, "Testing of polymeric materials", in: "Comprehensive Materials Processing", pp. 35–70, Elsevier, 2014.

[106] M. Anderson, J. Keyak & H. Skinner, "Compressive mechanical properties of human cancellous bone after gamma irradiation", *Journal of Bone and Joint Surgery*, vol. 74-A, (1992), pp. 747–752.

[107] A. Odgaard & F. Linde, "The underestimation of young's modulus in compressive testing of cancellous bone specimens", *Journal of Biomechanics*, vol. 24, (1991), pp. 691–698.

[108] T. Keaveny, R. Borchers, L. Gibson & W. Hayes, "Theoretical analysis of the experimental artifact in trabecular bone compressive modulus", *Journal of Biomechanics*, vol. 26, (1993), pp. 599–607.

[109] M. Zhu, T. Keller & D. Spengler, "Effects of specimen load-bearing and free surface layers on the compressive mechanical properties of cellular materials", *Journal of Biomechanics*, vol. 27, (1994), pp. 57–66.

[110] T. Cloete, A. Van Der Westhuizen, S. Kok & G. Nurick, "A tapered striker pulse shaping technique for uniform strain rate dynamic compression of bovine bone", *EDP Sciences*, vol. 1, (2009), pp. 901–907.

[111] M. Prot & T. J. Cloete, "A tandem momentum trap for dynamic specimen recovery during split hopkinson pressure bar testing of cancellous bone", *Journal of Dynamic Behavior of Materials*, vol. 2, no. 1, (2016), pp. 50–58.

[112] Robert H. Riffenburgh & Daniel L. Gillen, *Techniques to Aid Analysis*, chap. 27.6, pp. 574–585, Elsevier, 4th edn., 2020.

[113] R. A. Wannamaker, S. P. Lipshitz, J. Vanderkooy & J. N. Wright, "A theory of nonsubtractive dither", *IEEE Transactions on Signal Processing*, vol. 48, no. 2, (2000), pp. 499–516.

[114] J. Vanderkooy & S. P. Lipshitz, "Resolution below the least significant bit in digital systems with dither", *Journal of the Audio Engineering Society*, vol. 32, no. 3, (1984), pp. 106–113.

[115] R. Etchenique & J. Aliaga, "Resolution enhancement by dithering", *American Association of Physics Teachers*, vol. 72, (2004), p. 159.

[116] S. Kalidindi, A. Abusafieh & E. Ei-Danaf, "Accurate characterization of machine compliance for simple compression testing", *Experimental Mechanics*, vol. 37, (1997), pp. 210–215.

[117] P. Augat, T. Link, T. Lang & et al., "Anisotropy of the elastic modulus of trabecular bone specimens from different anatomical locations", *Medical Engineering and Physics*, vol. 20, (1998), pp. 124–131.

[118] S. Timoshenko & J. N. Goodier, *Theory of Elasticity*, McGraw-Hill, 3rd ed. edn., 1970.

[119] R. G. Budynas & J. K. Nisbett, *Shigley's Mechanical Engineering Design*, McGraw-Hill Higher Education, 2019.

[120] Thyssenkrupp Materials UK, "Aluminium 1050-h14 data sheet", n.d., URL `https://d2zo35mdb530wx.cloudfront.net/_legacy/UCPthyssenkruppBAMXUK/assets.files/material-data-sheets/aluminium/1050-h14.pdf`, accessed: 2025-02-11.

[121] N. Daras, *Degradation behaviour of the mechanical properties of bovine cortical bone*, Ph.D. thesis, University of Cape Town, 2024.

[122] Prasanta Basak, Indrani Basak & N. Balakrishnan, "Estimation for the three-parameter lognormal distribution based on progressively censored data", *Computational Statistics and Data Analysis*, vol. 53, (2009), pp. 3580–3592.

[123] Rodrigo J. Aristizabal, *Estimating the Parameters of the Three-Parameter Lognormal Distribution*, Ph.D. thesis, Florida International University, 2012.

[124] Eckhard Limpert, Werner A. Stahel & Markus Abbt, "Log-normal distributions across the sciences: Keys and clues", *Bioscience*, vol. 51, (2001), pp. 341–352.

[125] A. Clifford Cohen & Betty Jones Whitten, "Estimation in the three-parameter lognormal distribution", *Journal of the American Statistical Association*, vol. 75, (1980), pp. 399–404.

[126] A. D. Speirs, M. A. Hotz, T. R. Oxland, R. Häusler & L.-P. Nolte, "Biomechanical properties of sterilized human auditory ossicles", *Journal of Biomechanics*, vol. 32, (1999), pp. 485–491.

[127] E. F. Morgan, O. C. Yeh, W. C. Chang & T. M. Keaveny, "Nonlinear behavior of trabecular bone at small strains", *Journal of Biomechanical Engineering*, vol. 123, (2001), pp. 1–9.

[128] L. Grassi & H. Isaksson, "Extracting accurate strain measurements in bone mechanics: A critical review of current methods", *Journal of the Mechanical Behavior of Biomedical Materials*, vol. 50, (2015), pp. 43–54.

[129] L. Cyganik, M. Binkowski, G. Kokot *et al.*, "Prediction of young's modulus of trabeculae in microscale using macro-scale's relationships between bone density and mechanical properties", *Journal of the Mechanical Behavior of Biomedical Materials*, vol. 36, (2014), pp. 120–134.

[130] L. Grassi, S. P. Väänänen, S. A. Yavari *et al.*, "Full-field strain measurement during mechanical testing of the human femur at physiologically relevant strain rates", *Journal of Biomechanical Engineering*, vol. 136, (2014), p. 111010.

Appendices

Appendix A

Sample Calculations

The stiffness of a specimen is given by:

$$k = \frac{EA}{L} \tag{A.1}$$

where:

- E = Elastic modulus (2.9 GPa for PMMA and 2.9 GPa for Al)
- A = Cross-sectional area (πr^2)
- L = Height of the specimen (mm)

A.1 PMMA Stiffness Calculations

A.1.1 In Theory

For short specimens ($d = 5$ mm, $L = 5$ mm):

$$k_{\text{short}} = \frac{2.9 \times \pi \times 2.5^2}{5} = 11.39 \text{ kN/mm} \tag{A.2}$$

For tall specimens ($d = 5$ mm, $L = 10$ mm):

$$k_{\text{tall}} = \frac{2.9 \times \pi \times 2.5^2}{10} = 5.69 \text{ kN/mm} \tag{A.3}$$

Thus, the stiffness ratio:

$$\frac{k_{\text{tall}}}{k_{\text{short}}} = \frac{5.69}{11.39} = 0.5 \tag{A.4}$$

as proven in Section 3.3.3.

A.1.2 In Practice

The sub-press has its own stiffness k_{sp}. Using the relationship:

$$\frac{1}{k_{\text{spec, apparent}}} = \frac{1}{k_{\text{spec}}} + \frac{1}{k_{\text{sp}}} \tag{A.5}$$

For flat platens ($k_{\text{sp}} = 305$ kN/mm):

$$\frac{1}{k_{\text{short, apparent}}} = \frac{1}{11.39} + \frac{1}{305} \tag{A.6}$$

$$k_{\text{short, apparent}} = 10.98 \text{ kN/mm} \tag{A.7}$$

$$\frac{1}{k_{\text{tall, apparent}}} = \frac{1}{5.69} + \frac{1}{305} \tag{A.8}$$

$$k_{\text{tall, apparent}} = 5.59 \text{ kN/mm} \tag{A.9}$$

Thus, the apparent stiffness ratio:

$$\frac{k_{\text{tall, apparent}}}{k_{\text{short, apparent}}} = \frac{5.59}{10.98} = 0.509 \tag{A.10}$$

For hyperbolic frustum platens ($k_{\text{sp}} = 201$ kN/mm):

$$\frac{1}{k_{\text{short, apparent}}} = \frac{1}{11.39} + \frac{1}{201} \tag{A.11}$$

$$k_{\text{short, apparent}} = 10.78 \text{ kN/mm} \tag{A.12}$$

$$\frac{1}{k_{\text{tall, apparent}}} = \frac{1}{5.69} + \frac{1}{201} \tag{A.13}$$

$$k_{\text{tall, apparent}} = 5.53 \text{ kN/mm} \tag{A.14}$$

Thus, the apparent stiffness ratio:

$$\frac{k_{\text{tall, apparent}}}{k_{\text{short, apparent}}} = \frac{5.53}{10.78} = 0.513 \tag{A.15}$$

A.2 Aluminium Stiffness Calculations

A.2.1 In Theory

For short specimens ($d = 5$ mm, $L = 5$ mm):

$$k_{\text{short}} = \frac{71 \times \pi \times 2.5^2}{5} = 278.82 \text{ kN/mm} \tag{A.16}$$

For tall specimens ($d = 5$ mm, $L = 10$ mm):

$$k_{\text{tall}} = \frac{71 \times \pi \times 2.5^2}{10} = 139.41 \text{ kN/mm} \tag{A.17}$$

Thus, the stiffness ratio:

$$\frac{k_{\text{tall}}}{k_{\text{short}}} = \frac{139.41}{278.82} = 0.5 \tag{A.18}$$

A.2.2 In Practice

For flat platens ($k_{\text{sp}} = 305$ kN/mm):

$$\frac{1}{k_{\text{short, apparent}}} = \frac{1}{278.82} + \frac{1}{305} \tag{A.19}$$

$$k_{\text{short, apparent}} = 145.66 \text{ kN/mm} \tag{A.20}$$

$$\frac{1}{k_{\text{tall, apparent}}} = \frac{1}{139.41} + \frac{1}{305} \tag{A.21}$$

$$k_{\text{tall, apparent}} = 95.68 \text{ kN/mm} \tag{A.22}$$

Thus, the apparent stiffness ratio:

$$\frac{k_{\text{tall, apparent}}}{k_{\text{short, apparent}}} = \frac{95.68}{145.66} = 0.66 \tag{A.23}$$

For hyperbolic frustum platens ($k_{\text{sp}} = 201$ kN/mm):

$$\frac{1}{k_{\text{short, apparent}}} = \frac{1}{278.82} + \frac{1}{201} \tag{A.24}$$

$$k_{\text{short, apparent}} = 116.80 \text{ kN/mm} \tag{A.25}$$

$$\frac{1}{k_{\text{tall, apparent}}} = \frac{1}{139.41} + \frac{1}{201} \tag{A.26}$$

$$k_{\text{tall, apparent}} = 82.32 \text{ kN/mm} \tag{A.27}$$

Thus, the apparent stiffness ratio:

$$\frac{k_{\text{tall, apparent}}}{k_{\text{short, apparent}}} = \frac{82.32}{116.80} = 0.705 \tag{A.28}$$

A.3 Expected Range

The expected range for the apparent stiffness ratio spans from the most compliant material (PMMA) to the least compliant material (Aluminium):

- For the flat platens: 0.509 to 0.66, with an expected stiffness ratio close to the average:

$$\frac{0.509 + 0.66}{2} = 0.585 \tag{A.29}$$

- For the hyperbolic frustum platens: 0.513 to 0.705, with an expected stiffness ratio close to the average:

$$\frac{0.513 + 0.705}{2} = 0.61 \tag{A.30}$$

Appendix B

Stress-Strain Data Analysis

A Python script was used for data processing. First, the script prompts the user to select the UTM test data file and choose a specific specimen for analysis. It then generates a displacement versus time plot for the selected specimen. The user manually selects six points on this plot, and the nearest data rows are identified. Straight lines are fitted between these points to capture key transitions, and the times of these transitions are calculated based on the intersection of the fitted lines.

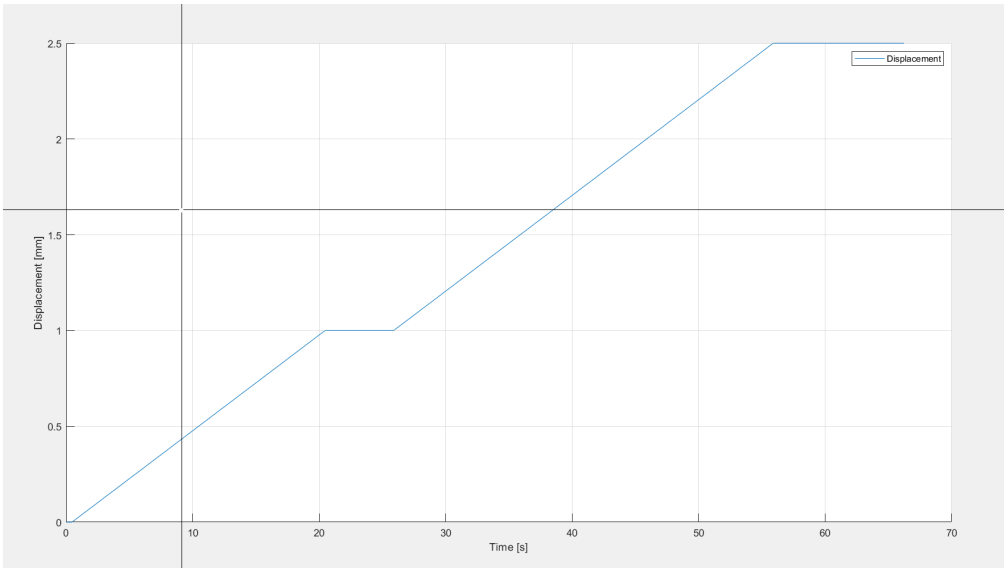

Figure B.1 Displacement vs time data from the Zwick UTM.

Next, the data is truncated to remove irrelevant sections before the datum, and displacement, force, and time values are zeroed for further analysis. The script interpolates the data at regular intervals (0.1 seconds) to create a consistent time series. Verification plots of displacement and force versus time are generated to ensure accuracy. A similar process is applied to sub-press data, where displacement values are smoothed and converted from μm to mm. The UTM and sub-press data are then synchronized and combined into a single dataset.

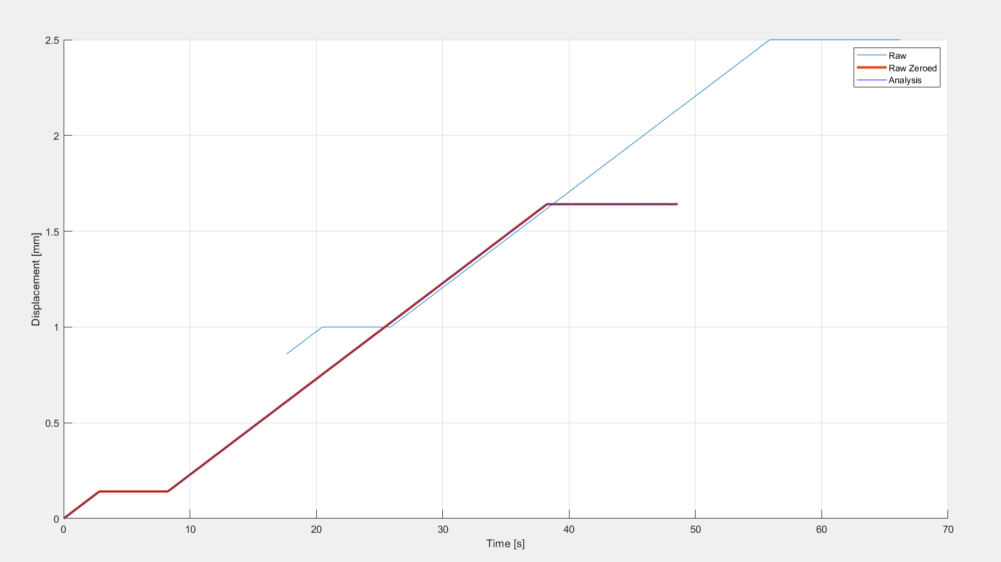

Figure B.2 Zeroed displacement vs time data from the Zwick UTM.

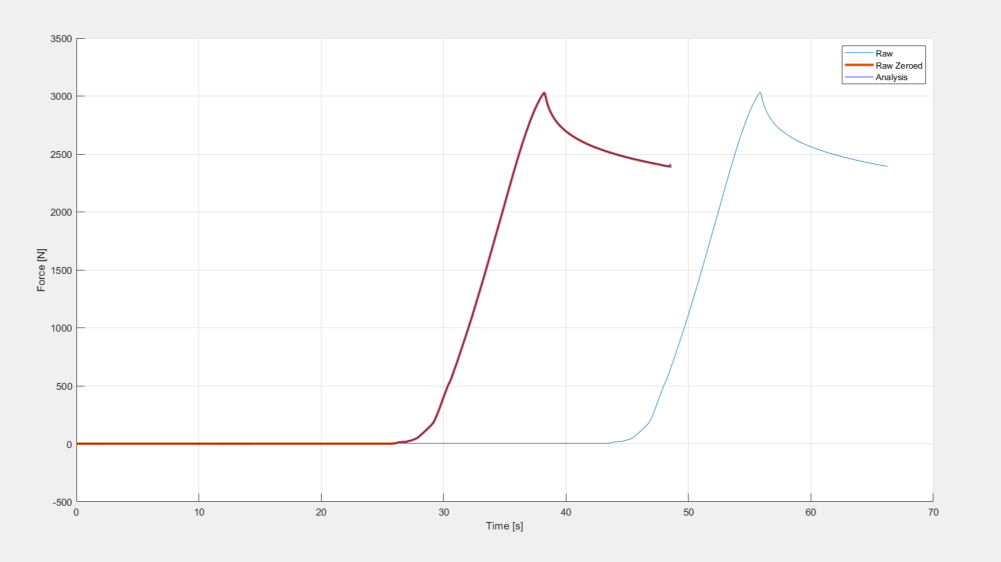

Figure B.3 Force vs time data from the Zwick UTM.

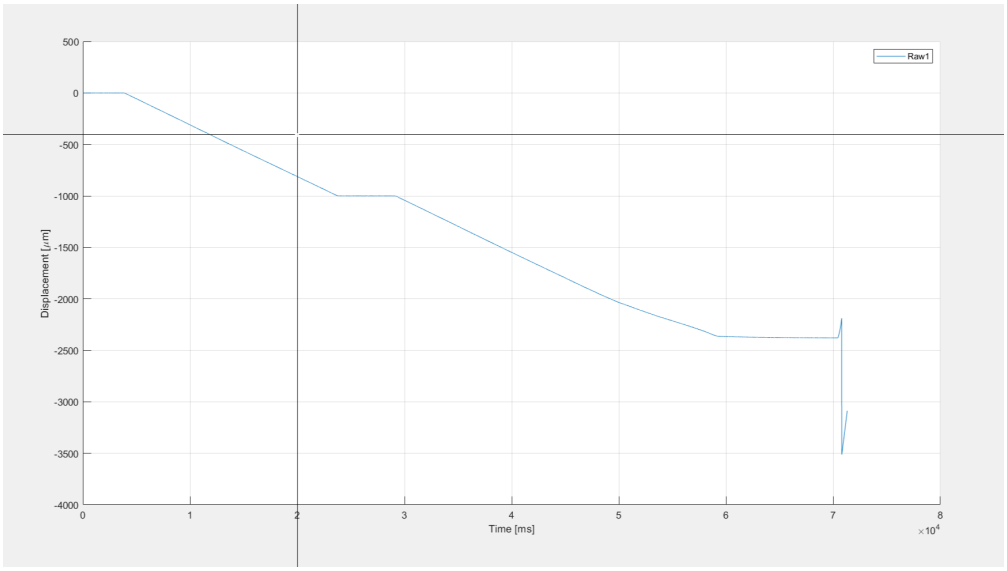

Figure B.4 Averaged displacement vs time data from the sub-press.

Following this, the script calculates stress and strain values based on user-provided specimen dimensions (diameter, height, and weight). The calculated stress and strain data are added to the combined dataset. A raw stress-strain and strain rate plot is generated and a gradient calculation of the elastic portion is made to determine the modulus.

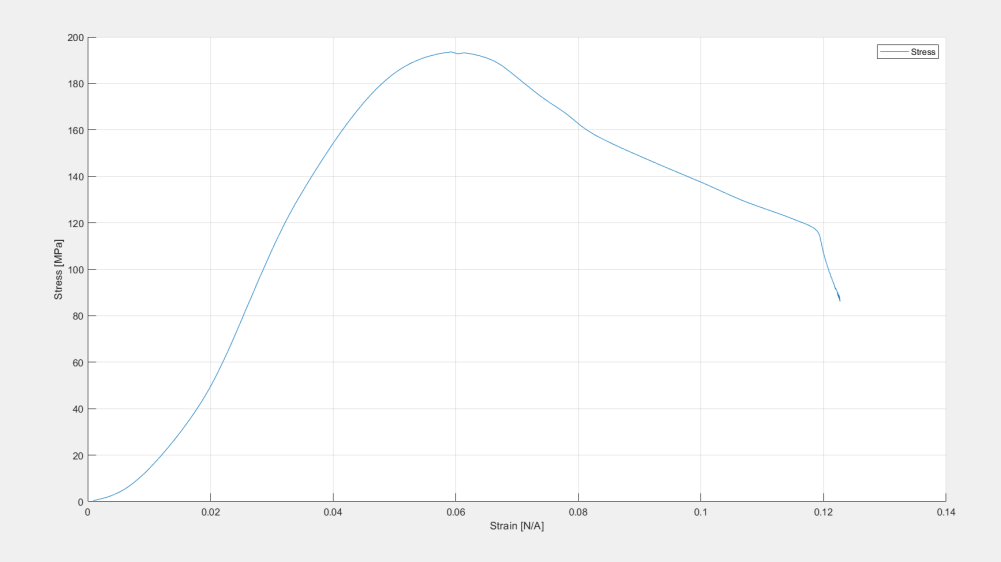

Figure B.5 Raw stress vs strain data.

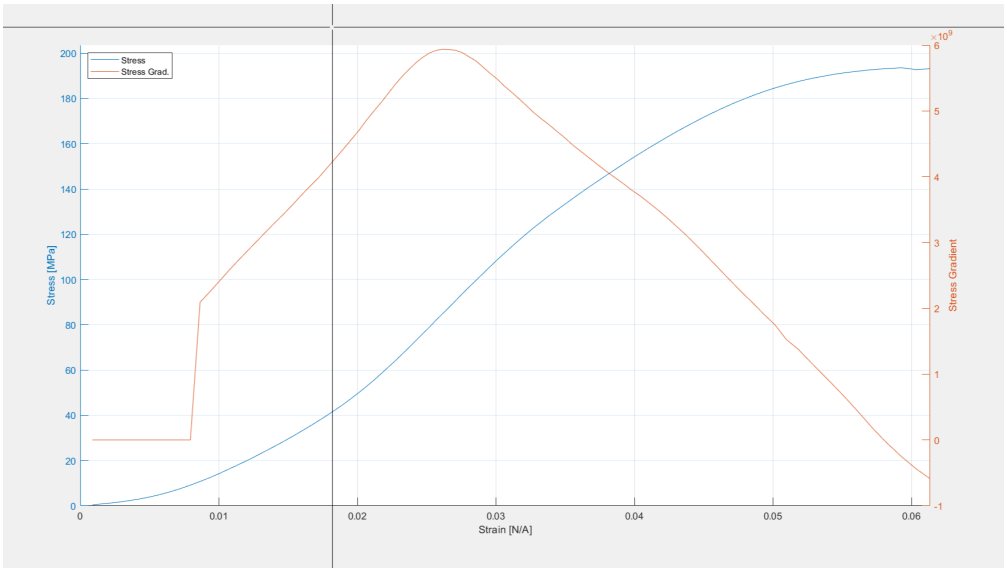

Figure B.6 Stress vs strain vs strain gradient data.

Finally, the stress-strain curve is shifted so that the modulus runs through the origin. The results are exported as a CSV file for further analysis.

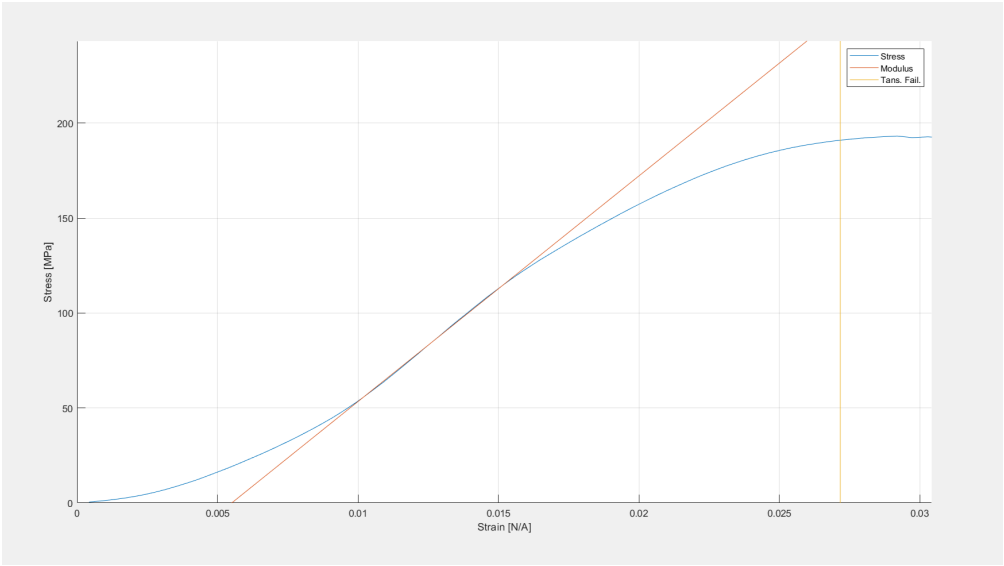

Figure B.7 Raw stress vs strain data with modulus and point of incipient failure superimposed.

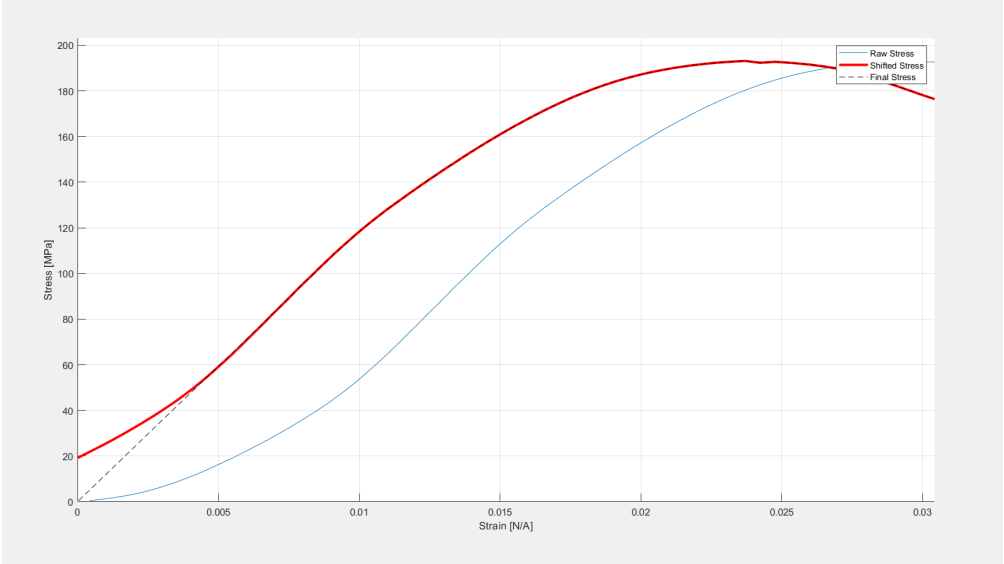

Figure B.8 Final, shifted stress vs strain data.

Appendix C

Log-normal Distributions

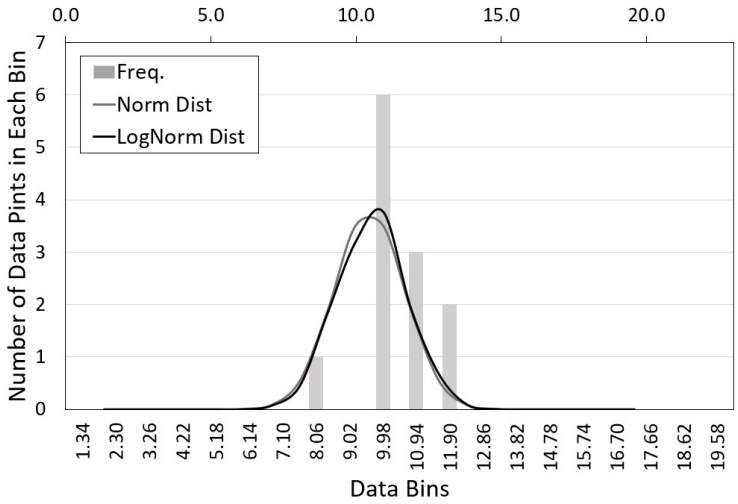

Figure C.1 Apparent moduli for "machine-freeze" specimens after one month in storage, with both normal and log-normal distributions displayed.

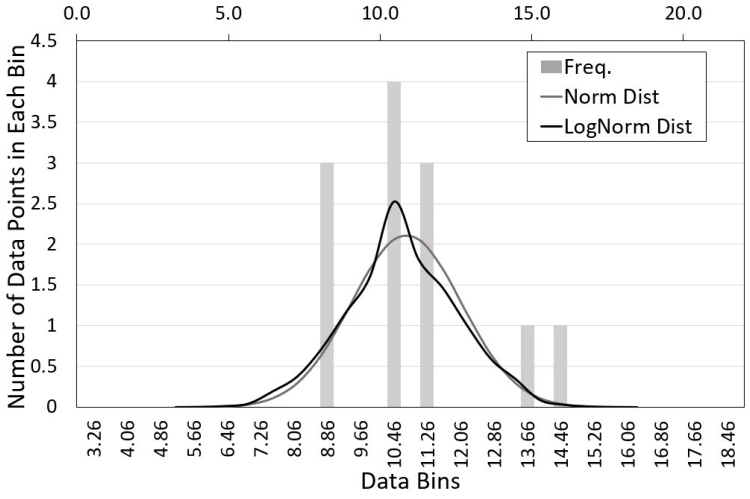

Figure C.2 Apparent moduli for "freeze-machine" specimens after one month in storage, with both normal and log-normal distributions displayed.

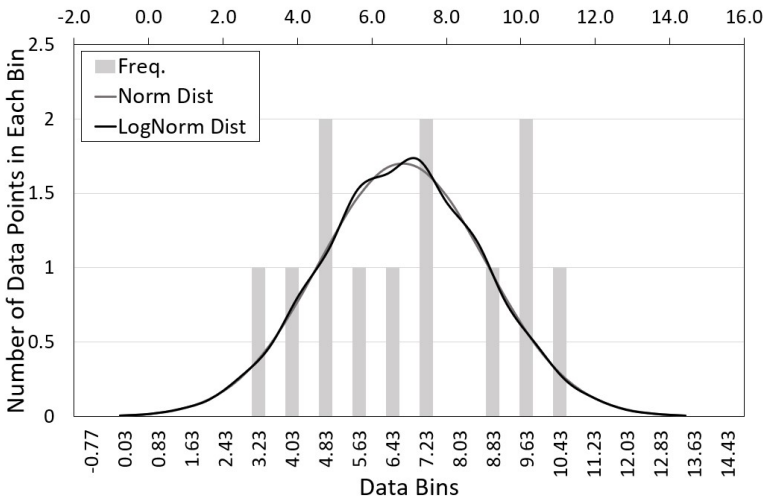

Figure C.3 Apparent moduli for "machine-freeze" specimens after three months in storage, with both normal and log-normal distributions displayed.

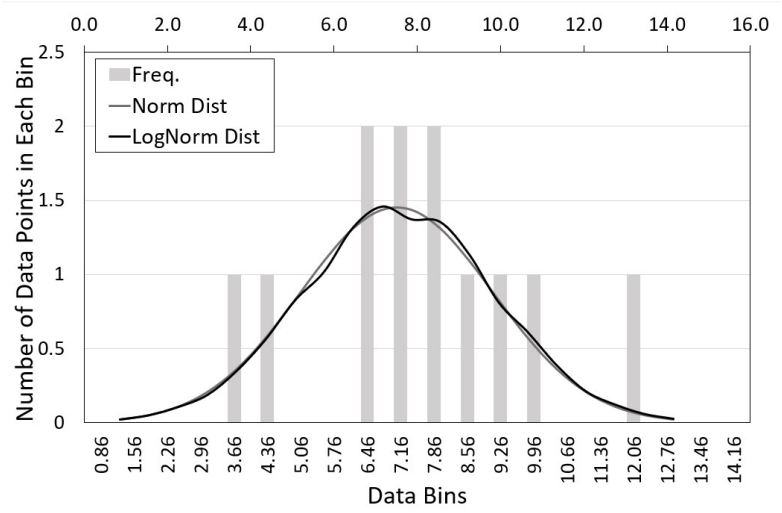

Figure C.4 Apparent moduli for "freeze-machine" specimens after three months in storage, with both normal and log-normal distributions displayed.

Appendix D

Ethical Clearance Forms

UNIVERSITY OF CAPE TOWN
IYUNIVESITHI YASEKAPA • UNIVERSITEIT VAN KAAPSTAD

PRE-SCREENING QUESTIONNAIRE OUTCOME LETTER

STU-EBE-2023-PSQ000305

2023/04/12

Dear Lia Carstens,

Your Ethics pre-screening questionnaire (PSQ) has been evaluated by your departmental ethics representative. Based on the information supplied in your PSQ, it has been determined that you do not need to make a full ethics application for the research project in question.

You may proceed with your research project titled:

Degradation of Mechanical Properties of Bovine Cortical Bone During Long-Term Whole Bone Storage.

Please note that should aspect(s) of your current project change, you should submit a new PSQ in order to determine whether the changed aspects increase the ethical risks of your project. It may be the case that project changes could require a full ethics application and review process.

Regards,

Faculty Research Ethics Committee

To Whom It May Concern

Dear Sir/Madam

This purpose of this letter is to confirm the ethical process by which we, Bill Riley Meat cc, have provided biological material for research to be conducted by Mr Nicholas Daras and Dr Trevor Cloete at the University of Cape Town.

The biological material provided by us for the purpose of research was all by-product of the standard operations at our facility and no harm was done to any animal specifically for the purpose of research.

Signed by candidate

BILL RILE (MEAT) PT LTD
2 STEENBRAS ST.
BROOKLYN
TEL: 021 511 5522 -

Appendix E

Design Drawings

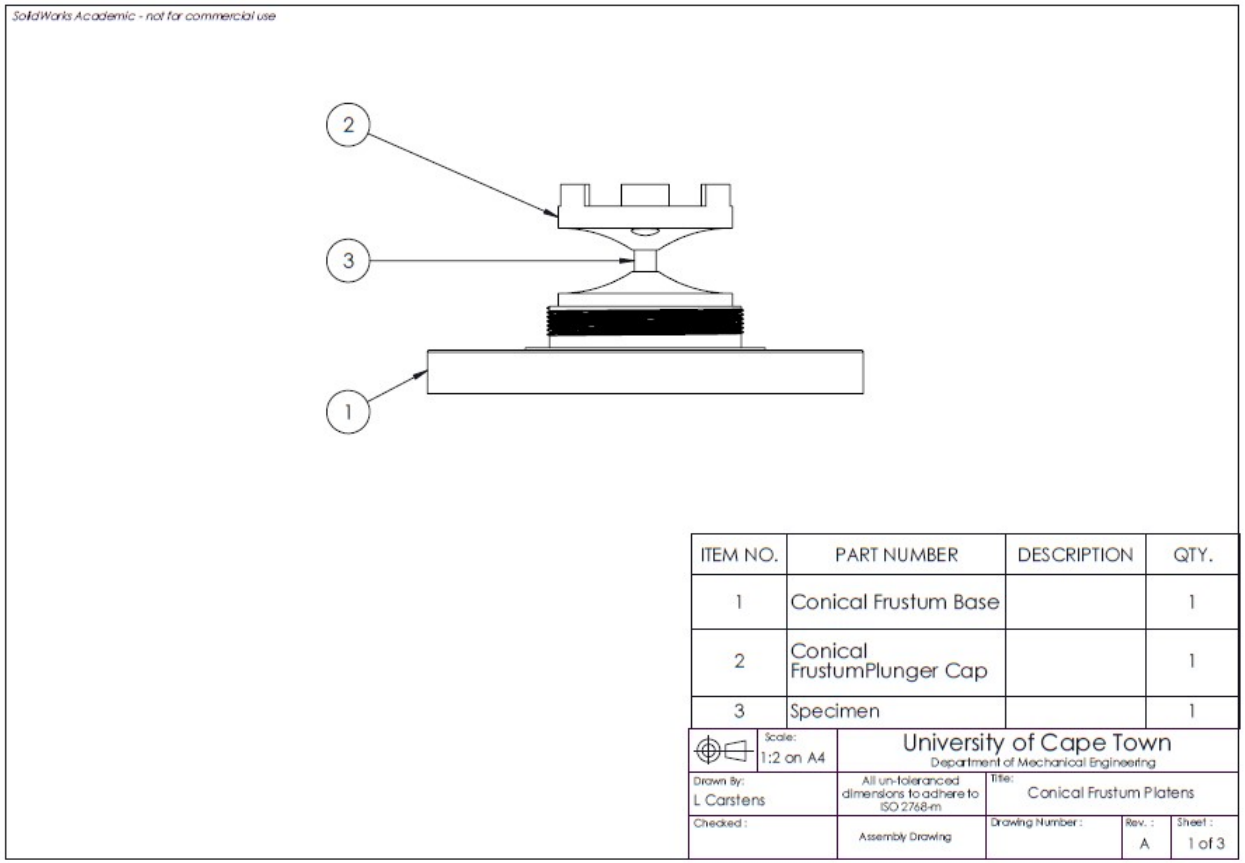

Figure E.1 Assembly drawing for the conical frustum platens.

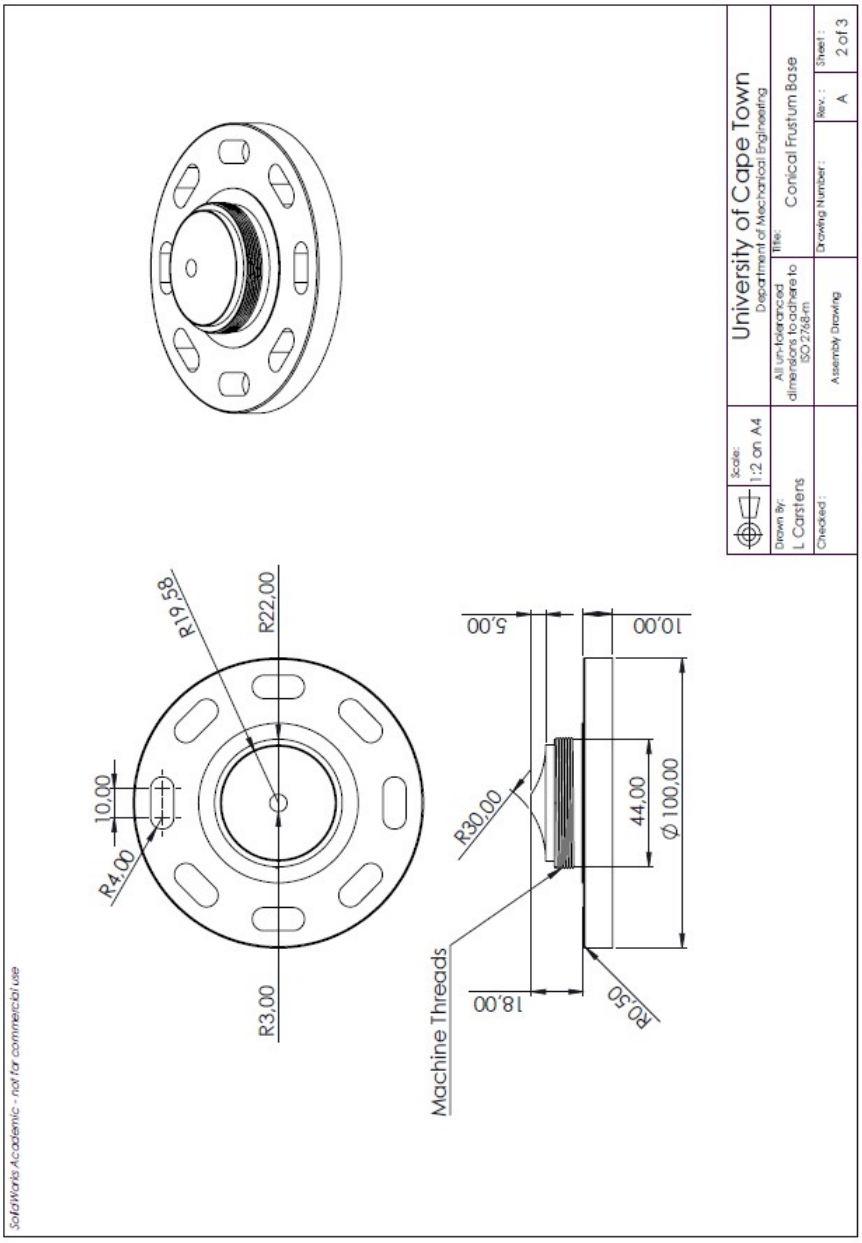

Figure E.2 Part drawing for the conical frustum base.

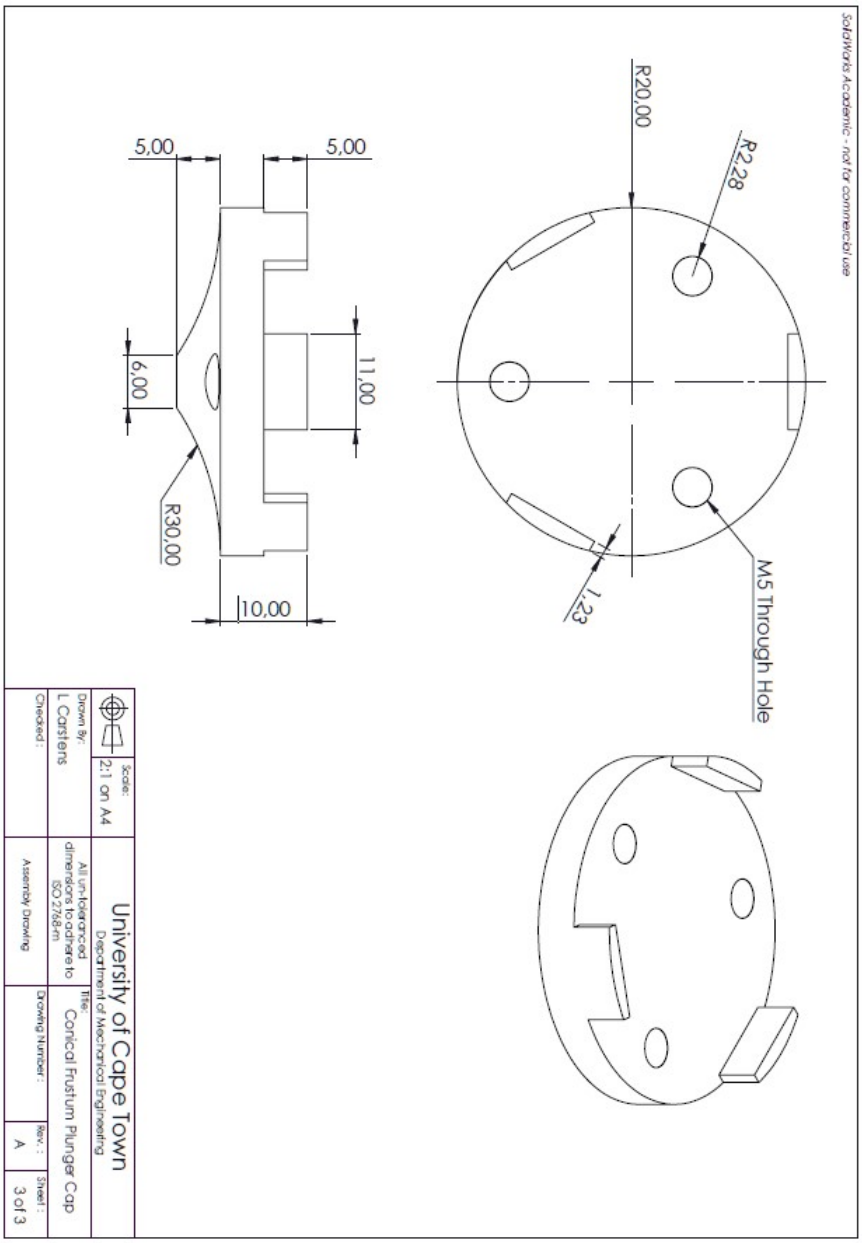

Figure E.3 Part drawing for the conical frustum plunger cap.

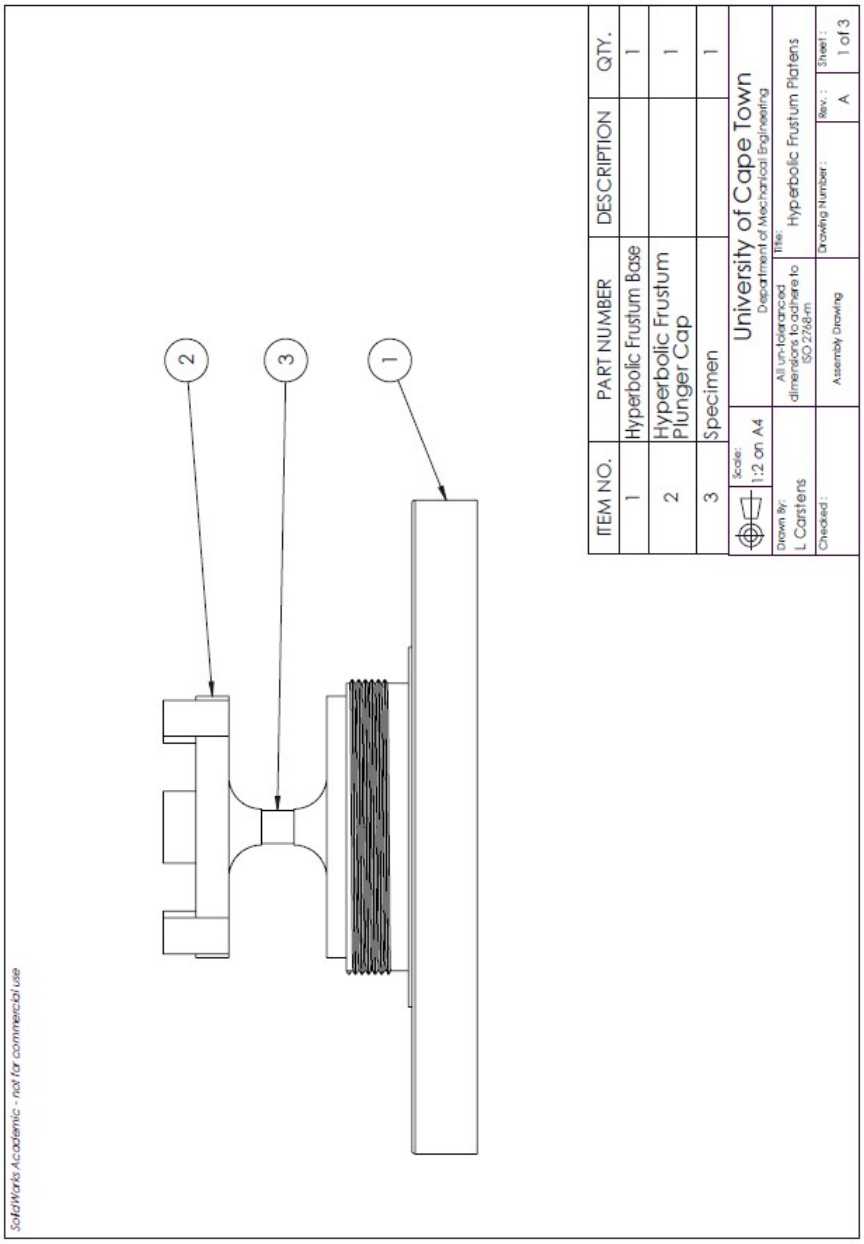

Figure E.4 Assembly drawing for the hyperbolic frustum platens.

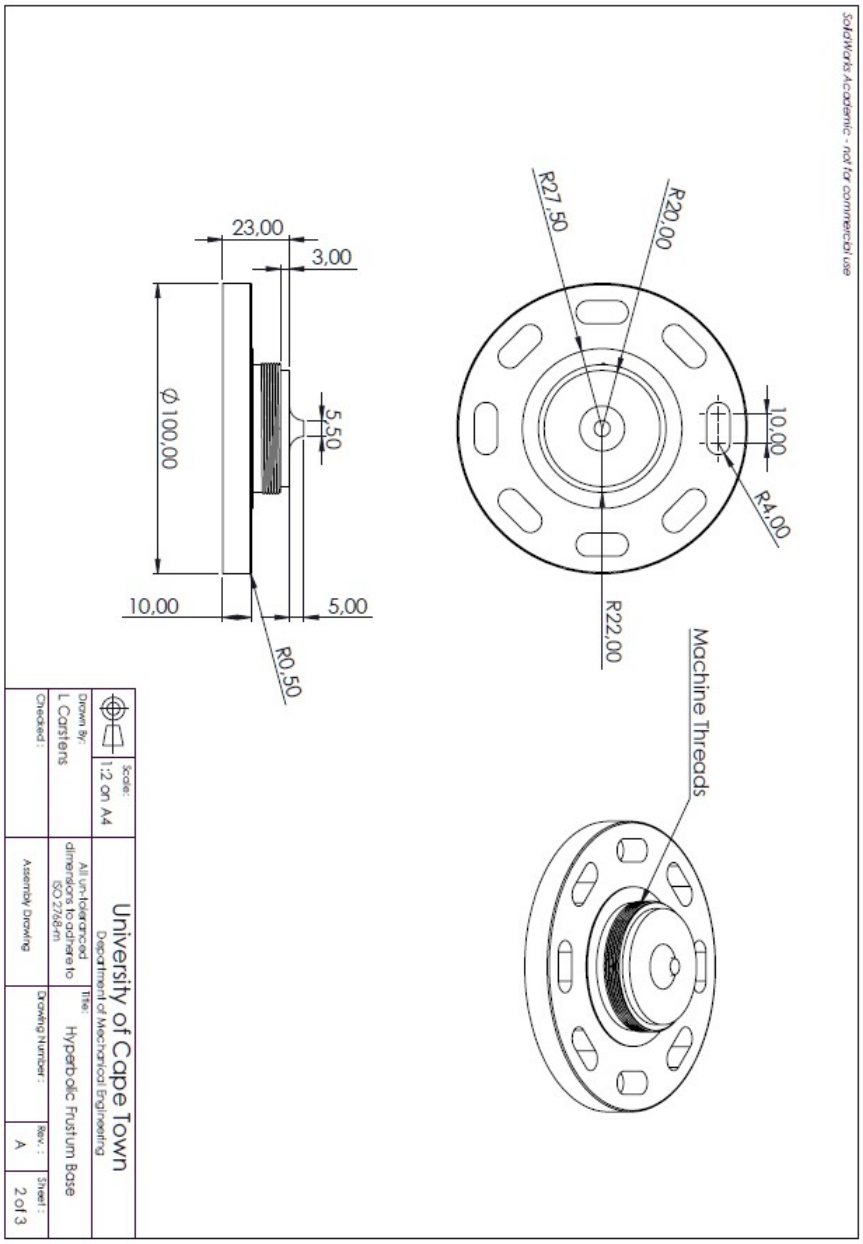

Figure E.5 Part drawing for the hyperbolic frustum base.

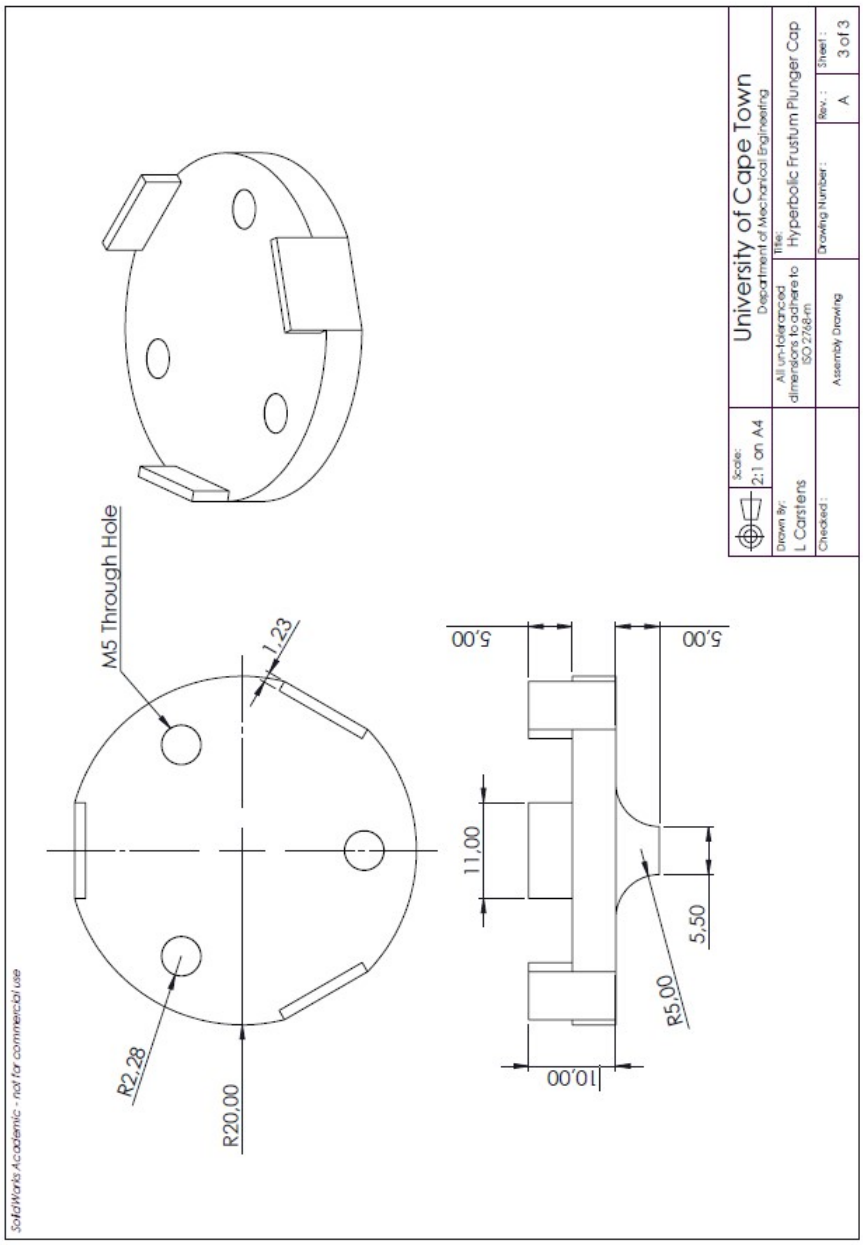

Figure E.6 Part drawing for the hyperbolic frustum plunger cap.

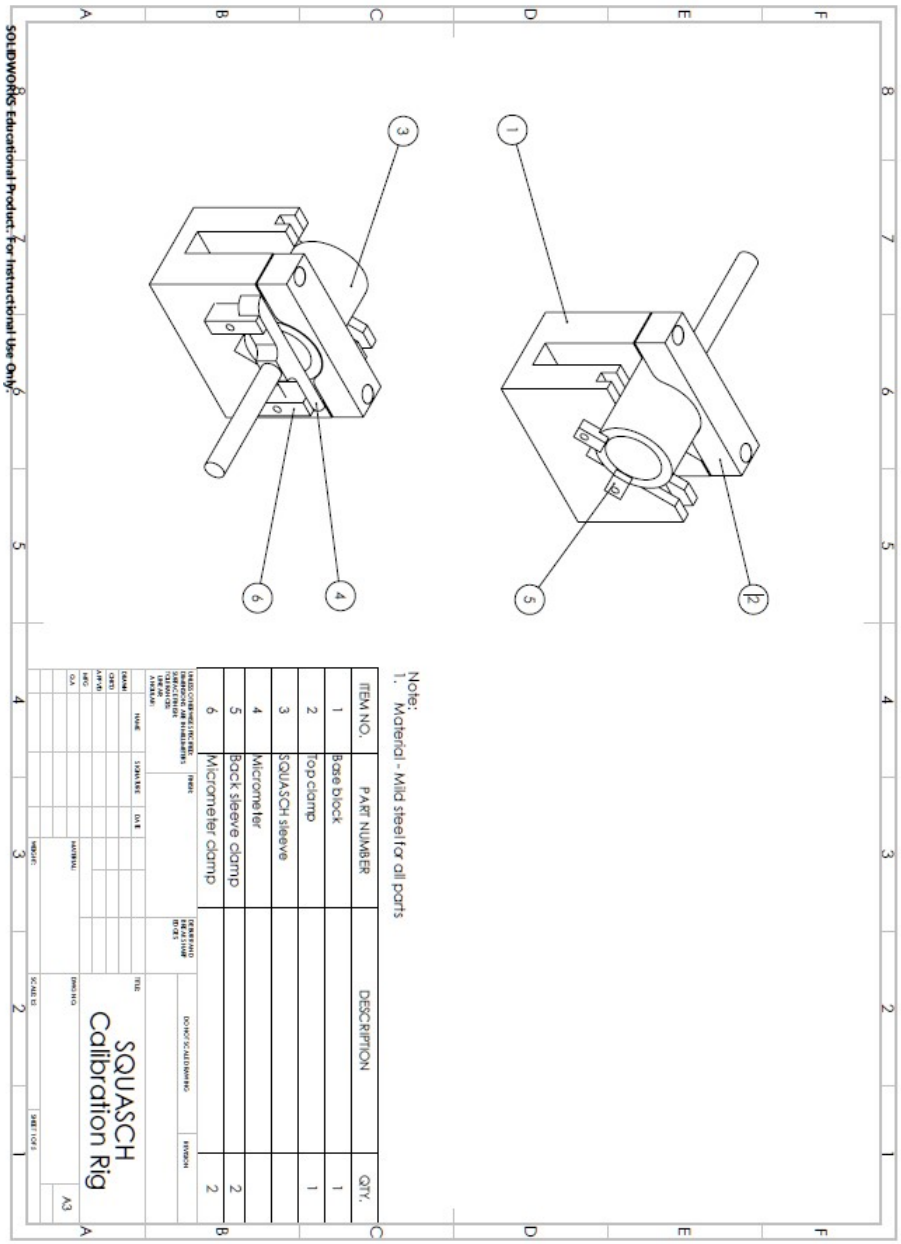

Figure E.7 Assembly drawing for the sub-press calibration mounting fixture.

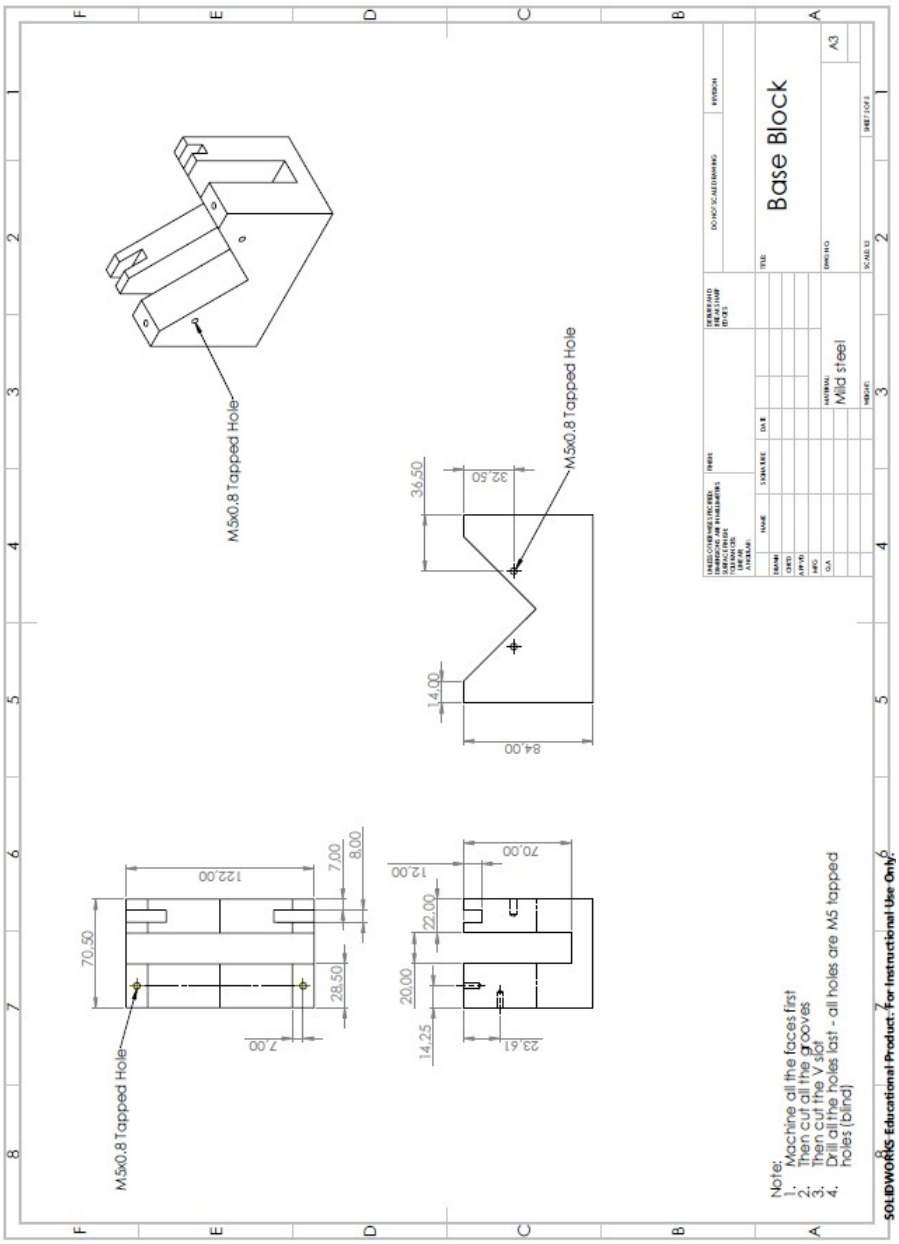

Figure E.8 Part drawing for the mounting fixture base block.

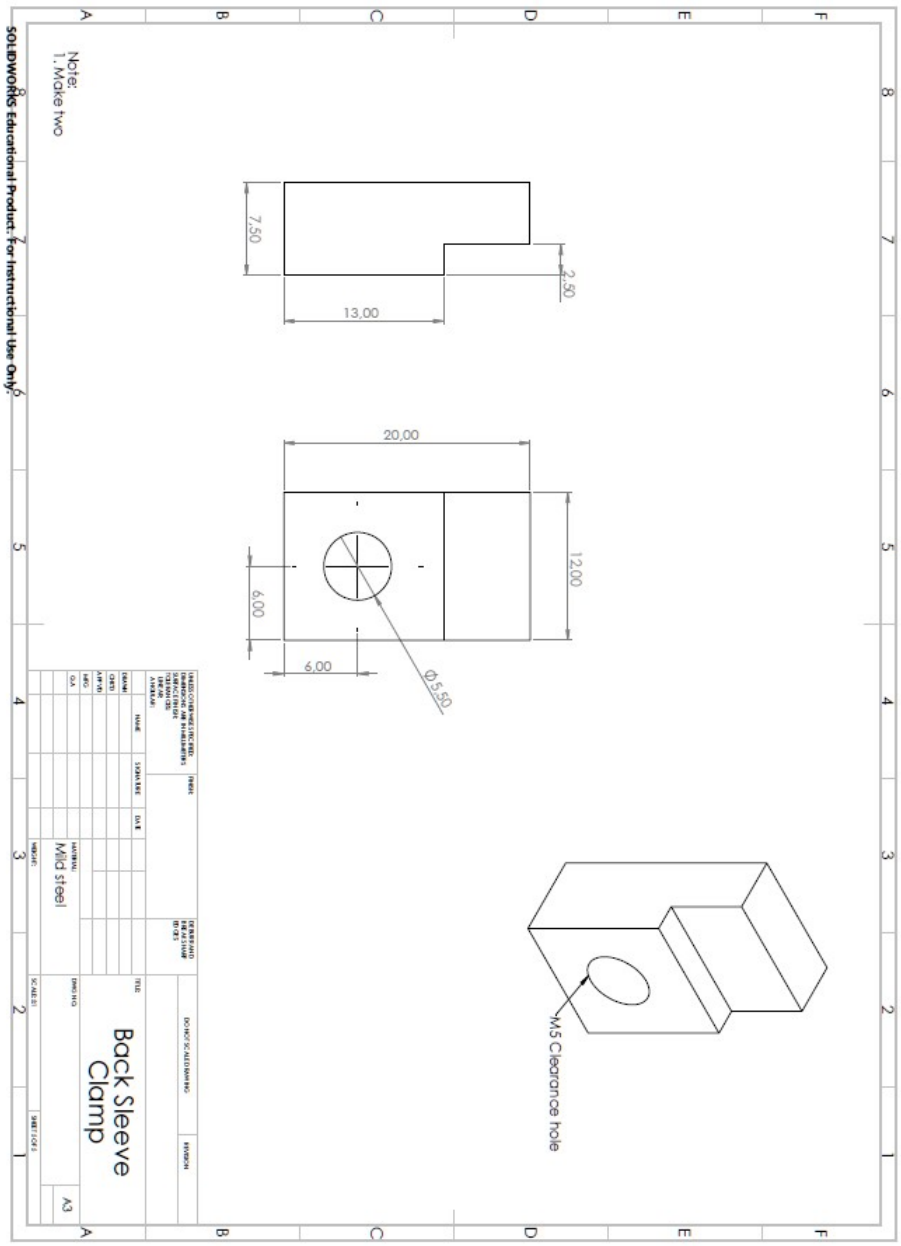

Figure E.9 Part drawing for the sub-press sleeve back clamp.

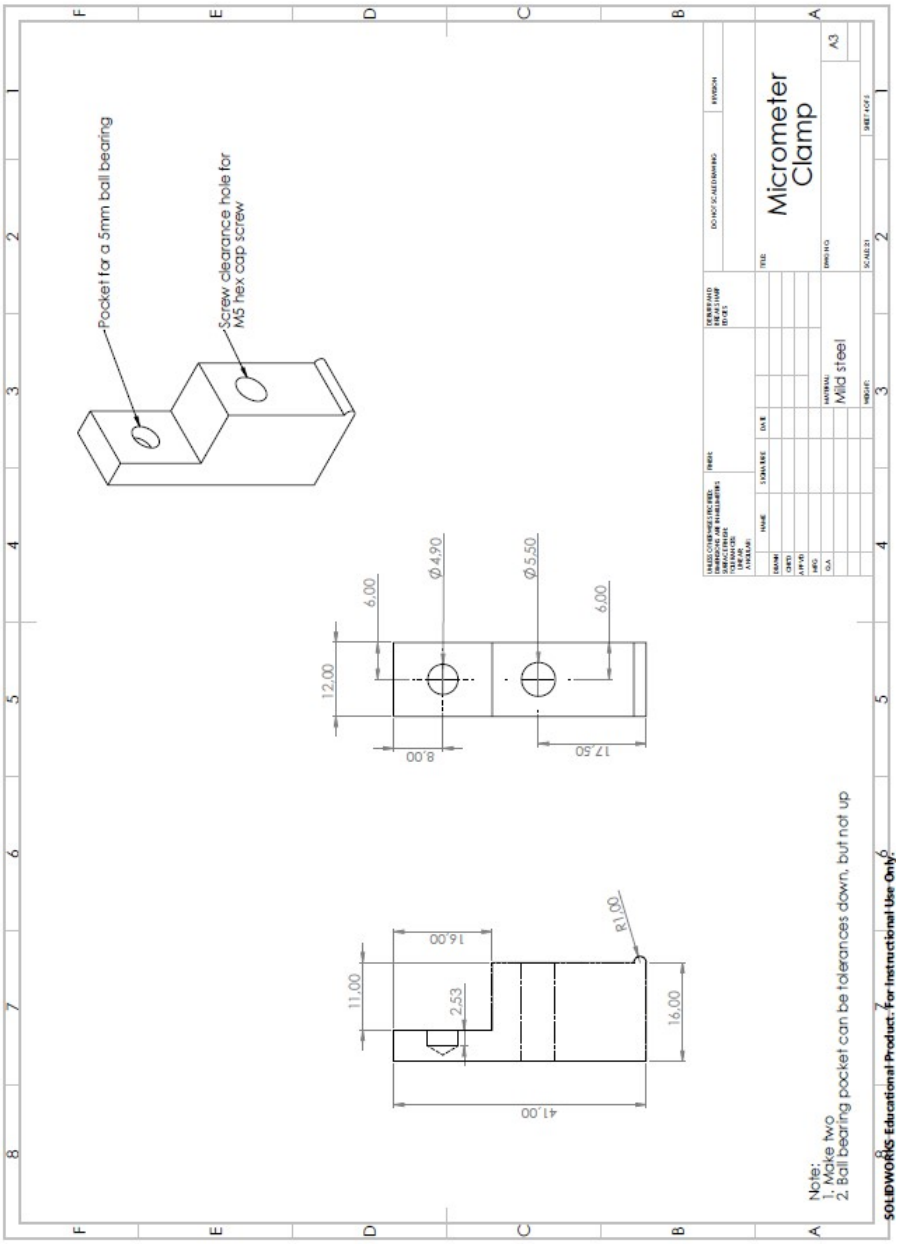

Figure E.10 Part drawing for the mounting fixture micrometer clamp.

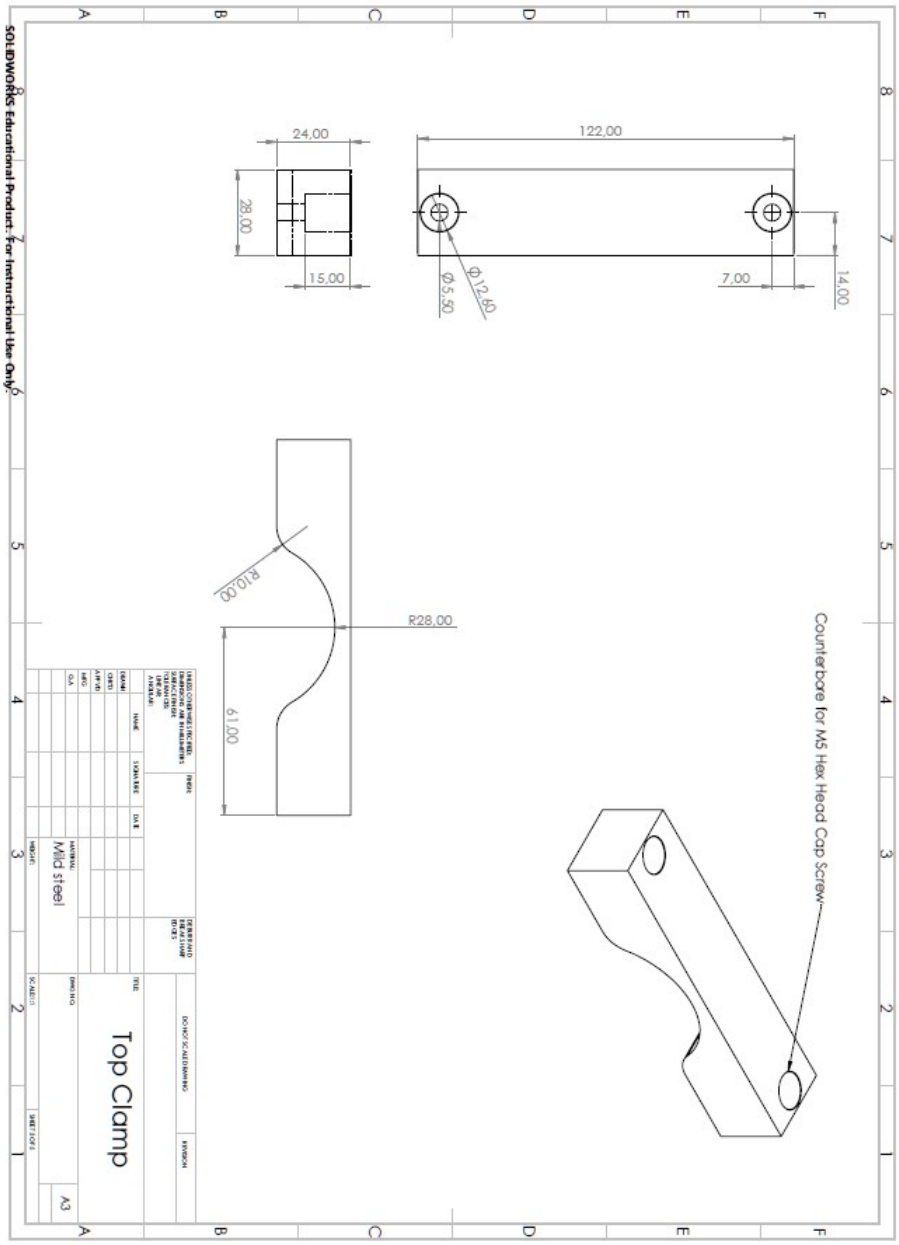

Figure E.11 Part drawing for the sub-press sleeve top clamp.